THE UNIVERSITY OF MICHIGAN

5548-5-T

AFCRL-66-124

THEORETICAL AND EXPERIMENTAL STUDY OF THE SCATTERING BEHAVIOR OF A CIRCUMFERENTIALLY-LOADED SPHERE

by

V. V. Liepa and T. B. A. Senior

February 1966

Scientific Report No. 5

Contract AF 19(628)-2374
Project 5635
Task 563502

Prepared for

Air Force Cambridge Research Laboratories
Office of Aerospace Research
L. G. Hanscom Field
Bedford, Massachusetts

ABSTRACT

The electromagnetic scattering behavior of a metallic sphere loaded with a circumferential slot in a plane perpendicular to the direction of incidence is investigated. The slot is assumed of small but finite width with a constant electric field across it, and under this assumption, the analysis of external fields is exact. The scattered field is obtained by superposition of the field diffracted by an unloaded sphere and that radiated from the excited slot, with the radiation strength and phase determined by the loading parameters. Thus the scattering behavior is determined by the loading admittance and the position of this slot.

The numerical study is restricted to the frequency range corresponding to $0 < ka \leqslant 10.0$, and the results presented are primarily for passive loading. The maximum and minimum back scattering cross sections and the loading needed to attain these are presented for different loading positions. The bistatic scattering patterns are computed for a sphere loaded for zero back scattering and from these the back scattering null widths are obtained. The extreme total scattering cross sections are evaluated using the forward scattering theorem and, for small values of ka, the result is compared with that obtained by direct integration of the differential cross sections.

Experimental data, obtained using a metallic sphere with an equatorial slot backed by a radial cavity of adjustable depth, is presented for the surface field and back scattering measurements. The results are compared with the computed data.

ACKNOWLEDGMENTS

The authors wish to acknowledge the assistance of Miss A. Maldups and Mr. T. L. Boynton for computer programming and of Mr. H. E. Hunter and Mr. G. Antones for hand computations and technical illustrations respectively.

TABLE OF CONTENTS

CHAPTER I

INTRODUCTION

When an electromagnetic wave encounters a conducting object, a current is induced which, in turn, reradiates to produce a scattered field. At present, one of the major problems in scattering theory is to develop ways to control this scattering through modification of the shape of the object or by changing the current distribution on its surface. It has long been recognized that minor shape changes can be effective in decreasing (or even enhancing) the scattering cross section, especially at high frequencies, and with the development of absorbing coatings during the past decade, the application of these materials has become one of the most important tools for cross section reduction. However, it is desirable to investigate other means of cross section control, particularly those which are effective in the resonance region and can be used either to decrease or increase the radar cross section. One such method is surface or impedance (admittance) loading and in the last few years it has received increased attention. An additional advantage of this technique is that its application does not require alteration of the body shape or the surface characteristics as do the shaping techniques and the application of microwave absorbers, respectively.

In essence, the method is to introduce an impedance over a restricted portion of the surface using a cavity-backed slot, lumped network, or some other type of microwave circuit, and as such is only a special case of the general theory of surface impedance effects. Mathematically at least, it is similar to the application of absorbers, but in practice differs both in the localized nature of the region where the loading is employed and in the greater variety of impedances that can be achieved either to enhance or decrease the scattered field.

The idea of using loading to reduce the reradiated fields dates back to the 1920's (Meissner, 1929) when it was common practice to use lumped inductors and capacitors to detune the broadcast transmitting antenna supporting structures whenever their lengths were near resonance and interfered with the antenna radiation

patterns. The first reported application of the loading technique for scattering reduction at microwave frequencies was by Iams (1950), who used a coaxial loading to decrease the scattering from the metallic posts in a parallel plate pillbox structure. King (1956) investigated the change in the current distribution on a thin cylindrical rod when a central load is introduced, and later Hu (1958) and Ås and Schmitt (1958) showed that a high reactive impedance can appreciably affect the scattering behavior of such a rod. However, it was not until the recent study by Chen and Liepa (1964a) that the capability of loading for cross section reduction was fully demonstrated. For normal incidence on a thin cylinder of length ℓ, $0 < \ell < 2\lambda$, the induced current was calculated as a function of an arbitrary central load, and the results were confirmed by detailed current measurements on a model. The back scattering cross section was then determined, and it was found that for every value of ℓ/λ within the chosen range, a loading exists for which the cross section is zero. The real and imaginary parts of the corresponding optimum impedances were obtained as functions of ℓ/λ, and whereas the required loading was passive when $\ell < \lambda$, that for $\lambda < \ell < 2\lambda$ was primarily active.

Chen and Liepa (1964b) also considered the scattering in directions other than normal to the surface and extended the analysis to oblique incidence; later Chen (1965a) showed that by using two symmetrically placed loads on a cylinder, its cross section can be reduced with passive loading up to length 2λ. Valuable as this work is, however, its usefulness for most applications is limited by the requirement that the cylinder be thin (radius much less than the wavelength). Although Sletten et al (1964) have shown experimentally that reactive loading is still effective when the cylinder is thick, a theoretical treatment of loading of moderately thick cylinders by Chen (1965b) shows that in this case, different loading must be supplied for each circumferential mode, which would be rather complicated to achieve even at a single frequency.

A somewhat different and more abstract approach to reactive loading is to represent the body as a one-port (Harrington, 1963; Green, 1963) or n-port (Weinberg, 1963; Harrington, 1964) device, which leads to the expression of the

scattered field in terms of commonly-defined antenna parameters. However, to use this method to obtain quantitative results it is necessary to determine the transmitting and receiving properties of the body, and for an accurate treatment this again involves the solution of the boundary value problems.

The most simple example of a "thick" body is a sphere, which we shall consider here. A plane wave is assumed to impinge on a perfectly conducting sphere loaded with a narrow slot in the plane perpendicular to the direction of incidence, and in this case only the asymmetric mode is excited. The field scattered in any direction can then be expressed as a superposition of the field diffracted by an unloaded sphere and that radiated by an excited slot at the position of the load. The radiation strength and its phase are determined by the loading characteristics of the slot, and by varying the admittance Y_l of the slot, a wide degree of scattering control can be exercised. Even if attention is confined to passive loads (admittance whose real parts are non-negative), substantial increases or decreases in the scattered amplitude in almost any specified direction can be achieved by an appropriate choice of Y_l and the slot position θ_o. Numerical results are presented, primarily for the case of back scattering and surface fields, and these are compared with the measurements made using a model with an equatorial slot backed by a radial cavity of adjustable depth. The agreement is excellent.

CHAPTER II

THEORETICAL FORMULATION

2.1 Summary of Mie Series

2.1.1 Surface Fields

Consider first an unloaded perfectly conducting sphere of radius a, whose center is located at the origin of a Cartesian coordinate system (x, y, z). A linearly polarized plane electromagnetic wave is incident in the direction of the negative z-axis, and since there is no loss of generality in taking its electric vector to lie in the x-direction, we choose

$$\underline{E}^i = \hat{x} e^{ikz} \qquad \text{and} \qquad \underline{H}^i = -\hat{y} Y e^{ikz}, \tag{2.1}$$

where k is the propagation constant and Y the intrinsic admittance of free space. For convenience, the electric field has been normalized to unity and the time factor $e^{i\omega t}$ suppressed.

If we also introduce spherical polar coordinates (r, θ, ϕ) such that

$$x = r\sin\theta\cos\phi, \qquad y = r\sin\theta\sin\phi, \qquad z = r\cos\theta$$

with $\theta = 0$ representing the back scattering direction and $\theta = \pi$ the forward one, the incident field may be written in the form (Stratton, 1941)

$$\underline{E}^i = \sum_{n=1}^{\infty} i^n \frac{2n+1}{n(n+1)} \left(\underline{M}_{o1n}^{(1)} - i\underline{N}_{e1n}^{(1)} \right) \tag{2.2a}$$

$$\underline{H}^i = iY \sum_{n=1}^{\infty} i^n \frac{2n+1}{n(n+1)} \left(\underline{N}_{o1n}^{(1)} - i\underline{M}_{e1n}^{(1)} \right), \tag{2.2b}$$

where $\underline{M}^{(1)}$ and $\underline{N}^{(1)}$ are the spherical wave functions

$$\underline{M}_{\substack{e \\ o}mn}^{(1)} = \hat{\theta}\left[\frac{m}{\sin\theta} h_n(ka) P_n^m(\cos\theta) \begin{Bmatrix} -\sin m\phi \\ \cos m\phi \end{Bmatrix} \right] + \hat{\phi}\left[-h_n(kr) \frac{d}{d\theta} P_n^m(\cos\theta) \begin{Bmatrix} \cos m\phi \\ \sin m\phi \end{Bmatrix} \right]$$

$$\underset{e}{\underset{o}{\underline{N}}}^{(1)}_{mn} = \hat{r}\left[n(n+1)\frac{h_n(kr)}{kr} P_n^m(\cos\theta)\begin{Bmatrix}\cos m\phi\\ \sin m\phi\end{Bmatrix}\right] + \hat{\theta}\left[\frac{[krh_n(kr)]'}{kr}\frac{d}{d\theta} P_n^m(\cos\theta)\begin{Bmatrix}\cos m\phi\\ \sin m\phi\end{Bmatrix}\right]$$

$$+ \hat{\phi}\left[m\frac{[krh_n(kr)]'}{kr\sin\theta} P_n^m(\cos\theta)\begin{Bmatrix}-\sin m\phi\\ \cos m\phi\end{Bmatrix}\right] .$$

The prime refers to the derivative with respect to kr. From the requirement that the scattered field represent an outgoing wave at infinity, we are led to assume the scattered field to be of the form

$$\underline{E}^s = \sum_{n=1}^{\infty}\left(A_n \underline{M}_{o1n}^{(4)} + iB_n \underline{N}_{e1n}^{(4)}\right) \tag{2.3a}$$

$$\underline{H}^s = iY\sum_{n=1}^{\infty}\left(A_n \underline{N}_{o1n}^{(4)} + iB_n \underline{M}_{e1n}^{(4)}\right) , \tag{2.3b}$$

where $\underline{M}^{(4)}$ and $\underline{N}^{(4)}$ differ from $\underline{M}^{(1)}$ and $\underline{N}^{(1)}$ in having the spherical Bessel function $j_n(kr)$ replaced by the spherical Hankel function $h_n(kr)$ of the second kind. Application of the boundary condition

$$\hat{r}\times(\underline{E}^i + \underline{E}^s) = 0$$

at $r = a$ then determines A_n and B_n.

The total field is the sum of $(\underline{E}^i, \underline{H}^i)$ and $(\underline{E}^s, \underline{H}^s)$, and the only nonzero components (at the surface of the sphere) are E_r, H_θ and H_ϕ. The last two are of direct concern to us, and they can be expressed, in the notation of Kazarinoff and Senior (1962), as

$$H_\theta = Y\sin\phi\, T_1(\theta) \tag{2.4a}$$

$$H_\phi = Y\cos\phi\, T_2(\theta) , \tag{2.4b}$$

where

$$T_1(\theta) = \frac{1}{ka} \sum_{n=1}^{\infty} i^{n+1} \frac{2n+1}{n(n+1)} \left\{ \frac{1}{\zeta_n'(ka)} \frac{P_n^1(\cos\theta)}{\sin\theta} + \frac{i}{\zeta_n(ka)} \frac{\partial}{\partial\theta} P_n^1(\cos\theta) \right\} \quad (2.5a)$$

$$T_2(\theta) = \frac{1}{ka} \sum_{n=1}^{\infty} i^{n+1} \frac{2n+1}{n(n+1)} \left\{ \frac{1}{\zeta_n'(ka)} \frac{\partial}{\partial\theta} P_n^1(\cos\theta) + \frac{i}{\zeta_n(ka)} \frac{P_n^1(\cos\theta)}{\sin\theta} \right\} . \quad (2.5b)$$

Here, $\zeta_n(x) = x h_n(x)$, and the prime denotes differentiation with respect to the entire argument. $P_n^1(\cos\theta)$ is the Legendre function of degree n and order unity as defined, for example, by Stratton (1941).

2.1.2 Scattered Far Fields

In the far zone the expressions for the scattered field are obtained by replacing $h_n(kr)$ and its derivatives in equations (2.3) by the leading terms of their asymptotic expansions for large arguments. Using the notation* of Senior and Goodrich (1964), we write

$$E_\theta^s = i\cos\phi \frac{e^{-ikr}}{kr} S_1^s(\theta) \quad (2.6a)$$

$$E_\phi^s = -i\sin\phi \frac{e^{-ikr}}{kr} S_2^s(\theta) , \quad (2.6b)$$

where $S_1^s(\theta)$ and $S_2^s(\theta)$ are defined as the far field scattering amplitudes and are given by

$$S_1^s(\theta) = \sum_{n=1}^{\infty} (-1)^n \frac{2n+1}{n(n+1)} \left\{ \frac{\psi_n'(ka)}{\zeta_n'(ka)} \frac{\partial}{\partial\theta} P_n^1(\cos\theta) - \frac{\psi_n(ka)}{\zeta_n(ka)} \frac{P_n^1(\cos\theta)}{\sin\theta} \right\} \quad (2.7a)$$

$$S_2^s(\theta) = \sum_{n=1}^{\infty} (-1)^n \frac{2n+1}{n(n+1)} \left\{ \frac{\psi_n'(ka)}{\zeta_n'(ka)} \frac{P_n^1(\cos\theta)}{\sin\theta} - \frac{\psi_n(ka)}{\zeta_n(ka)} \frac{\partial}{\partial\theta} P_n^1(\cos\theta) \right\} \quad (2.7b)$$

* Note the change in time convention.

with $\psi_n(x) = x j_n(x)$. In the back ($\theta = 0$) and forward ($\theta = \pi$) directions

$$\left[\frac{P_n^1(\cos\theta)}{\sin\theta}\right]_{\theta=0} = \left[\frac{\partial}{\partial\theta} P_n^1(\cos\theta)\right]_{\theta=0} = \frac{n(n+1)}{2} \tag{2.8a}$$

$$\left[\frac{P_n^1(\cos\theta)}{\sin\theta}\right]_{\theta=\pi} = -\left[\frac{\partial}{\partial\theta} P_n^1(\cos\theta)\right]_{\theta=\pi} = (-1)^{n+1}\frac{n(n+1)}{2} \tag{2.8b}$$

respectively. Hence, from equations (2.7)

$$S_1^s(0) = S_2^s(0) \tag{2.9a}$$

$$S_1^s(\pi) = -S_2^s(\pi) \tag{2.9b}$$

implying that for forward and back scattering the field has the same linear polarization as the incident field. In other directions, however, the field is elliptically polarized.

2.2 Radiation Problem

We now consider a separate but related problem of a perfectly conducting sphere with a narrow slot symmetrically placed with respect to the z-axis (and hence, with respect to the incident field direction in the problem just discussed). The slot occupies the region $\theta_o - \frac{\delta}{2} \leqslant \theta \leqslant \theta_o + \frac{\delta}{2}$ (see Fig. 2-1) and its angular width δ is such that $ka\,\delta \ll 1$. Within the gap, the tangential electric field is specified, and in view of our intention to regard the slot as a passive or semi-active* device excited by the incident field, the excitation must be chosen in accordance with the surface field behavior shown in equation (2.4b). It is therefore assumed that for $|\theta - \theta_o| < \delta/2$

$$E_\theta = -\frac{1}{\delta a} v\cos\phi \tag{2.10a}$$

$$E_\phi = 0\ . \tag{2.10b}$$

* By a semi-active device it is implied here that the real part of the loading admittance (or impedance) is negative.

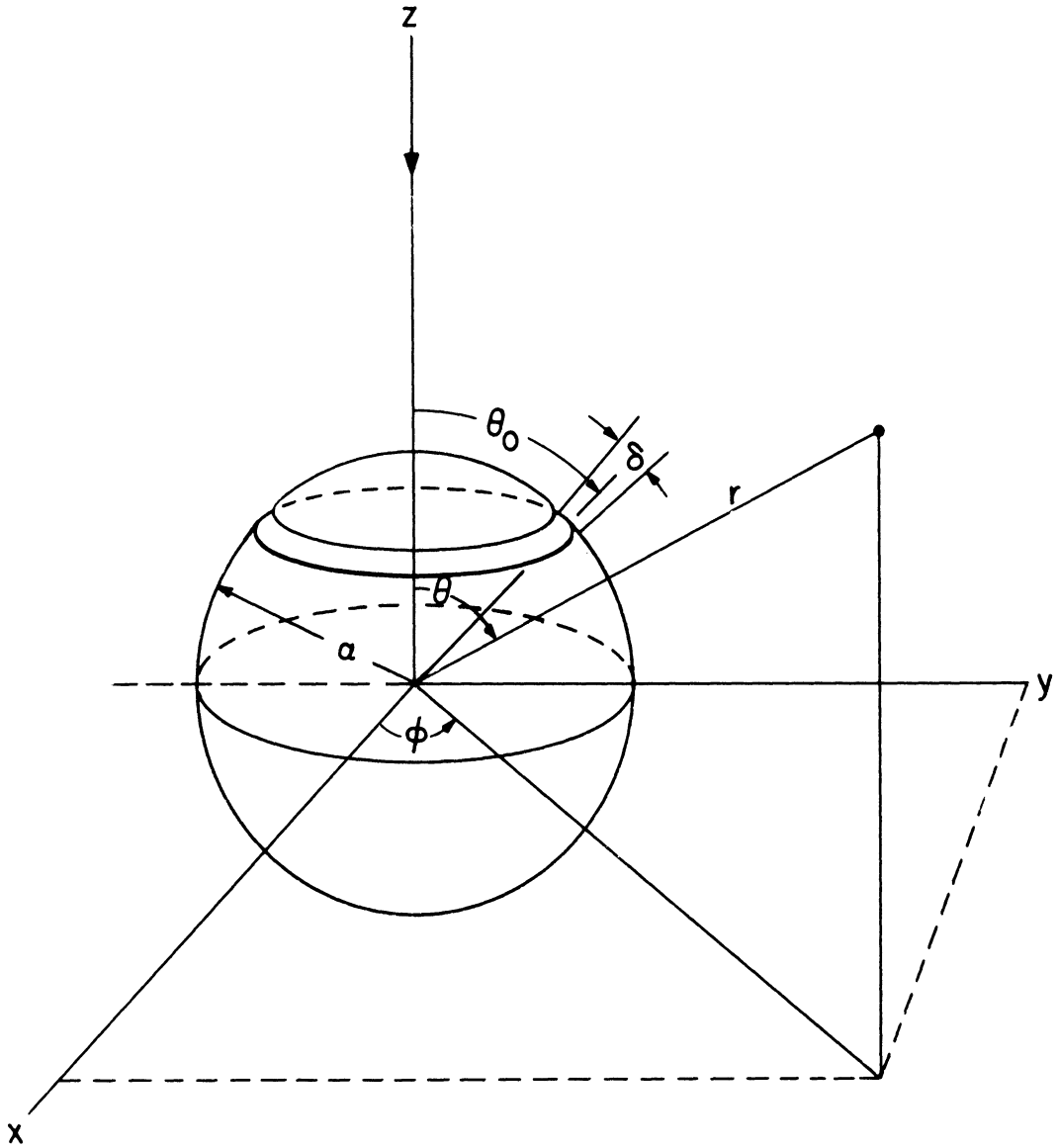

FIG. 2-1: SPHERE GEOMETRY.

This corresponds to a constant (but asymmetrical) voltage $v\cos\phi$ applied across the gap. Over the rest of the sphere, E_θ and E_ϕ are both zero, as is appropriate for a perfectly conducting surface.

To calculate the field $(\underline{E}^r, \underline{H}^r)$ radiated by the slot, we again postulate a field of the form shown in equations (2.3), but with A_n and B_n replaced by new constants C_n and D_n respectively, so that

$$\underline{E}^r = \sum_{n=1}^{\infty} \left(C_n \underline{M}_{o1n}^{(4)} + iD_n \underline{N}_{e1n}^{(4)} \right) \tag{2.11a}$$

$$\underline{H}^r = iY \sum_{n=1}^{\infty} \left(C_n \underline{N}_{o1n}^{(4)} + iD_n \underline{M}_{e1n}^{(4)} \right) . \tag{2.11b}$$

When these are substituted into the boundary conditions at $r = a$, we obtain

$$\sum_{n=1}^{\infty} \left\{ C_n \zeta_n(ka) \frac{P_n^1(\cos\theta)}{\sin\theta} + iD_n \zeta_n'(ka) \frac{\partial}{\partial\theta} P_n^1(\cos\theta) \right\} = -\frac{kv}{\delta} , \quad |\theta - \theta_o| < \frac{\delta}{2}$$
$$= 0 , \quad \text{otherwise} \tag{2.12a}$$

from the θ component, and

$$\sum_{n=1}^{\infty} \left\{ C_n \zeta_n(ka) \frac{\partial}{\partial\theta} P_n^1(\cos\theta) + iD_n \zeta_n'(ka) \frac{P_n^1(\cos\theta)}{\sin\theta} \right\} = 0 , \quad \text{all } \theta . \tag{2.12b}$$

from the ϕ component. Moreover, from Bailin and Silver (1956)

$$\int_0^{\pi} \left\{ P_n^1(\cos\theta) \frac{\partial}{\partial\theta} P_m^1(\cos\theta) + P_m^1(\cos\theta) \frac{\partial}{\partial\theta} P_n^1(\cos\theta) \right\} d\theta = 0$$

and

$$\int_0^{\pi} \left\{ \frac{\partial}{\partial\theta} P_n^1(\cos\theta) \frac{\partial}{\partial\theta} P_m^1(\cos\theta) + \frac{1}{\sin^2\theta} P_n^1(\cos\theta) P_m^1(\cos\theta) \right\} \sin\theta \, d\theta = \Lambda_{nm} ,$$

where

$$\Lambda_{nm} = \begin{cases} 0 & n \neq m \\ \dfrac{2n^2(n+1)^2}{2n+1} & n = m \end{cases} .$$

Hence, by application of these relations to (2.12)

$$C_n = -\frac{kv}{\zeta_n(ka)} \frac{2n+1}{2n^2(n+1)^2} \frac{1}{\delta} \int_{\theta_o - \frac{\delta}{2}}^{\theta_o + \frac{\delta}{2}} P_n^1(\cos\theta) d\theta$$

$$= \frac{kv}{\zeta_n(ka)} \frac{2n+1}{2n^2(n+1)^2} \frac{P_n(+) - P_n(-)}{\delta} \qquad (2.13a)$$

and

$$D_n = i \frac{kv}{\zeta_n'(ka)} \frac{2n+1}{2n^2(n+1)^2} \frac{1}{\delta} \int_{\theta_o - \frac{\delta}{2}}^{\theta_o + \frac{\delta}{2}} \sin\theta \frac{\partial}{\partial\theta} P_n^1(\cos\theta) d\theta$$

$$\simeq i \frac{kv \sin\theta_o}{\zeta_n'(ka)} \frac{2n+1}{2n^2(n+1)^2} \frac{P_n^1(+) - P_n^1(-)}{\delta} , \qquad (2.13b)$$

where, for brevity, we have written

$$P_n^m(\pm) = P_n^m \left(\cos\left\{ \theta_o \pm \frac{\delta}{2} \right\} \right) .$$

In the evaluation of D_n it was assumed that the variation of $\sin\theta$ over the slot can be neglected and, as a consequence, the position of the slot is now limited by the condition

$$\epsilon \lesssim \theta_o \lesssim \pi - \epsilon$$

with $\epsilon \gg \delta$.

The expressions for the radiated field follow from equations (2.11) upon inserting the above formulae for C_n and D_n, and $\underline{M}^{(4)}$ and $\underline{N}^{(4)}$. The equations are rather lengthy, by straightforward. Thus, we proceed directly to formulas for the surface fields and the far fields.

2.2.1 Surface Fields

On the surface, $r = a$, only the magnetic field is of direct concern to us, and for this we write, analogously to equations (2.4),

$$H_\theta^r = vY \sin\phi \, T_1^r(\theta, \theta_o) \tag{2.14a}$$

$$H_\phi^r = vY \cos\phi \, T_2^r(\theta, \theta_o) \quad , \tag{2.14b}$$

where

$$T_1^r(\theta, \theta_o) = \frac{i}{2a} \sum_{n=1}^{\infty} \frac{2n+1}{n^2(n+1)^2} \left\{ \frac{\zeta_n(ka)}{\zeta_n'(ka)} \frac{\sin\theta_o}{\sin\theta} \left(\frac{P_n^1(+) - P_n^1(-)}{\delta} \right) P_n^1(\cos\theta) \right.$$
$$\left. + \frac{\zeta_n'(ka)}{\zeta_n(ka)} \left(\frac{P_n(+) - P_n(-)}{\delta} \right) \frac{\partial}{\partial\theta} P_n^1(\cos\theta) \right\} \tag{2.15a}$$

$$T_2^r(\theta, \theta_o) = \frac{i}{2a} \sum_{n=1}^{\infty} \frac{2n+1}{n^2(n+1)^2} \left\{ \frac{\zeta_n(ka)}{\zeta_n'(ka)} \sin\theta_o \left(\frac{P_n^1(+) - P_n^1(-)}{\delta} \right) \frac{\partial}{\partial\theta} P_n^1(\cos\theta) \right.$$
$$\left. + \frac{\zeta_n'(ka)}{\zeta_n(ka)} \frac{1}{\sin\theta} \left(\frac{P_n(+) - P_n(-)}{\delta} \right) P_n^1(\cos\theta) \right\} . \tag{2.15b}$$

The convergence of the above series is determined by the gap width δ. For non-zero values of δ the series are convergent, but rather slowly, and the number of terms that must be retained for numerical evaluation is in fact inversely proportional to δ. In the limit as $\delta \to 0$ the series for $T_1^r(\theta, \theta_o)$ actually diverges everywhere, but for $T_2^r(\theta, \theta_o)$ diverges only when $\theta \to \theta_o$. More discussion on the convergence and numerical computations of these series is given in Section 3.1.

2.2.2. Radiated Far Fields

In the far zone, on the other hand, the expressions for the radiated field components are convergent even for $\delta = 0$, corresponding to an infinitesimal gap across which a voltage $v\cos\phi$ is applied. We obtain the expressions from equation (2.11a) by replacing $h_n(kr)$ and its derivatives by the leading terms of their asymptotic expansion for large kr in the definitions for $\underline{M}^{(4)}$ and $\underline{N}^{(4)}$, and by replacing

$$\frac{P_n(+) - P_n(-)}{\delta} \quad \text{and} \quad \frac{P_n^1(+) - P_n^1(-)}{\delta}$$

in the expressions for C_n and D_n by the derivative forms

$$-P_n^1(\cos\theta_o) \quad \text{and} \quad \frac{\partial}{\partial\theta_o} P_n^1(\cos\theta_o)$$

respectively. Then, analogously to equations (2.6), we write

$$E_\theta^r = iv\cos\phi \frac{e^{-ikr}}{kr} S_1^r(\theta,\theta_o) \tag{2.16a}$$

$$E_\phi^r = -iv\sin\phi \frac{e^{-ikr}}{kr} S_2^r(\theta,\theta_o), \tag{2.16b}$$

where the radiated far field amplitudes are given by

$$S_1^r(\theta,\theta_o) = \frac{k}{2}\sin\theta_o \sum_{n=1}^{\infty} i^{n+1} \frac{2n+1}{n^2(n+1)^2} \left\{ \frac{1}{\zeta_n'(ka)} \frac{\partial}{\partial\theta} P_n^1(\cos\theta) \frac{\partial}{\partial\theta_o} P_n^1(\cos\theta_o) + \frac{i}{\zeta_n(ka)} \frac{P_n^1(\cos\theta)}{\sin\theta} \frac{P_n^1(\cos\theta_o)}{\sin\theta_o} \right\} \tag{2.17a}$$

$$S_2^r(\theta,\theta_o) = \frac{k}{2}\sin\theta_o \sum_{n=1}^{\infty} i^{n+1} \frac{2n+1}{n^2(n+1)^2} \left\{ \frac{1}{\zeta_n'(ka)} \frac{P_n^1(\cos\theta)}{\sin\theta} \frac{\partial}{\partial\theta_o} P_n^1(\cos\theta_o) + \frac{i}{\zeta_n(ka)} \frac{\partial}{\partial\theta} P_n^1(\cos\theta) \frac{P_n^1(\cos\theta_o)}{\sin\theta_o} \right\}. \tag{2.17b}$$

In the back and forward directions

$$S_1^r(0,\theta_o) = S_2^r(0,\theta_o) \tag{2.18a}$$

$$S_1^r(\pi,\theta_o) = -S_2^r(\pi,\theta_o). \tag{2.18b}$$

2.3 Radiation Admittance of Asymmetrically Excited Slot

It is customary to define the admittance of a slot as the ratio of the current flowing away from the slot to the gap voltage, where the latter is the line integral of the electric field across the gap. This definition, however, is unique only for TEM waves, and for other modes the admittance is usually defined to best suit the particular situation. In this problem of an asymmetrically excited slot, the total instantaneous current is in fact, zero, and we are led to introduce the concept of admittance density, defined as admittance per unit length of the slot.

We define the admittance density as twice the ratio of the complex power flow density to the modulus squared of the applied voltage. The complex power radiated per unit length of the slot is

$$w = \int_{\theta_o - \frac{\delta}{2}}^{\theta_o + \frac{\delta}{2}} \frac{1}{2}(\underline{E}^r \times \underline{\tilde{H}}^r) \cdot \hat{r}\, a\, d\theta$$

$$= -\frac{1}{2}\frac{v\cos\phi}{\delta} \int_{\theta_o - \frac{\delta}{2}}^{\theta_o + \frac{\delta}{2}} \tilde{H}_\phi^r\, d\theta ,$$

where the tilde denotes the complex conjugate, and the radiation admittance density is therefore

$$y_r = \frac{2\tilde{w}}{v\cos\phi\,\widetilde{v\cos\phi}}$$

$$= -\frac{1}{\delta\, v\cos\phi}\int_{\theta_o-\frac{\delta}{2}}^{\theta_o+\frac{\delta}{2}} H_\phi^r\, d\theta$$

$$= -\frac{Y}{\delta}\int_{\theta_o-\frac{\delta}{2}}^{\theta_o+\frac{\delta}{2}} T_2^r(\theta,\theta_o)\, d\theta\ .$$

The (total) radiation admittance is

$$Y_r = \int_0^{2\pi} y_r\, a\sin\theta_o\, d\phi \tag{2.19a}$$

and since y_r is independent of ϕ, we write

$$Y_r = -2\pi\sin\theta_o\, Y\frac{a}{\delta}\int_{\theta_o-\frac{\delta}{2}}^{\theta_o+\frac{\delta}{2}} T_2^r(\theta,\theta_o)d\theta\ . \tag{2.19b}$$

Using the expression for $T_2^r(\theta,\theta_o)$ given in equation (2.15b), together with the evaluation of the Legendre function integrals used in the determination of C_n and D_n, we get

$$Y_r = i\,Y\pi\sin^2\theta_o \sum_{n=1}^{\infty}\frac{2n+1}{n^2(n+1)^2}\left\{\frac{\zeta_n'(ka)}{\zeta_n(ka)}\left(\frac{P_n(+)-P_n(-)}{\delta\sin\theta_o}\right)^2 - \frac{\zeta_n(ka)}{\zeta_n'(ka)}\left(\frac{P_n^1(+)-P_n^1(-)}{\delta}\right)^2\right\}. \tag{2.20}$$

An equally acceptable definition for admittance density is the ratio of the current density flowing away from the slot to the applied voltage at a point specified by the azimuthal variable ϕ. In this case the resultant radiation admittance is of a different form, but, as we shall next show, it is not as well suited for our purposes.

The surface current density $\underline{J}$ is directly related to the tangential magnetic field by

$$\underline{J} = \hat{r} \times \underline{H} \tag{2.21a}$$

so that on the surface of a sphere

$$J_\theta = -H_\phi \qquad \text{and} \qquad J_\phi = H_\theta \,. \tag{2.21b}$$

The radiation admittance density is then

$$y'_r = \left. \frac{J^r_\theta}{v \cos\phi} \right|_{\theta=\theta'}$$

$$= -Y T^r_2(\theta', \theta_o)$$

and the (total) radiation admittance

$$Y'_r = \int_0^{2\pi} y_r \, a \sin\theta_o \, d\phi$$

$$= -2\pi Y \sin\theta_o \, a T^r_2(\theta', \theta_o) \tag{2.22}$$

The θ' denotes the edge of the slot and is given by either $\theta' = \theta_o + \frac{\delta}{2}$ or $\theta' = \theta_o - \frac{\delta}{2}$. Except for $\theta_o = \pi/2$ or when the gap width $\delta \to 0$, the two values give different results for Y_r, and although the numerical effect may be insignificant under most practical circumstances, it is undesirable that an expression should have that degree of arbitrariness. Another difference between this result and the one previously derived is that for Y_r the surface field component $T^r_2(\theta, \theta_o)$ is integrated across the slot (equation 2.19b), and as a consequence the convergence of the infinite series is accelerated by a factor $O(1/n)$.

2.4 Complete Problem

The final problem to be considered is the combination of the scattering and radiation problems in which the plane wave given in equation (2.1) is incident on

the slotted sphere. It is assumed that the same voltage $v\cos\phi$ is excited across the gap, and the expressions for the resulting total fields can be found by superposition of those associated with each individual problem. We therefore have

$$\underline{E} = \underline{E}^i + \underline{E}^s + \underline{E}^r \tag{2.23a}$$

and

$$\underline{H} = \underline{H}^i + \underline{H}^s + \underline{H}^r \ , \tag{2.23b}$$

where $(\underline{E}^i, \underline{H}^i)$, $(\underline{E}^s, \underline{H}^s)$ and $(\underline{E}^r, \underline{H}^r)$ are as defined before. In particular, in the far zone the components of the total scattered electric field are written, similarly to equations (2.6), as

$$E_\theta = i\cos\phi \frac{e^{-ikr}}{kr} S_1(\theta) \tag{2.24a}$$

$$E_\phi = -i\sin\phi \frac{e^{-ikr}}{kr} S_2(\theta) \ , \tag{2.24b}$$

where the total scattering amplitudes are now given by

$$S_1(\theta) = S_1^s(\theta) + v S_1^r(\theta, \theta_o) \tag{2.25a}$$

$$S_2(\theta) = S_2^s(\theta) + v S_2^r(\theta, \theta_o) \ . \tag{2.25b}$$

The expressions for $S_1^r(\theta, \theta_o)$ and $S_2^r(\theta, \theta_o)$ are, of course, independent of v, and if this voltage is excited across the slot by the currents induced by the incident field, the voltage can be related to the loading admittance of the slot.

To calculate this voltage, we apply the same technique that was used for determining Y_r. As before, the complex power entering the slot per unit length is obtained by integrating the Poynting vector over the slot. Hence,

$$w = -\frac{1}{2} \int_{\theta_o - \frac{\delta}{2}}^{\theta_o + \frac{\delta}{2}} (\underline{E} \times \underline{\tilde{H}}) \cdot \hat{r}\, a\, d\theta \ ,$$

where $(\underline{E}, \underline{H})$ are given by (2.23). But since

$$\underline{E} = -\frac{v\cos\phi}{\delta a}\hat{\theta} \quad ,$$

the slot admittance density is simply

$$y_\ell = \frac{1}{\delta v\cos\phi}\int_{\theta_o-\frac{\delta}{2}}^{\theta_o+\frac{\delta}{2}} \left(H_\phi^i + H_\phi^s + H_\phi^r\right) d\theta$$

which, by using equations (2.19), (2.17b), and (2.5b), can be written as

$$y_\ell = -y_r + \frac{Y}{\delta v}\int_{\theta_o-\frac{\delta}{2}}^{\theta_o+\frac{\delta}{2}} T_2(\theta)\, d\theta \quad .$$

For δ sufficiently small, the variation of $T_2(\theta)$ across the slot can be neglected, giving

$$y_\ell = -y_r + \frac{Y}{v}\, T_2(\theta_o)$$

and the (total) loading admittance of the slot is therefore

$$Y_\ell = -Y_r + \frac{Y}{v}\, 2\pi a \sin\theta_o T_2(\theta_o) \quad , \tag{2.26}$$

where $T_2(\theta)$ and Y_r are given in equations (2.5b) and (2.20), respectively. Solving for v from equation (2.26),

$$v = \frac{Y}{Y_\ell + Y_r}\, 2\pi a \sin\theta_o T_2(\theta_o) \tag{2.27}$$

and, when substituted in (2.25), the component scattering amplitudes for the loaded sphere are

$$S_1(\theta) = S_1^s(\theta) + \frac{Y}{Y_\ell + Y_r}\, 2\pi \sin\theta_o T_2(\theta_o)\, a S_1^r(\theta, \theta_o) \tag{2.28a}$$

$$S_2(\theta) = S_2^s(\theta) + \frac{Y}{Y_l + Y_r} 2\pi \sin\theta_o T_2(\theta_o) a S_2^r(\theta, \theta_o). \tag{2.28b}$$

Each scattering amplitude is a sum of the scattering amplitude for an unloaded sphere and the modification term accounting for the presence of the slot. This term contains radiation and loading admittances, a term for the value of the surface current at the position of the slot when the slot is not present, and the radiation pattern from the slotted sphere when it is excited by an asymmetric (unit) voltage across the gap.

In terms of these scattering functions, the bistatic radar cross section is

$$\sigma(\theta, \phi) = \sigma_\theta(\theta, \phi) + \sigma_\phi(\theta, \phi) , \tag{2.29}$$

where the component cross sections are given by

$$\sigma_\theta(\theta, \phi) = \frac{\lambda^2}{\pi} |S_1(\theta)|^2 \cos^2\phi$$

$$\sigma_\phi(\theta, \phi) = \frac{\lambda^2}{\pi} |S_2(\theta)|^2 \sin^2\phi .$$

In particular, for back scattering and forward scattering directions

$$\sigma(0) = \frac{\lambda^2}{\pi} |S_1(0)|^2 \tag{2.30a}$$

$$= \frac{\lambda^2}{\pi} |S_2(0)|^2 \tag{2.30b}$$

and

$$\sigma(\pi) = \frac{\lambda^2}{\pi} |S_1(\pi)|^2 \tag{2.31a}$$

$$= \frac{\lambda^2}{\pi} |S_2(\pi)|^2 \tag{2.31b}$$

respectively.

To make the scattering amplitude $S_1(\theta)$ zero in the direction $\theta = \theta'$ the required loading is

$$\left[Y_\ell\right]_0 = -Y_r - Y 2\pi \sin\theta_o T_2(\theta_o) \frac{a S_1^r(\theta', \theta_o)}{S_1^s(\theta')} . \tag{2.32a}$$

Similarly, to make $S_2(\theta)$ zero in the same direction, the required loading is

$$\left[Y_\ell\right]_0 = -Y_r - Y 2\pi \sin\theta_o T_2(\theta_o) \frac{a S_2^r(\theta', \theta_o)}{S_2^s(\theta')} \tag{2.32b}$$

and unless

$$\frac{a S_1^r(\theta', \theta_o)}{S_1^s(\theta')} = \frac{a S_2^r(\theta', \theta_o)}{S_2^s(\theta')} \tag{2.33}$$

the scattering cross section cannot be reduced to zero with a single slot loading of the form discussed here. This does not, however, rule out the possibility of significant reduction in scattering by a suitable choice of Y_ℓ. Moreover, in many cases of bistatic scattering only $S_1(\theta)$ or $S_2(\theta)$ is of interest, and in such a case zero scattering can be achieved.

The obvious exceptions to the above are back and forward scattering, in which cases equation (2.33) is satisfied. (See equations 2.9 and 2.18). Furthermore,

$$a S_1^r(0, \theta_o) = \frac{(ka)^2}{4} \sin\theta_o T_2(\theta_o) \tag{2.34a}$$

and hence the loading for zero $S_1(0)$ and $S_2(0)$ is

$$\left[Y_\ell\right]_0 = -Y_r - Y \frac{\pi}{2} \left\{ka \sin\theta_o T_2(\theta_o)\right\}^2 \left\{S_1^s(0)\right\}^{-1} . \tag{2.34b}$$

Similarly, in the forward direction we get

$$a S_1^r(\pi, \theta_o) = \frac{(ka)^2}{4} \sin\theta_o T_2(\pi - \theta_o) \tag{2.35a}$$

and consequently for zero $S_1(\pi)$ and $S_2(\pi)$

$$\left[Y_\ell\right]_0 = -Y_r - Y\frac{\pi}{2}(ka\sin\theta_o)^2 T_2(\theta_o)T_2(\pi - \theta_o)\left\{S_1^s(\pi)\right\}^{-1}. \tag{2.35b}$$

The fact that for a passive scatterer, zero scattering in the forward direction implies zero total scattering and absorption indicates that the above loading will have a negative real part, corresponding to an active slot for all values of ka and θ_o.

The expressions for the total surface field components can be obtained directly from the far field expressions. Since the technique used in the derivation of the far fields is quite general, the components of the total surface fields are obtained by replacing the far field formulae in (2.28) by the corresponding surface field expressions. Thus,

$$T_1^t(\theta) = T_1(\theta) + \frac{Y}{Y_\ell + Y_r} 2\pi \sin\theta_o T_2(\theta_o) a T_1^r(\theta, \theta_o) \tag{2.36a}$$

$$T_2^t(\theta) = T_2(\theta) + \frac{Y}{Y_\ell + Y_r} 2\pi \sin\theta_o T_2(\theta_o) a T_2^r(\theta, \theta_o) \tag{2.36b}$$

and, analogously to (2.4), the total surface field components are given by

$$H_\theta = Y \sin\phi\, T_1^t(\theta) \tag{2.37a}$$

$$H_\phi = Y \cos\phi\, T_2^t(\theta) \,. \tag{2.37b}$$

2.5 Low Frequency Approximation

The characteristics of the above derived formulae can, in general, be determined only by numerical computation of the functions involved. However, an exception is the case of small ka. Taking the leading term of the series expansions of spherical Bessel functions about ka = 0 (see, for example, Stratton, 1941),

$$j_n(ka) = 2^n (ka)^n \sum_{m=0}^{\infty} \frac{(-1)^m (n+m)!}{m!(2n+2m+1)!} (ka)^{2m}$$

$$y_n(ka) = \frac{-1}{2^n (ka)^{n+1}} \sum_{m=0}^{\infty} \frac{\Gamma(2n-2m+1)}{m!(n-m+1)} (ka)^{2m} \quad ,$$

we get

$$j_n(ka) \sim 2^n (ka)^n \frac{n!}{(2n+1)!} \quad , \qquad ka \ll 1$$

$$y_n(ka) \sim \frac{-1}{2^n (ka)^{n+1}} \frac{(2n)!}{n!} \quad , \qquad ka \ll 1$$

and when these are substituted into equations (2.7), the scattered far field amplitudes for an unloaded sphere reduce to

$$S_1^s(\theta) \sim -i \frac{(ka)^3}{2}(2\cos\theta + 1) + \frac{(ka)^6}{6}(1 - 4\cos\theta) \tag{2.38a}$$

$$S_2^s(\theta) \sim -i \frac{(ka)^3}{2}(2 + \cos\theta) + \frac{(ka)^6}{6}(\cos\theta - 4) \quad , \tag{2.38b}$$

and the radiated far field amplitudes, from equations (2.17), reduce to

$$a S_1^r(\theta, \theta_o) \sim -\frac{3}{8}(ka)^2 \sin\theta_o (1 + ika \cos\theta \cos\theta_o) \tag{2.39a}$$

$$a S_2^r(\theta, \theta_o) \sim -\frac{3}{8}(ka)^2 \sin\theta_o (\cos\theta + ika \cos\theta_o) \, . \tag{2.39b}$$

Similarly, for the surface field component $T_2(\theta)$, we obtain from equation (2.5b)

$$T_2(\theta) \sim -\frac{3}{2} - ika\left(\frac{3}{2}\cos\theta + \frac{5}{12}\frac{\sin 2\theta}{\sin\theta}\right) \quad , \tag{2.40}$$

and for the real part of the radiation admittance we obtain from equation (2.20)

$$\mathrm{Re}\frac{Y_r}{Y} \sim \frac{3}{4}\pi \sin^2\theta (ka)^2 .$$

Its counterpart, $\text{Im}\,\frac{Y_r}{Y}$, is not so easily expressible in closed form, however, and since there is no need for it in our investigation, no attempt is made to reduce it.

The scattering amplitudes for a loaded sphere are obtained by substituting the above small argument expansions into equations (2.28) and, in particular, with a slot at $\theta_o = 90^o$, their magnitudes are

$$|S_1(\theta)|^2 \sim \frac{(ka)^4}{4} \frac{1}{x^2+y^2} \left\{A_1 \cos^2\theta + A_2 \cos\theta + A_3\right\} \qquad (2.41a)$$

$$|S_2(\theta)|^2 \sim \frac{(ka)^4}{4} \frac{1}{x^2+y^2} \left\{A_3 \cos^2\theta + A_2 \cos\theta + A_1\right\} \quad , \qquad (2.41b)$$

where

$$A_1 = 4(ka)^2x^2 + 4(ka)^2y^2$$

$$A_2 = 4(ka)^2x^2 + 4(ka)^2y^2 + 9\pi(ka)y$$

$$A_3 = (ka)^2x^2 + (ka)^2y^2 + \frac{9}{2}\pi(ka)y + \frac{81}{16}\pi^2$$

with $x = \text{Re}\,\frac{1}{Y}(Y_\ell + Y_r)$ and $y = \text{Im}\,\frac{1}{Y}(Y_\ell + Y_r)$.

The loading needed to make either $|S_1(\theta')|^2$ or $|S_2(\theta')|^2$ zero in the direction $\theta = \theta'$ follows directly from equations (2.32). For $\theta = 0$, the two are identical, and if $\theta_o = 90^o$, the loading is

$$\frac{Y_\ell}{Y} + \frac{Y_r}{Y} \sim -i\frac{3}{4}\pi\frac{1}{ka} \quad .$$

When substituted in equations (2.41) this gives

$$|S_1(\theta)|^2 = |S_2(\theta)|^2$$

$$= (ka)^6(1-\cos\theta)^2 \quad .$$

Since the moduli of the scattering components are equal, the scattering is independent of ϕ, which, for a vector problem, is rather surprising. However, a further examination of equations (2.38) and (2.39) reveals that this is a special case and occurs when the imaginary terms in (2.39) disappear, i.e. when $\theta_o = 90^o$. In other words, the radiation field is a "mirror image" in ϕ of the scattered field and when the two are combined, the result is independent of ϕ.

For presentation purposes it is convenient to write the results in terms of component cross sections (equation 2.29) and then normalize the resulting values to the back scattering cross section σ_o of an unloaded sphere. Thus, for an unloaded sphere,

$$\frac{\sigma_o(\theta,\phi)}{\sigma_o} \sim \frac{1}{9}\left\{(2\cos\theta+1)^2\cos^2\phi+(2\cos\theta+1)^2\sin^2\phi\right\} \qquad (2.42a)$$

and, for the sphere loaded for zero back scattering,

$$\frac{\sigma(\theta,\phi)}{\sigma_o} \sim \frac{4}{9}(1-\cos\theta)^2 \ . \qquad (2.42b)$$

The results for $\phi = 0$ and $\phi = \pi/2$ are plotted in Figs. 2-2 and 2-3 respectively.

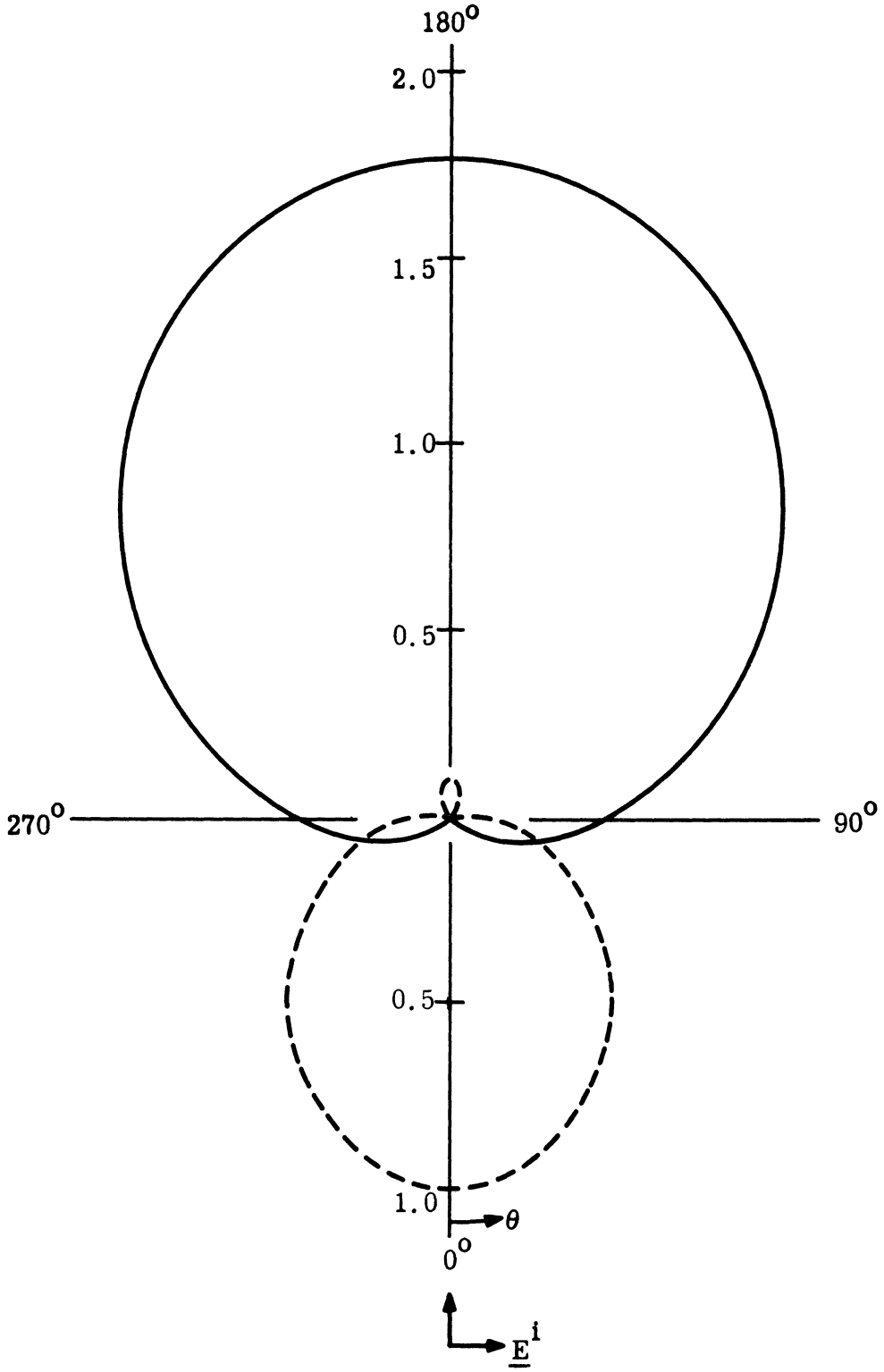

FIG. 2-2: NORMALIZED SCATTERING PATTERNS FOR LOADED (——) AND UNLOADED (– – –) SPHERES IN E-PLANE ($\phi = 0$) WITH $\theta_o = 90^o$ AS $ka \rightarrow 0$.

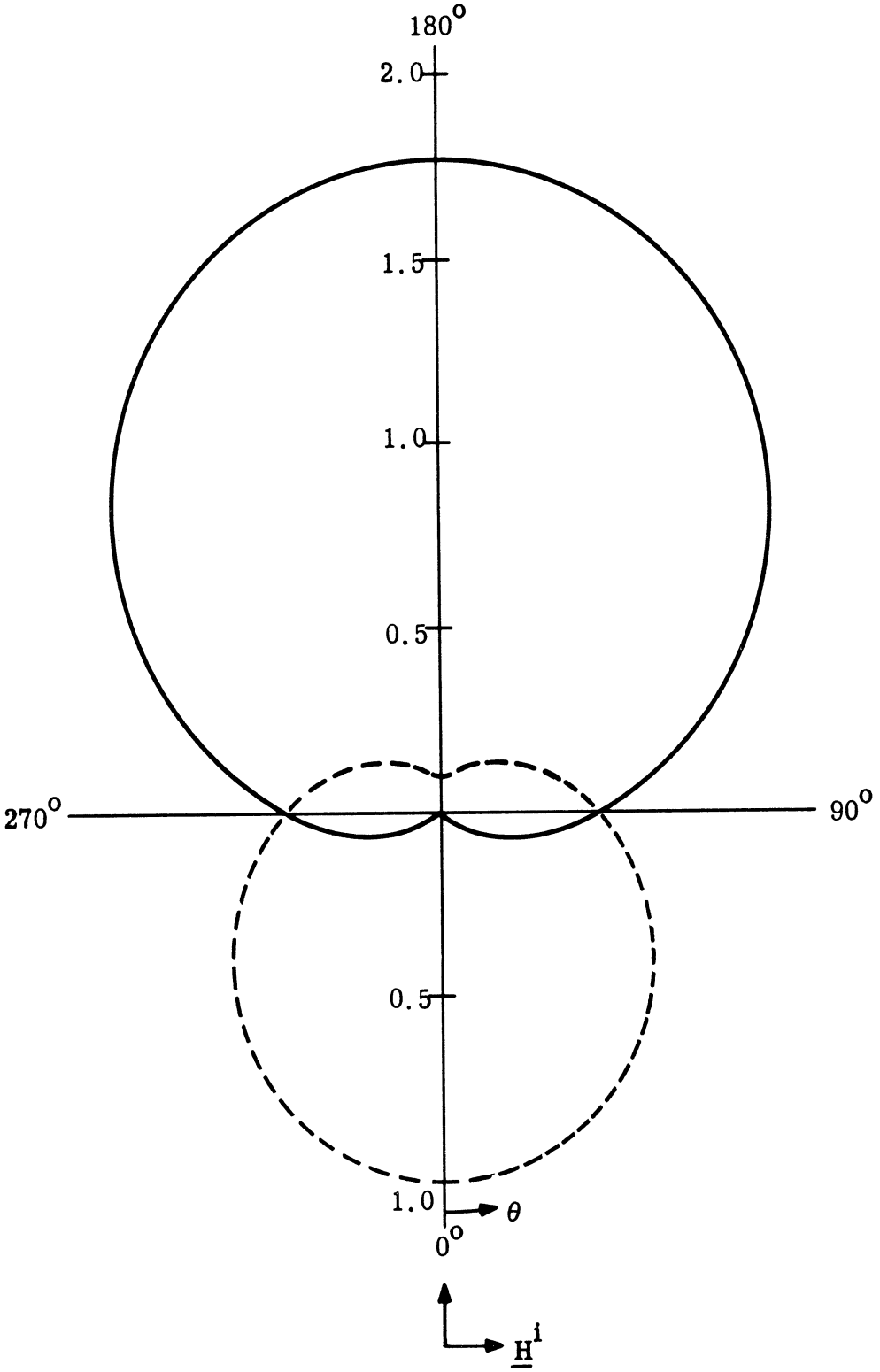

FIG. 2-3: NORMALIZED SCATTERING PATTERNS FOR LOADED (——) AND UNLOADED (– – –) SPHERES IN H-PLANE ($\phi = \pi/2$) WITH $\theta_o = 90^o$ AS $ka \to 0$.

CHAPTER III

NUMERICAL COMPUTATIONS

3.1 Computation of Pertinent Functions

The expressions of all pertinent functions derived in Chapter II were programmed for computation on the University of Michigan IBM 7090 computer. These included the surface and far field expressions (equations 2.5 and 2.7 respectively) for a solid sphere, radiated surface and far fields (equations 2.15 and 2.17 respectively) due to radiation from an excited slot, and the radiation admittance (equation 2.20) of this slot. Except in the cases of the radiated surface fields, $T_1^r(\theta,\theta_o)$ and $T_2^r(\theta,\theta_o)$, and the radiation admittance Y_r, the computations were straightforward. The infinite series were approximated by the same, but truncated series and the number N of terms retained in any given series was determined essentially by the machine. A criterion was set to terminate the series whenever the magnitudes of successive terms fell below 10^{-7}. On the average, only about 4 terms were required for $ka = 0.1$, but as many as 30 for $ka = 10.0$.

The spherical Hankel and Legendre functions are contained in all the series and their evaluation was carried out using external subroutines. The function $\zeta'(ka)$ was written in the form

$$\zeta'(x) = \frac{1}{2n+1}\left\{ nh_{n-1}(x) - (n+1)h_{n+1}(x) \right\} + h_n(x),$$

and $h_n(x)$ was itself broken up according to

$$h_n(x) = j_n(x) - iy_n(x).$$

The spherical Bessel functions of the first kind, $j_n(x)$, were evaluated by numerical integration of the finite integral expression

$$j_n(x) = \frac{(x/2)^n}{n!} \int_0^{\pi/2} \cos(x\sin\phi)\cos^{2n+1}\phi\, d\phi$$

(see, for example, Adams and Hippisley, 1947). The range of integration was

subdivided into $40+2n$ increments, and judging from spot checks, the resulting evaluations were accurate to six significant figures for $n \leqslant 20$ and to five for $n \leqslant 44$. The number $n = 44$ was the largest value, consistent with machine capacity, for which $j_n(x)$ could be evaluated. The spherical Bessel functions of the second kind were evaluated from the finite series expansion

$$y_n(x) = \frac{(-1)^{n+1}}{x} \left\{ \cos\left(x+\frac{n\pi}{2}\right) \sum_{r=0}^{\leqslant n/2} \frac{(-1)^r (n+2r)!}{(2r)!\,(n-2r)!\,(2x)^{2r}} - \sin\left(x+\frac{n\pi}{2}\right) \sum_{r=0}^{\leqslant \frac{n-1}{2}} \frac{(-1)^r (n+2r+1)!}{(2r+1)!\,(n-2r-1)!\,(2x)^{2r+1}} \right\}$$

(Watson, 1948), giving seven digit accuracy for $n \leqslant 20$ and better than five for $n \leqslant 44$.

The Legendre functions were computed from the recurrence relations

$$P_{n+1}(\cos\theta) = \frac{2n+1}{n+1} \cos\theta\, P_n(\cos\theta) - \frac{n}{n+1} P_{n-1}(\cos\theta)$$

and

$$P^1_{n+1}(\cos\theta) = \frac{2n+1}{n} \cos\theta\, P^1_n(\cos\theta) - \frac{n+1}{n} P^1_{n-1}(\cos\theta)$$

starting with $P_0(\cos\theta) = 1, \quad P_1(\cos\theta) = \cos\theta$

and $P^1_1(\cos\theta) = \sin\theta, \quad P^1_2(\cos\theta) = \frac{3}{2}\sin 2\theta$

respectively. The differential form $\frac{\partial}{\partial\theta} P^1_n(\cos\theta)$ was then obtained from the relation

$$\frac{\partial}{\partial\theta} P^1_n(\cos\theta) = n\cos\theta \frac{P^1_n(\cos\theta)}{\sin\theta} - (n+1) \frac{P^1_{n-1}(\cos\theta)}{\sin\theta}$$

with the conditionals

$$\left[\frac{\partial}{\partial\theta} P_n^1(\cos\theta)\right]_{\theta=0} = \frac{n(n+1)}{2}$$

$$\left[\frac{\partial}{\partial\theta} P_n^1(\cos\theta)\right]_{\theta=\pi} = (-1)^n \frac{n(n+1)}{2} .$$

The values of the Legendre functions computed in this manner are believed to be accurate to seven significant figures for $n \leqslant 50$, but the subroutine has been used up to $n = 300$ with no appreciable loss in accuracy.

For reference purposes, the back scattering cross section for an unloaded (solid) sphere, normalized to the physical optics value πa^2, is presented as a function of ka in Fig. 3-1. The formula for computing these values is given either by equation (2.30a) or (2.30b), but since there are already adequate tabulations of the back scattering cross sections in the literature (Bechtel, 1962; Hey et al, 1956), no direct computations were performed.

The evaluation of the series for the radiation admittance Y_r is complicated by the slow convergence of its imaginary part for all non-zero δ. This is a consequence of the local capacitance in the vicinity of the gap and, indeed, in the limit as the gap width tends to zero, the series for the imaginary part fails to converge. In contrast, the series for the real part is rapidly convergent even for $\delta = 0$.

The first N terms of the series are treated exactly, and to facilitate the computations, the subsequent terms are replaced by their asymptotic forms for large n. Since

$$\frac{\zeta_n'(ka)}{\zeta_n(ka)} \sim -\frac{n}{ka}$$

for $n \gg ka$, and

$$P_n(\cos\theta) \sim \sqrt{\frac{2}{n\pi \sin\theta}} \cos\left\{(n+\tfrac{1}{2})\theta - \frac{\pi}{4}\right\}$$

$$P_n^1(\cos\theta) \sim -\sqrt{\frac{2n}{\pi \sin\theta}} \cos\left\{(n+\tfrac{1}{2})\theta + \frac{\pi}{4}\right\}$$

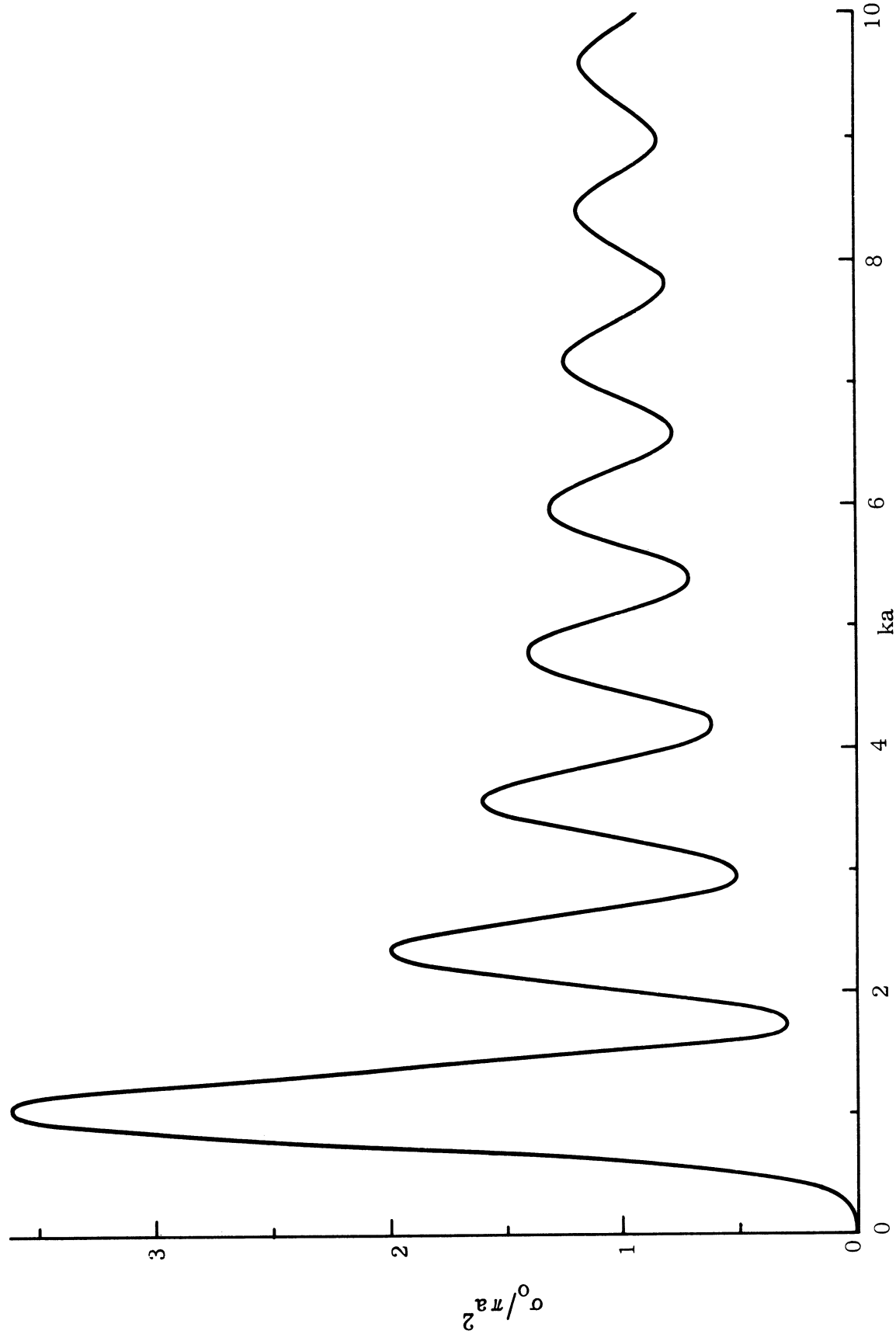

FIG. 3-1: NORMALIZED BACK SCATTERING CROSS SECTION OF UNLOADED SPHERE.

for $n \gg \operatorname{cosec}\theta$, substitution of these expressions into the higher order terms of (2.20) gives

$$\frac{Y_r}{Y} \simeq i\pi \sin^2\theta_o \sum_{n=1}^{N} \frac{2n+1}{n^2(n+1)^2} \left\{ \frac{\zeta_n'(ka)}{\zeta_n(ka)} \left(\frac{P_n(+) - P_n(-)}{\delta \sin\theta_o} \right)^2 - \frac{\zeta_n(ka)}{\zeta_n'(ka)} \left(\frac{P_n^1(+) - P_n^1(-)}{\delta} \right)^2 \right\}$$

$$+ i \sum_{n=N+1}^{\infty} \frac{2n+1}{(n+1)^2} \left(\frac{\sin\frac{n\delta}{2}}{\frac{n\delta}{2}} \right)^2 \left[ka \sin\theta_o \left\{ 1 + \sin(2n+1)\theta_o \right\} - \frac{1}{ka \sin\theta_o} \left\{ 1 - \sin(2n+1)\theta_o \right\} \right], \tag{3.1}$$

In all of the computations, N was given the largest value consistent with machine capacity, and 1000 terms were retained in the second series. This last is certainly more than sufficient for our purposes, and the only possible source of error then lies in the use of asymptotic formulae. To get some feeling for the probable magnitude of these errors, Y_r/Y was computed for $ka = 5.0$, $\delta = 0.0392$ and $\theta_o = 90^o$ using four different values for the upper limit of the summation variable in the first series, and the results are summarized below:

$$N = 10\ , \qquad Y_r/Y = 15.255 + i29.686,$$

$$N = 15\ , \qquad Y_r/Y = 15.255 + i30.385,$$

$$N = 20\ , \qquad Y_r/Y = 15.255 + i30.676,$$

$$N = 24\ , \qquad Y_r/Y = 15.255 + i30.748.$$

($N = 24$ is the maximum attainable by the machine for $ka = 5.0$). The rapid convergence of the series for $\mathrm{Re}\frac{Y_r}{Y}$ is reflected in the constancy of the real parts above, and if the trend of the imaginary parts remains the same as N is increased still further, the computed magnitude of $\mathrm{Im}\frac{Y_r}{Y}$ with $N = 24$ should be within one percent of the correct value.

Since Y_r is symmetric about $\theta = \pi/2$, it is sufficient to restrict attention to $\theta_o \leq 90^o$. The gap width chosen for computation was $\delta = 0.0392$ (approximately

2.25^{o}), and this was determined by the equivalent slot width of the experimental model (Section 4.1). The sample computations of Y_r/Y for $0 < ka \leqslant 10.0$ with slot positions at $\theta_o = 45^{o}$ and $\theta_o = 90^{o}$ are shown in Figs. 3-2 and 3-3 respectively, and from these it appears that the change of the slot position does not affect the general character of the loading behavior. The real parts are zero for $ka = 0$ and rise through positive values with a small but regular oscillation as ka increases. The imaginary parts, on the other hand, have a negative singularity at $ka = 0$, but as a consequence of the asymmetric excitation, they become positive at ka around unity, and then remain as such.

To investigate the effect of the slot width on the radiation admittance, Y_r/Y was computed as a function of δ for $ka = 4.28$ with $\theta_o = 90^{o}$. As shown in Fig. 3-4, the real part is essentially constant for the full range of δ considered, but the imaginary part shows a significant variation due to local capacitance across the gap. At $\delta = 0$ the imaginary part has a positive singularity and then is monotonically decreasing as δ increases.

Computation of the radiated surface field components $T_1^r(\theta, \theta_o)$ and $T_2^r(\theta, \theta_o)$, given by equations (2.15), is even more involved than that of the radiation admittance Y_r/Y. Whereas the terms in the series for Y_r/Y are $O(1/n^3)$ for n large, for $aT_1^r(\theta, \theta_o)$ and $aT_2^r(\theta, \theta_o)$ they* are $O(1/n)$ and $O(1/n^2)$ respectively. Fortunately, the terms in the series alternate in sign in groups of $2\pi/\delta$ terms, and therefore may be treated as an alternating series. The first 43 terms (or less, whenever the machine capacity was exceeded) were computed exactly. From there on, to facilitate the computation, the ratios of the Hankel functions were replaced by their asymptotic form

$$\frac{\zeta'(x)}{\zeta(x)} \sim -\frac{2(n+1)(2n-1)-(n-1)x^2}{2(2n-1)x+x^3} + \frac{1}{x}, \quad n \gg x$$

* The factor a has been incorporated to make equations (2.15) functions of ka rather than ka and k.

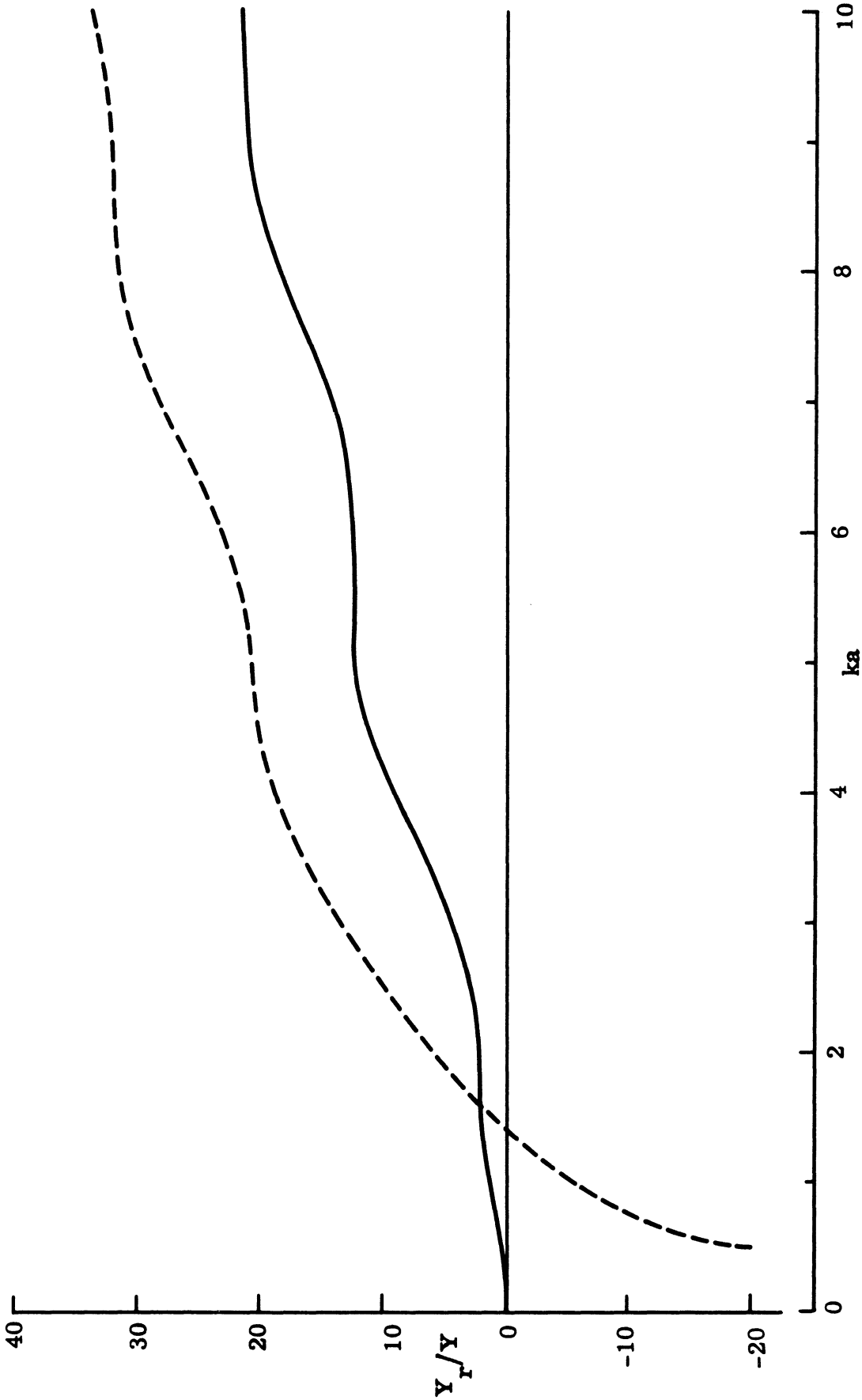

FIG. 3-2: REAL (——) AND IMAGINARY (– – –) PARTS OF NORMALIZED RADIATION ADMITTANCE FOR $\theta_o = 45^o$ AND $\delta = 0.0392$.

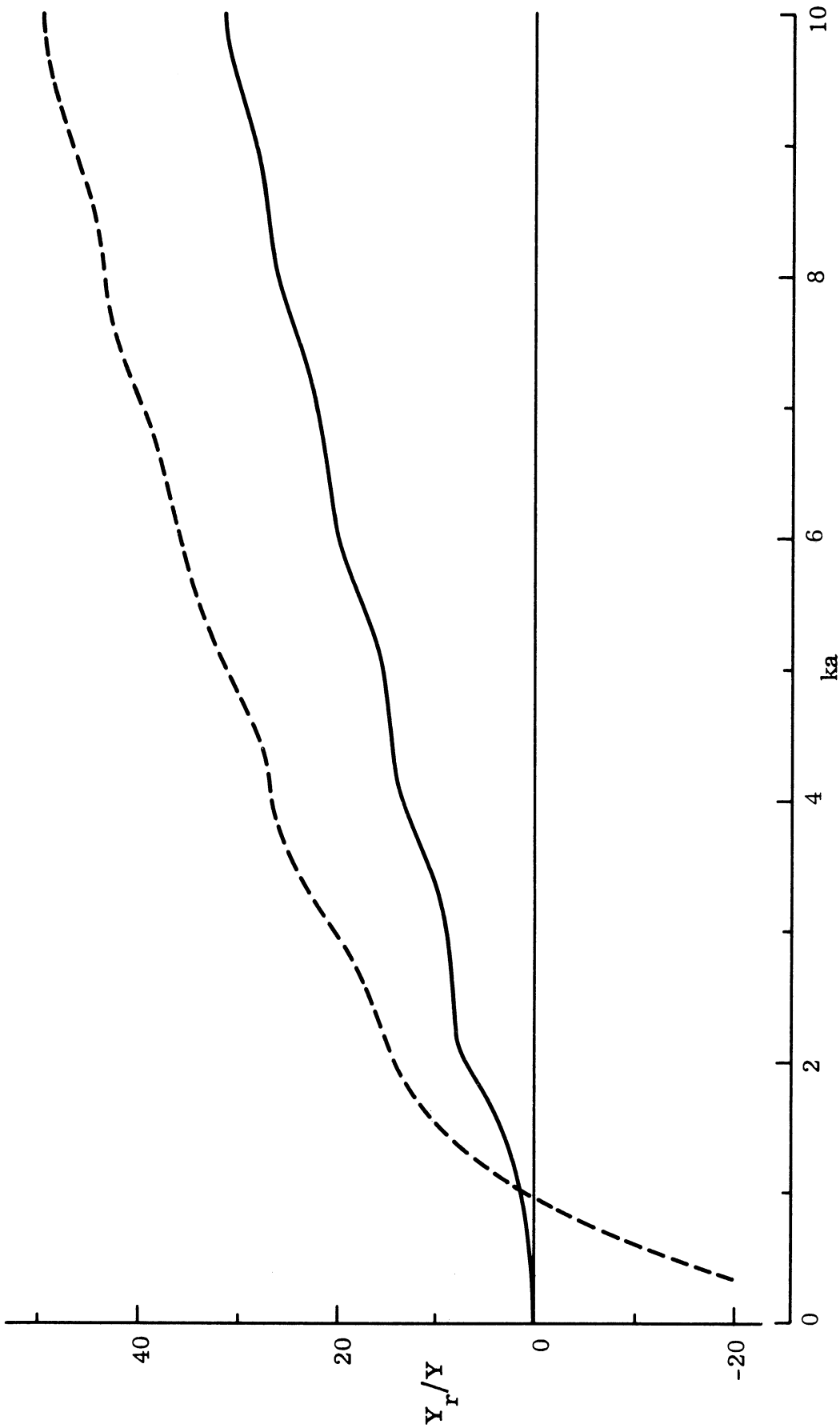

FIG. 3-3: REAL (——) AND IMAGINARY (– – –) PARTS OF NORMALIZED RADIATION ADMITTANCE FOR $\theta_o = 90^o$ AND $\delta = 0.0392$.

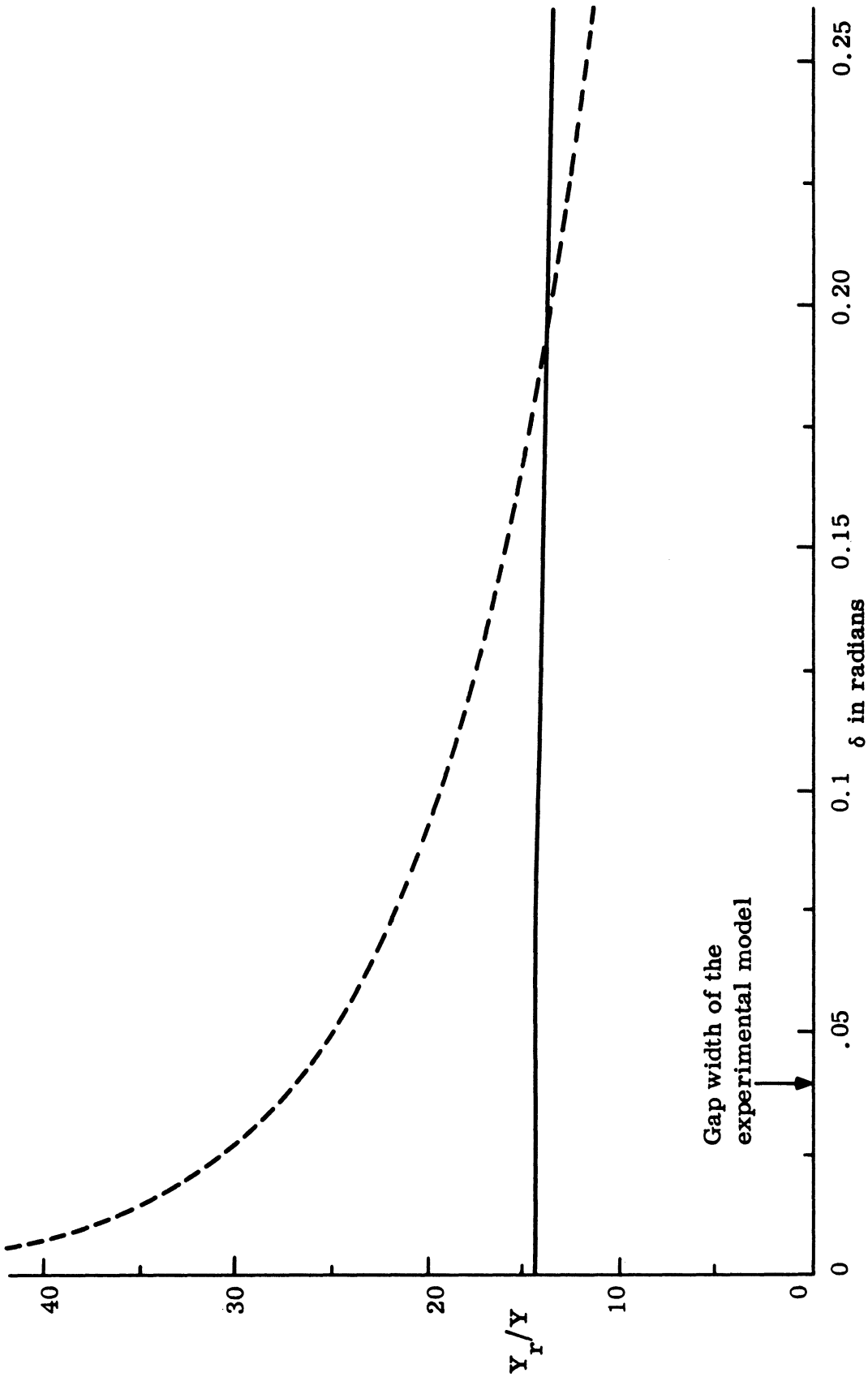

FIG. 3-4: REAL (——) AND IMAGINARY (- - -) PARTS OF NORMALIZED RADIATION ADMITTANCE FOR ka = 4.28 AND $\theta_o = 90^o$.

and the Legendre functions by their corresponding asymptotic forms, but only when $n \geqslant 100$. As such, the terms for both series contained the same factor $\sin\frac{n\delta}{2}$, and approached zero as

$$\frac{n\delta}{2} \rightarrow m\pi, \qquad m = 1, 2, 3 \ldots \quad .$$

A comparison of partial sums terminated at

$$n \sim \frac{2m\pi}{\delta}$$

showed that for $m \geqslant 3$ the results, for all practical purposes, were identical. To ensure good accuracy for the numerical evaluation, the series were terminated at $m = 6$, and with $\delta = 0.0392$ this corresponded to 962 terms. A sample computation for the amplitude of $T_2^r(\theta, \pi/6)$ with $ka = 1.03$ and $\theta_o = 30^o$ is shown in Fig. 3-5. The amplitude at the front ($\theta = 0$) is rather large, as compared to that at the back, and becomes even larger (but finite) in the region near the slot. A similar computation for $T_2^r(\theta, \pi/2)$ was also performed for $ka = 4.28$ with $\theta_o = 90^o$. The field, as one would expect, is symmetric about 90^o, but its amplitude is more uniformly distributed over the surface of the sphere.

3.2 Loading for Zero Back Scattering

Once the numerical results for $S_1^s(0)$, $T_2(\theta_o)$ and Y_r/Y are available, it is a simple matter to determine the loading admittance $\left[Y_\ell\right]_0$ for zero back scattering from equation (2.34b). In Figs. 3-6 through 3-10 the real and imaginary parts of the loading admittance are presented for $0 < ka \leqslant 10$, with $\theta_o = 30^o$, 45^o, 60^o, 90^o and 120^o respectively. All the curves are quite irregular and, as $ka \rightarrow 0$, the imaginary part becomes infinite. The real part is, however, of more importance. Bearing in mind that the non-negative values of the real part correspond to a passive load and the negative values to an active load, it is apparent that zero back scattering can be obtained with a passive load only when $\mathrm{Re}\left[Y_\ell\right]_0 \geqslant 0$. As we see from the graphs, the loading is quite dependent on the slot position θ_o, with

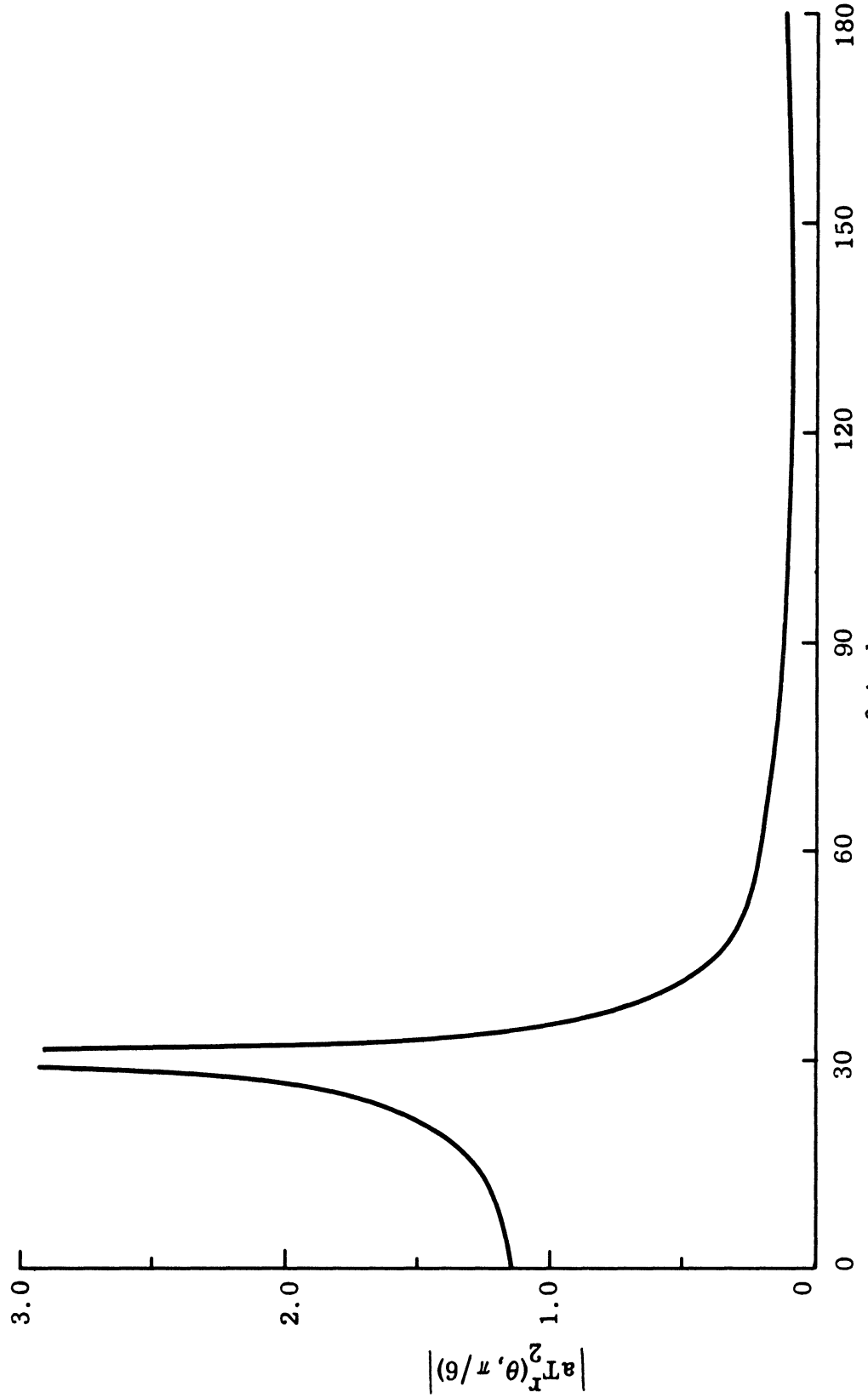

FIG. 3-5: AMPLITUDE OF RADIATED SURFACE FIELD COMPONENT $aT_2^r(\theta, \pi/6)$ FOR $ka = 1.03$ AND $\theta_o = 30^o$.

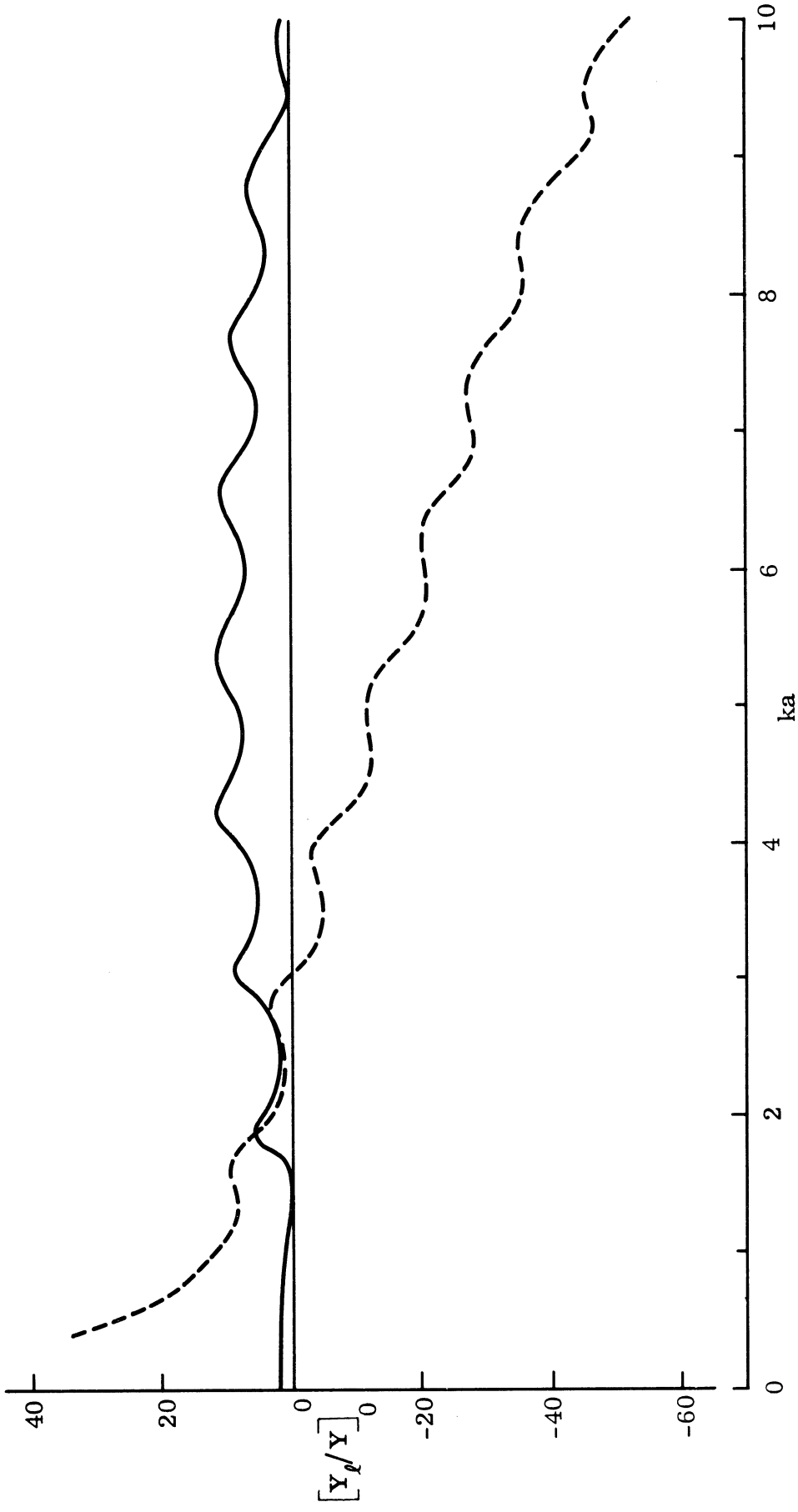

FIG. 3-6: REAL (——) AND IMAGINARY (– – –) PARTS OF NORMALIZED LOADING ADMITTANCE FOR ZERO BACK SCATTERING WITH $\theta_o = 30^o$.

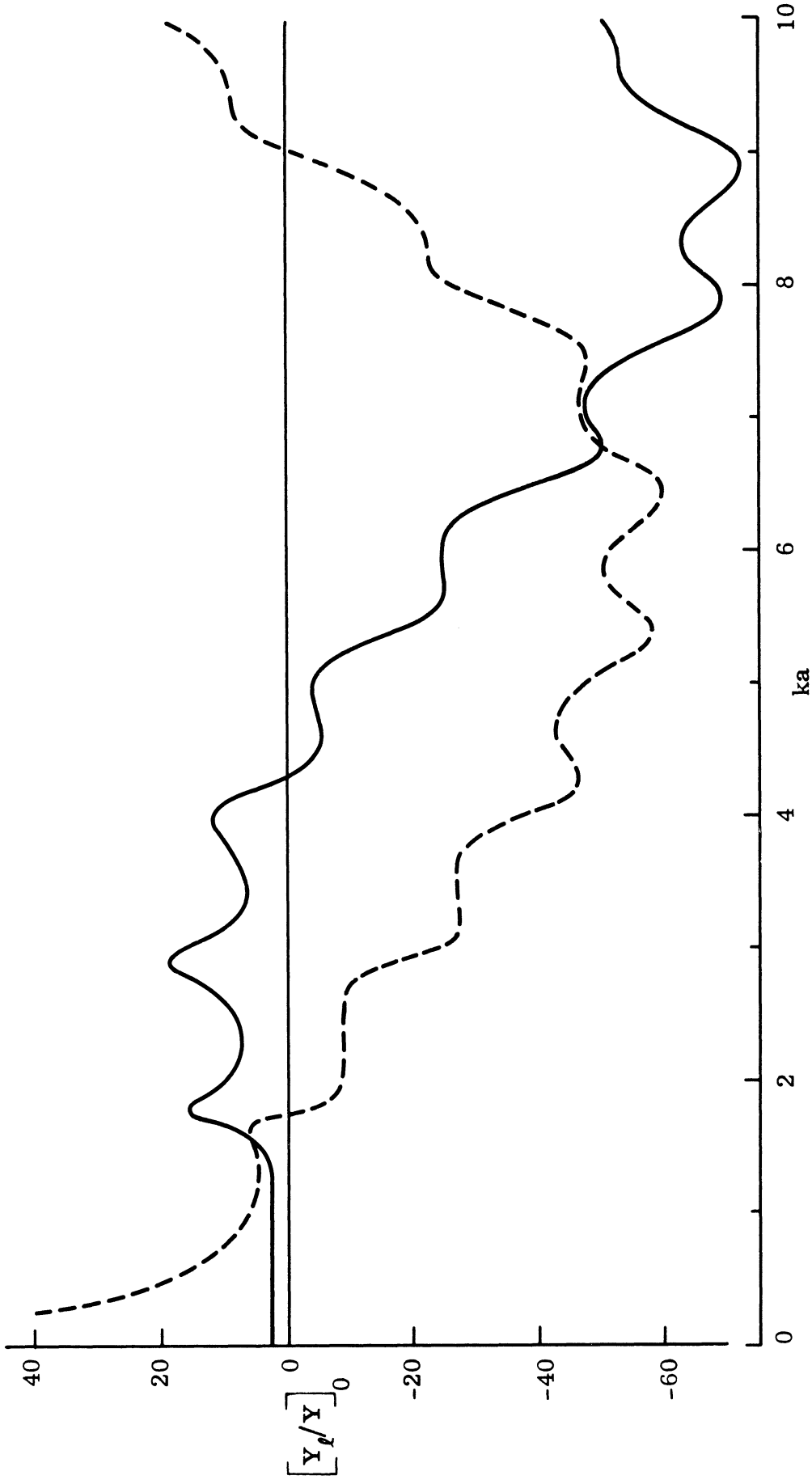

FIG. 3-7: REAL (——) AND IMAGINARY (- - - -) PARTS OF NORMALIZED LOADING ADMITTANCE FOR ZERO BACK SCATTERING WITH $\theta_o = 45^o$.

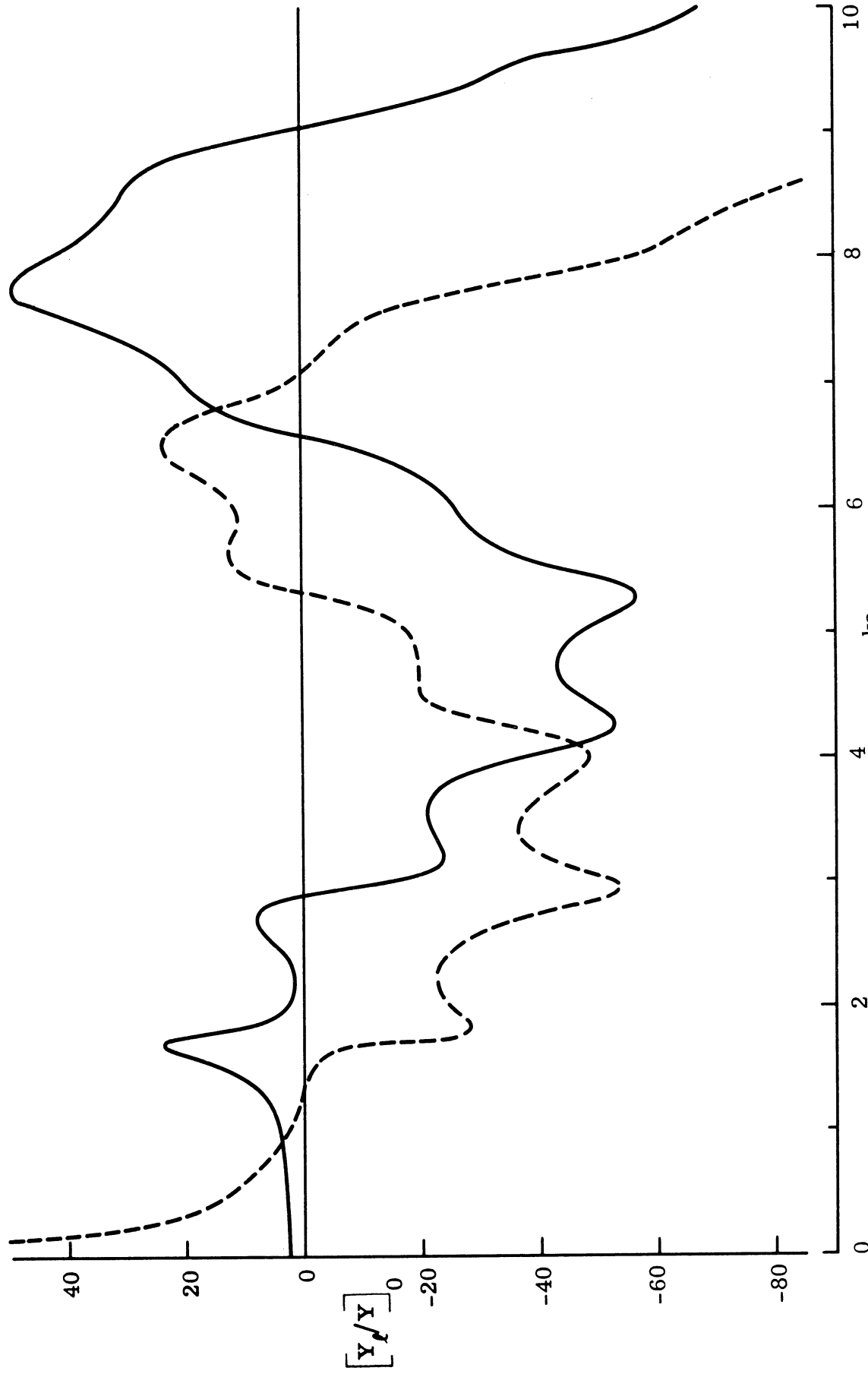

FIG. 3-8: REAL (——) AND IMAGINARY (– – –) PARTS OF NORMALIZED LOADING ADMITTANCE FOR ZERO BACK SCATTERING WITH $\theta_o = 60^o$

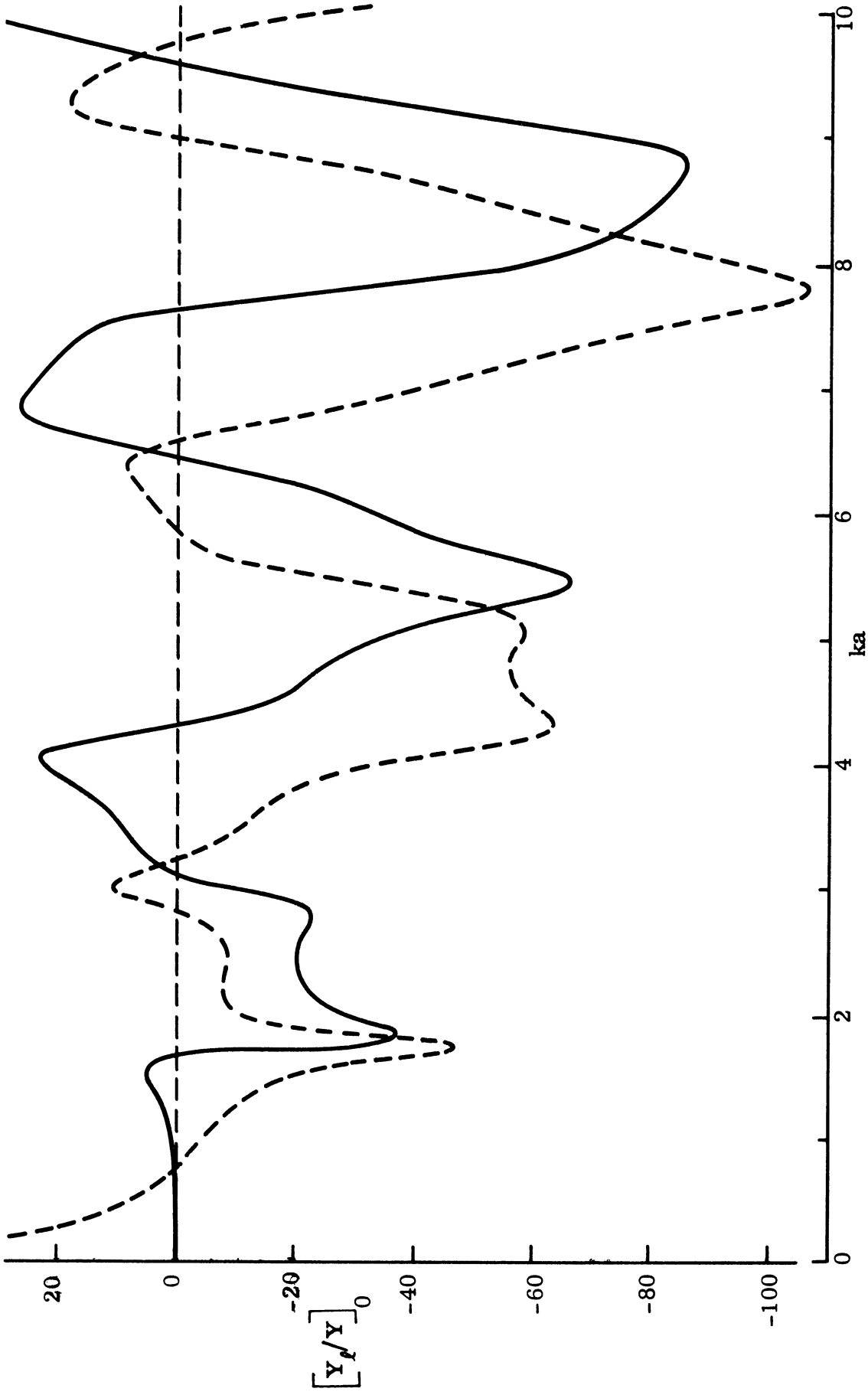

FIG. 3-9: REAL (——) AND IMAGINARY (- - -) PARTS OF NORMALIZED LOADING ADMITTANCE FOR ZERO BACK SCATTERING WITH $\theta_o = 90^o$.

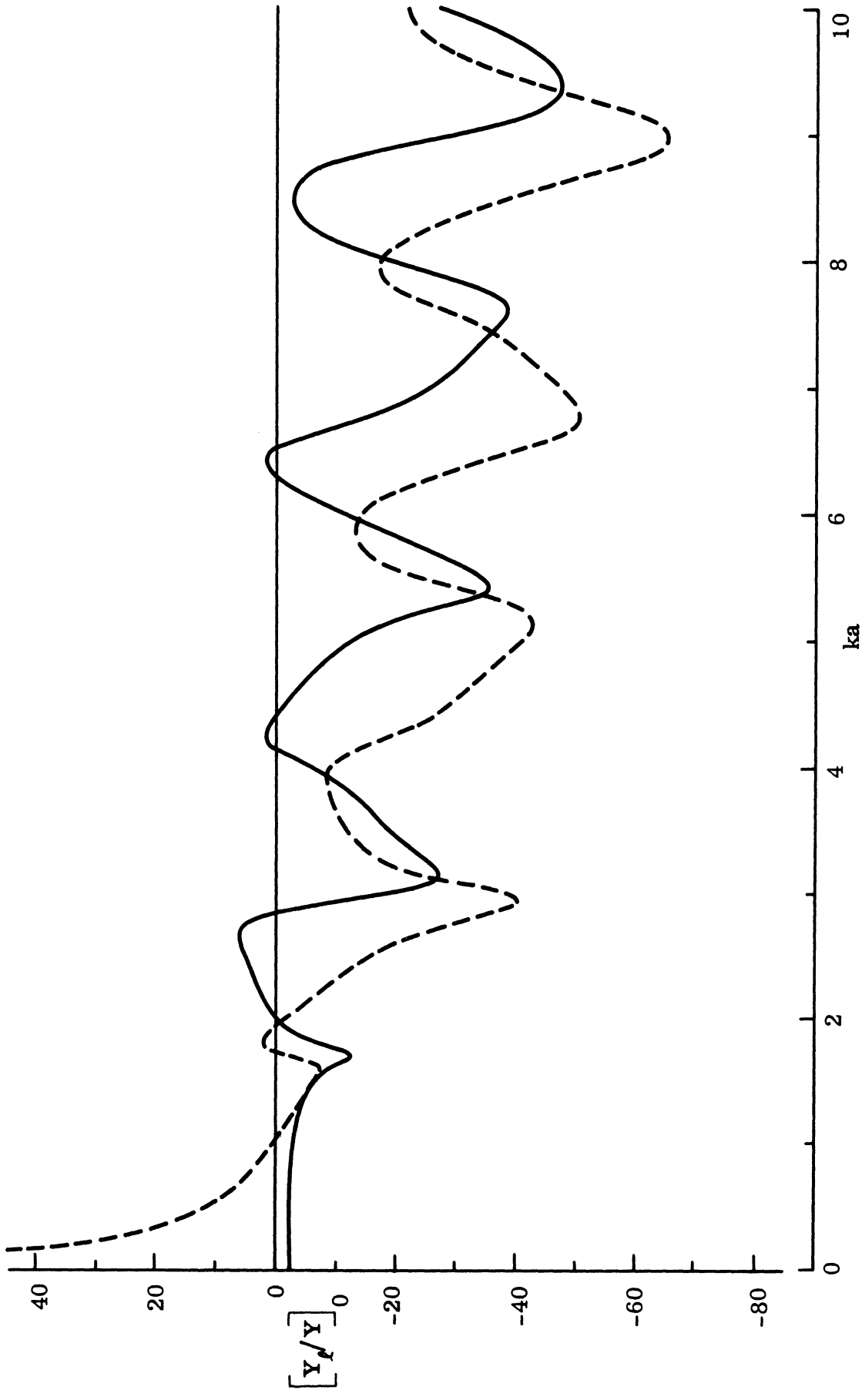

FIG. 3-10: REAL (——) AND IMAGINARY (– – –) PARTS OF NORMALIZED LOADING ADMITTANCE FOR ZERO BACK SCATTERING WITH $\theta_o = 120^o$.

increasing irregularity as θ_o increases. For instance, with $\theta_o = 30^o$, the real part is non-negative for almost the entire range of ka considered, but as θ_o goes to 90^o, or even 120^o, both the real and imaginary parts become rapidly varying about the zero axis. This variation can be directly associated with the spacial separation between the slot and the equivalent phase center for the returned signal from an unslotted sphere. This phase center is located somewhere near the front of the sphere. An increase in separation makes the load more frequency sensitive, while a decrease has the opposite effect. Unfortunately, as the slot is moved towards the front, its total circumferential length decreases, and the amount of energy available for "reradiation" is not sufficient to cancel out the far field. In such a case an active load is required. In Fig. 3-6, for $\theta_o = 30^o$, we see the cross-over appearing at about ka = 1.5 with the values of $\mathrm{Re}\left[Y_\ell/Y\right]_0$ being just slightly negative. When the slot was moved to $\theta_o = 25^o$, an exploratory calculation showed that the real part is even more negative.

3.3 Optimum Passive Loading

Since passive loading is of most interest, let us now consider the maximum and minimum values of back scattering cross sections that are attainable with such a loading. From equations (2.28), (2.30) and (2.34) we can write the back scattering cross section $\sigma(0)$ for a loaded sphere, relative to the back scattering cross section σ_o for an unloaded sphere, as

$$\frac{\sigma(0)}{\sigma_o} = \left| 1 + \frac{a+ib}{x+iy} \right|^2 \tag{3.2a}$$

$$= 1 + \frac{a^2+b^2}{x^2+y^2} + \frac{2ax}{x^2+y^2} + \frac{2by}{x^2+y^2} , \tag{3.2b}$$

where

$$a+ib = \frac{\pi \left\{ ka \sin\theta_o T_2(\theta_o) \right\}^2}{2 S_1^s(0)} \frac{Y}{Y_\ell + Y_r}$$

$$x+iy = \frac{Y_\ell}{Y} + \frac{Y_r}{Y}$$

with a, b, x and y being real quantities. The maximum and minimum values of the above cross section ratio, as well as the passive loading that is required to attain them, are determined in Appendix A. By passive loading we here mean only that $\mathrm{Re}\ \frac{Y_\ell}{Y} \geqslant 0$ and, by no means, that the resultant loading admittance is always physically realizable. A discussion of synthesis methods is presented in Section 6.1

The computed results for the extreme cross sections and for the corresponding passive load are presented for various slot positions, θ_o, in Figs. 3-11 through 3-19. First, taking the minima, we observe that there is a complete reduction in the cross section wherever $\mathrm{Re}\left[Y_\ell/Y\right]_0 \geqslant 0$. For example, with $\theta_o = 30^o$ (Fig. 3-11) the cross section is zero for almost all ka, $0 < ka \leqslant 10.0$. (At $ka = 1.5$, the real part does cross the zero axis, but even then the reduction is over 40 db.) Next, let us consider the result with $\theta_o = 45^o$ in Fig. 3-12. Here the return is zero for $ka < 4.25$, but as $\mathrm{Re}\left[Y_\ell/Y\right]_0$ in Fig. 3-7 swings from a positive to a negative value, the minimum return increases from zero and rises to a peak value at $ka \simeq 8.0$ which is only infinitesimally less than for an unloaded sphere. It then appears to fall back to zero somewhere around $ka = 12.0$. The pattern apparently is repeated without end. Any further displacement of the slot towards and into the shadow region ($\theta_o > 90^o$) compresses this "stop and pass band" pattern and decreases the total ka range over which the scattering can be appreciably reduced. For instance, with $\theta_o = 30^o$ almost the entire band $0 < ka \leqslant 10$ is covered, whereas with $\theta_o = 60^o$ the coverage has decreased to 53 percent and with $\theta_o = 120^o$ to only 33 percent.

If, on the other hand, we aim for the maximum return, an arbitrarly large enhancement can be achieved in all cases by taking ka sufficiently small, but since this is only a consequence of a higher order zero in the normalized function σ_o, the result is somewhat misleading. To consider an enhancement that is more realistic, we shall confine our attention values of $ka \geqslant 1.0$. The maximum return, in such a case, appears to be close to 20 db for a particular value of ka and with

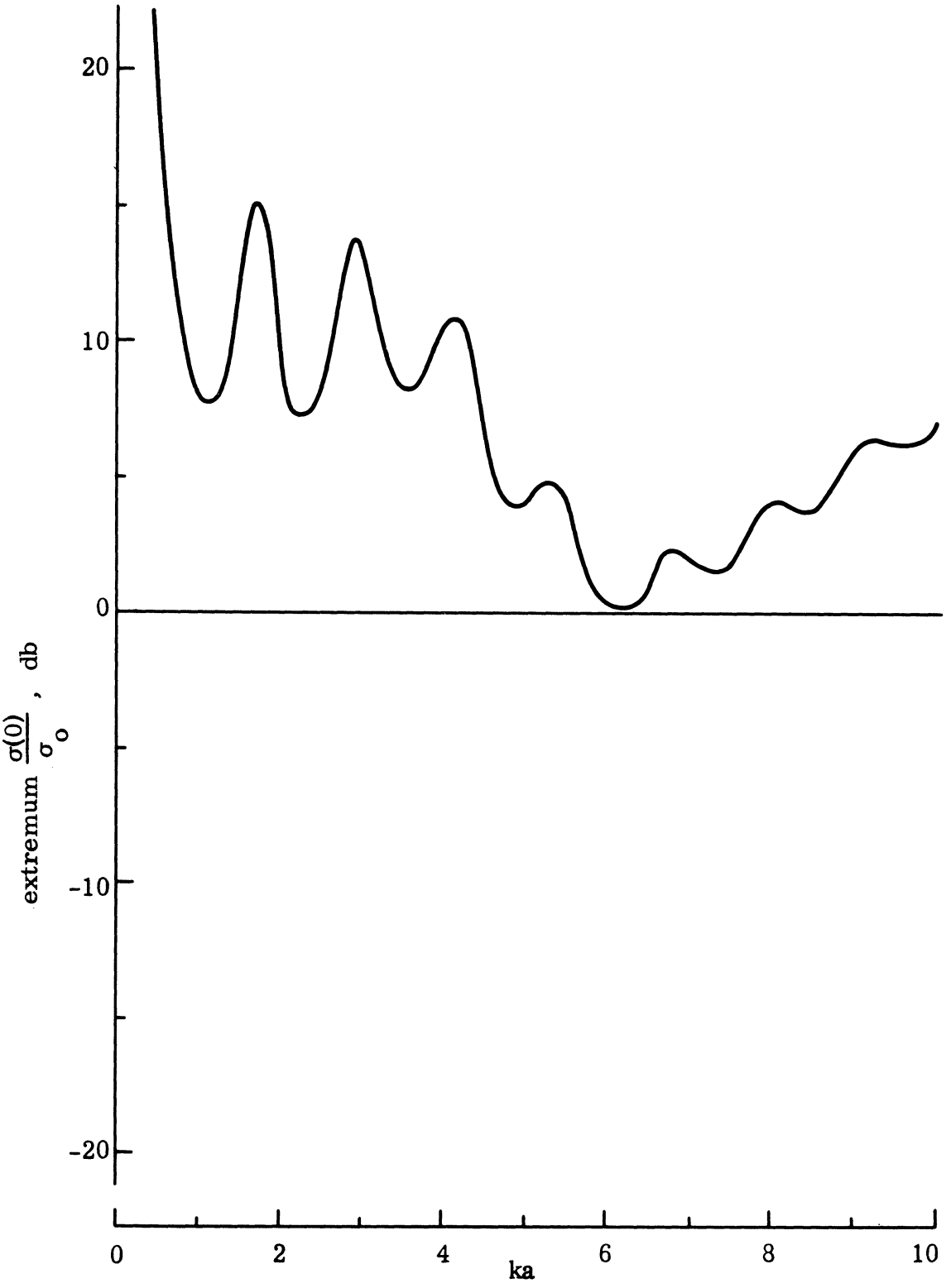

FIG. 3-11: MAXIMUM AND MINIMUM RELATIVE BACK SCATTERING CROSS SECTIONS FOR PASSIVE LOADING AT $\theta_o = 30^o$.

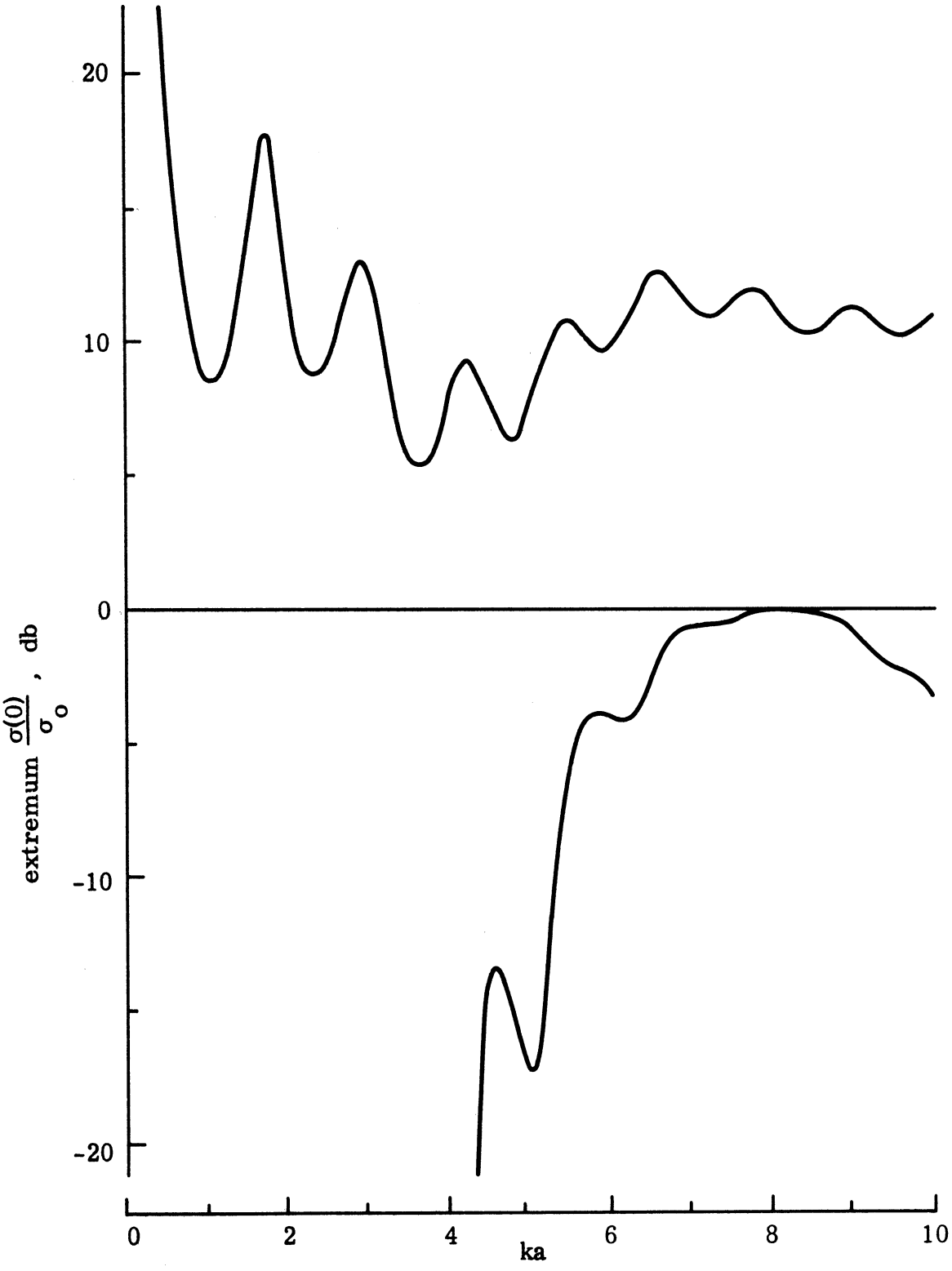

FIG. 3-12: MAXIMUM AND MINIMUM RELATIVE BACK SCATTERING CROSS SECTIONS FOR PASSIVE LOADING AT $\theta_o = 45^o$.

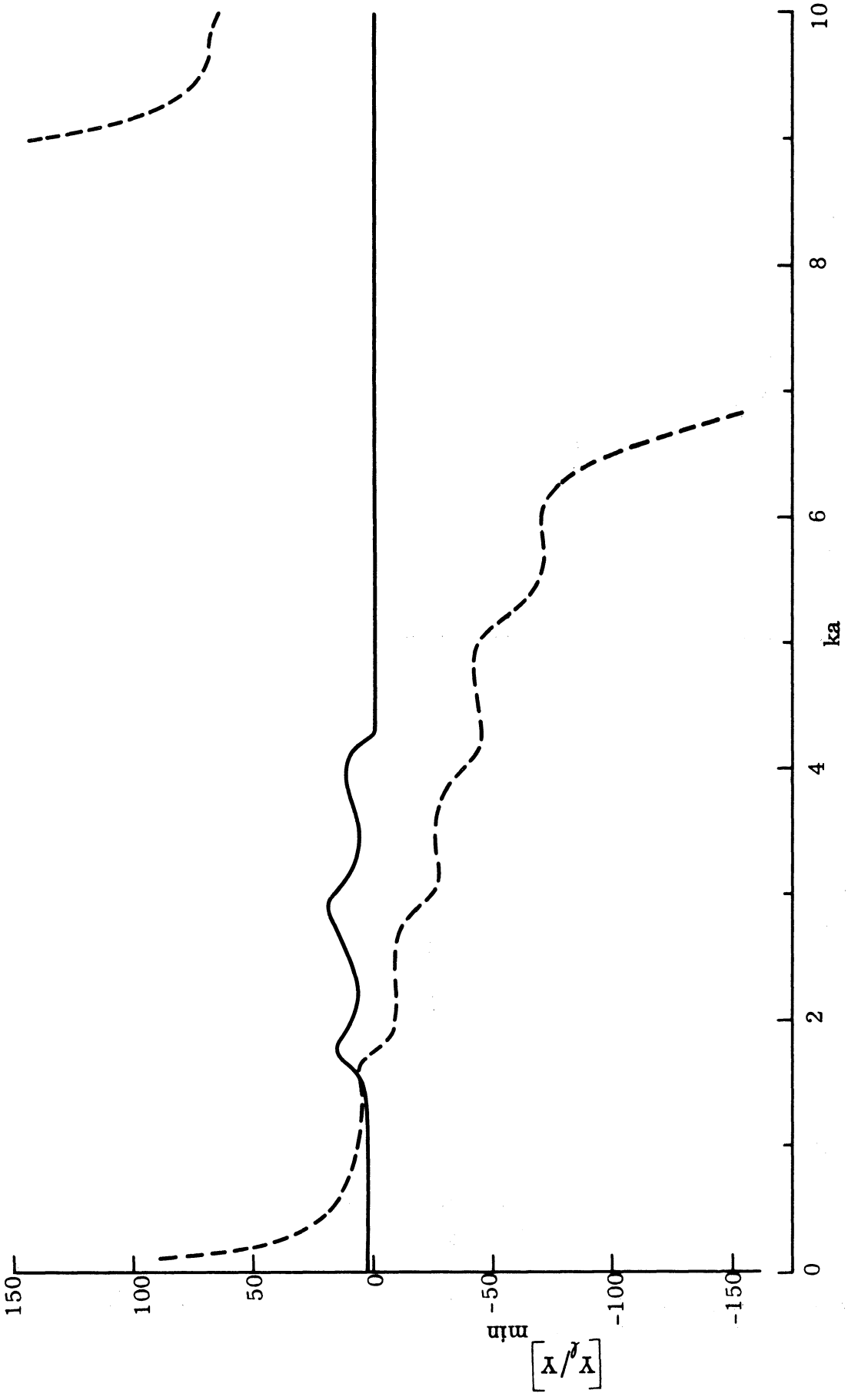

FIG. 3-13: REAL (——) AND IMAGINARY (- - -) PARTS OF NORMALIZED PASSIVE ADMITTANCE FOR MINIMUM BACK SCATTERING WITH $\theta_o = 45^o$.

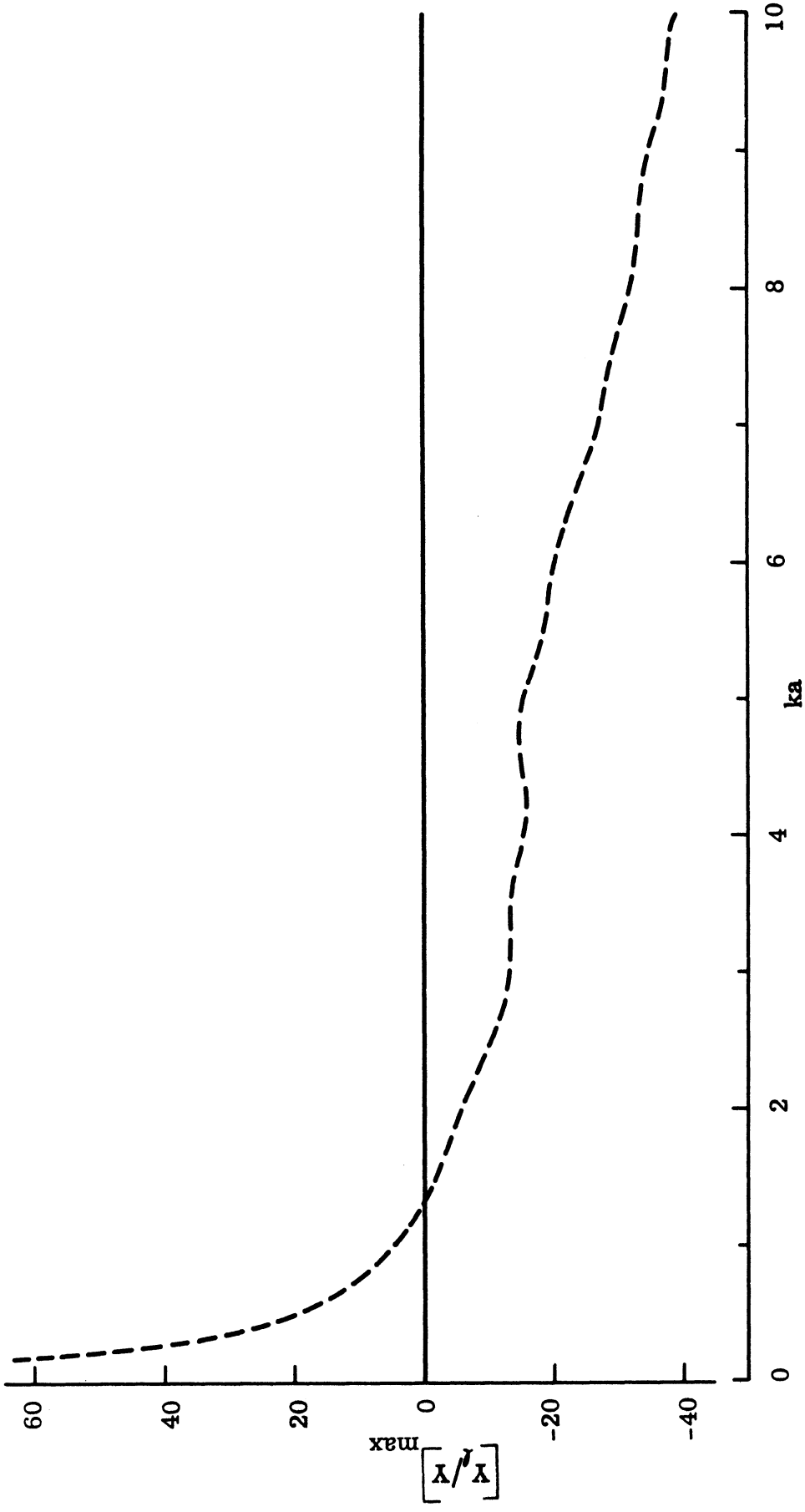

FIG. 3-14: REAL (——) AND IMAGINARY (- - -) PARTS OF NORMALIZED PASSIVE LOADING ADMITTANCE FOR MAXIMUM BACK SCATTERING WITH $\theta_o = 45^o$.

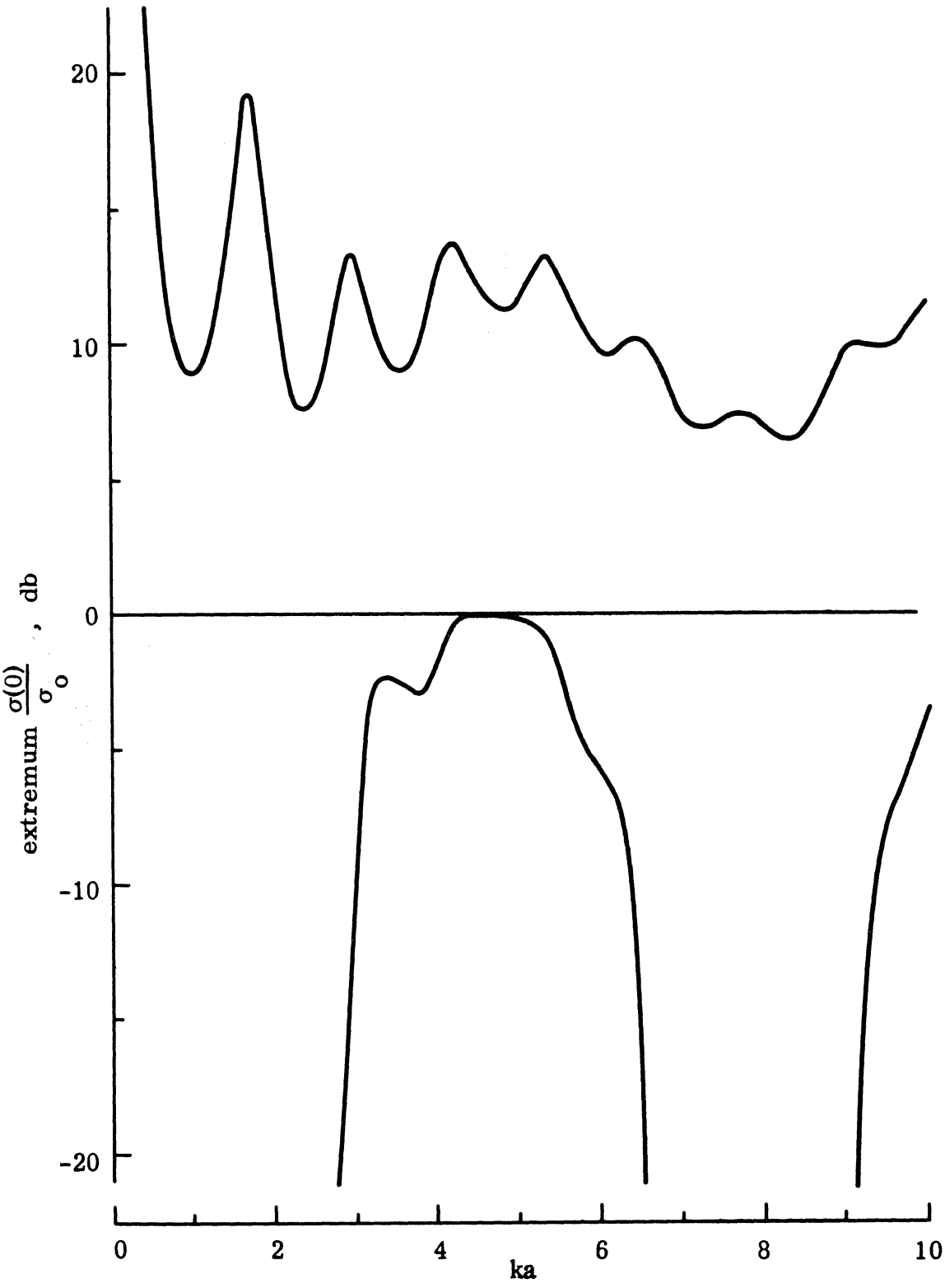

FIG. 3-15: MAXIMUM AND MINIMUM RELATIVE BACK SCATTERING CROSS SECTIONS FOR PASSIVE LOADING AT $\theta_o = 60^o$.

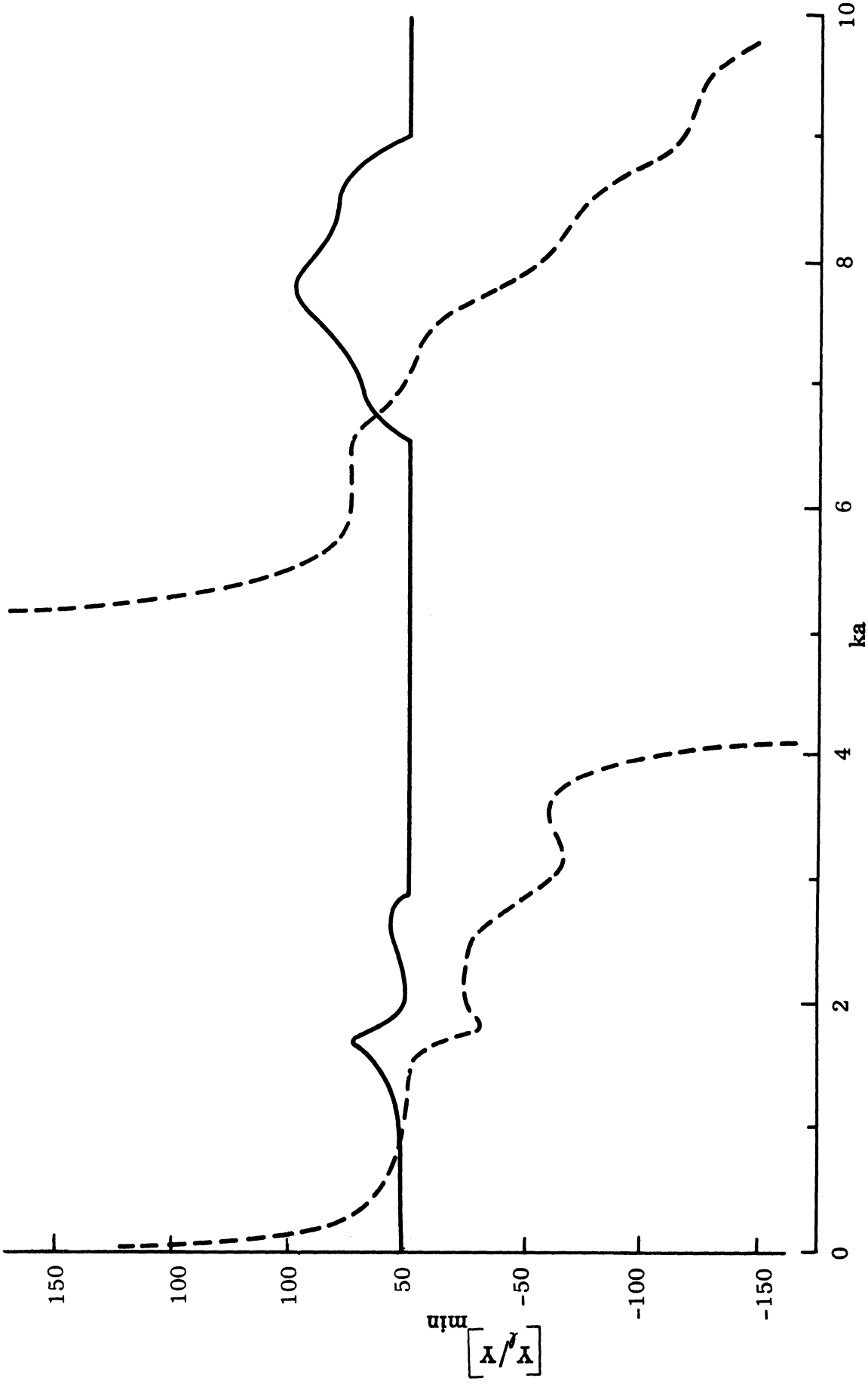

FIG. 3-16: REAL (——) AND IMAGINARY (- - -) PARTS OF NORMALIZED PASSIVE LOADING ADMITTANCE FOR MINIMUM BACK SCATTERING WITH $\theta_o = 60^o$.

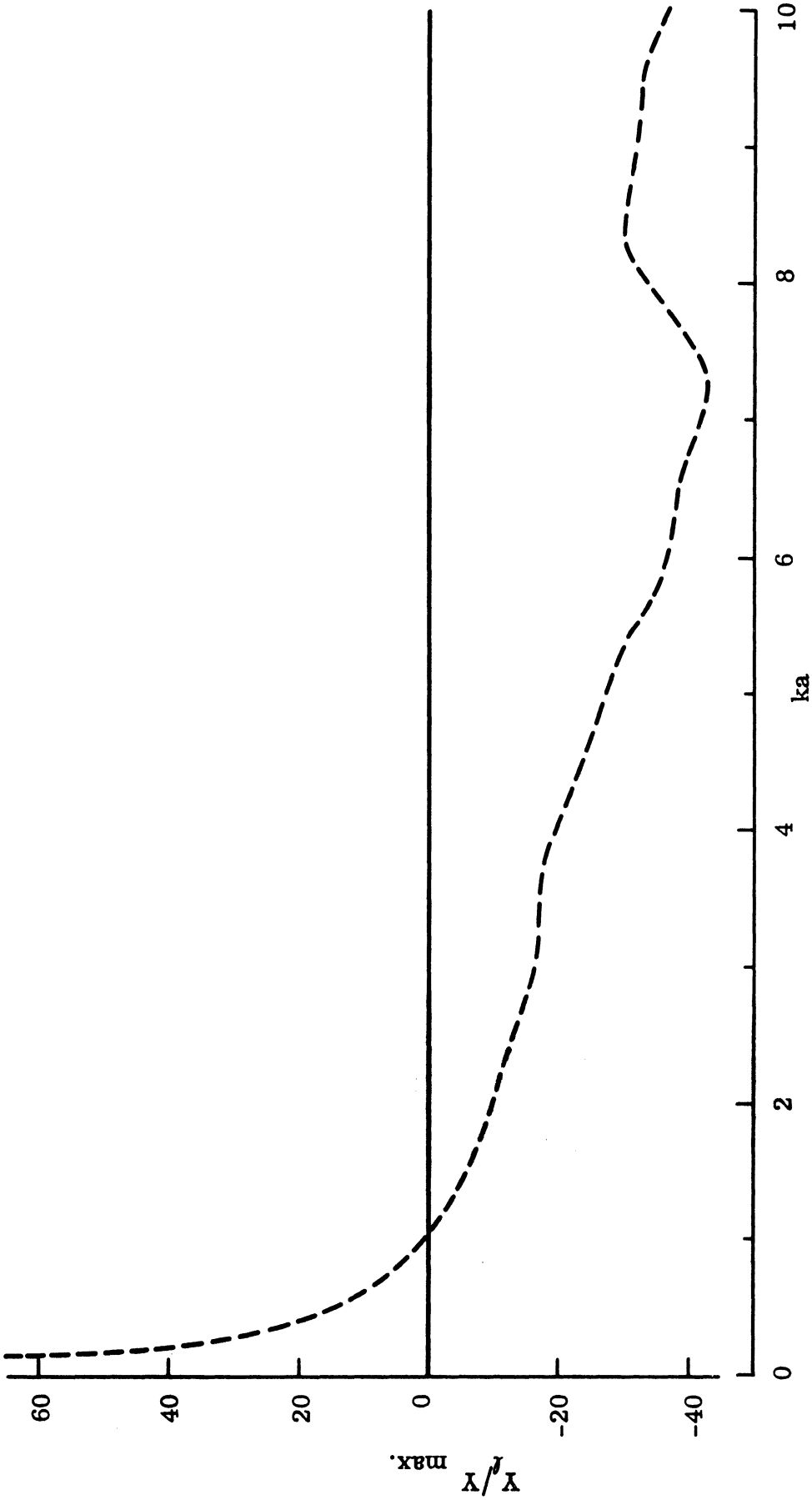

FIG. 3-17: REAL (——) AND IMAGINARY (– – –) PARTS OF NORMALIZED PASSIVE LOADING ADMITTANCE FOR MAXIMUM BACK SCATTERING WITH $\theta_o = 60^o$.

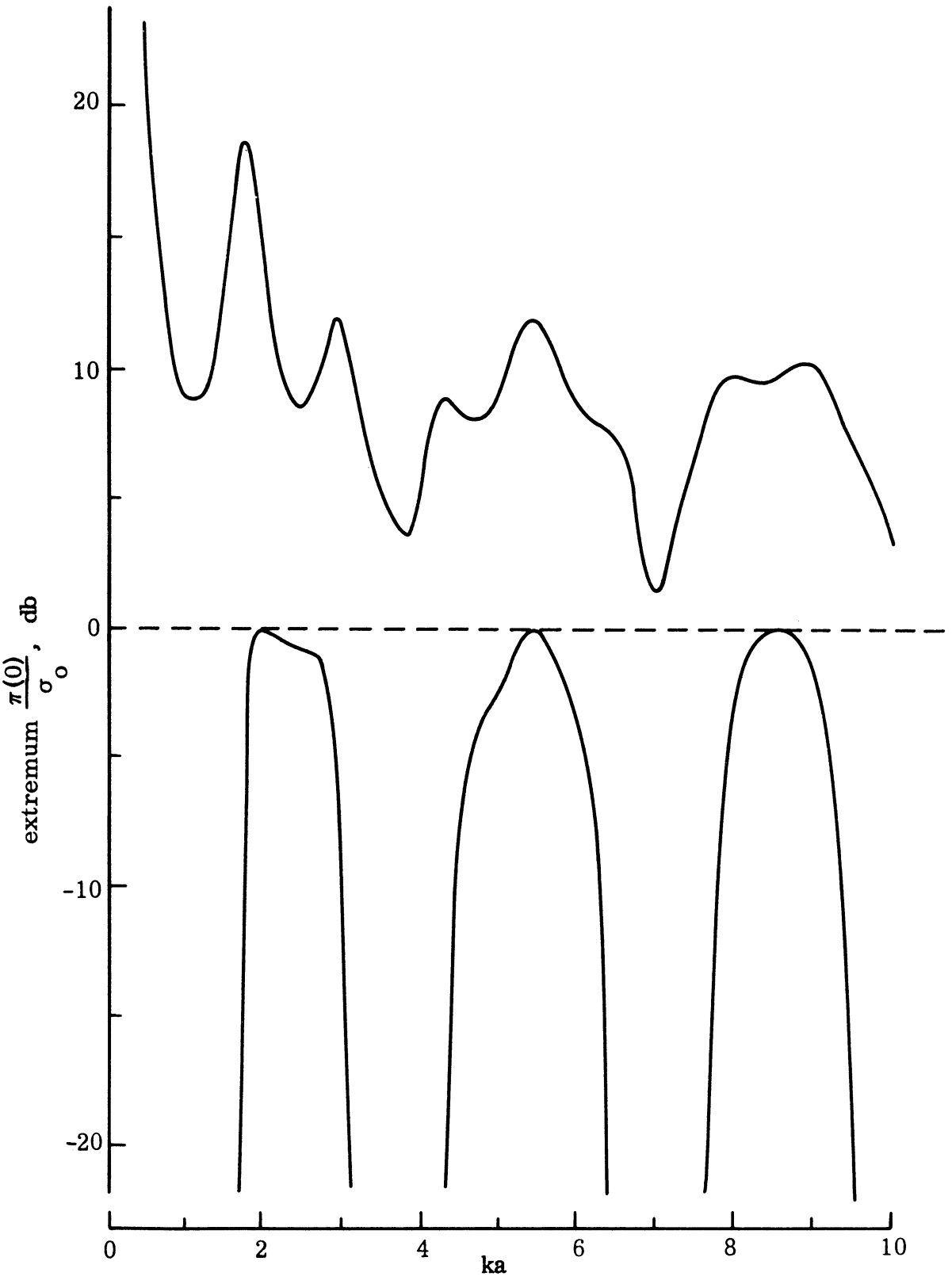

FIG. 3-18: MAXIMUM AND MINIMUM RELATIVE BACK SCATTERING CROSS SECTION FOR PASSIVE LOADING AT $\theta_o = 90^o$.

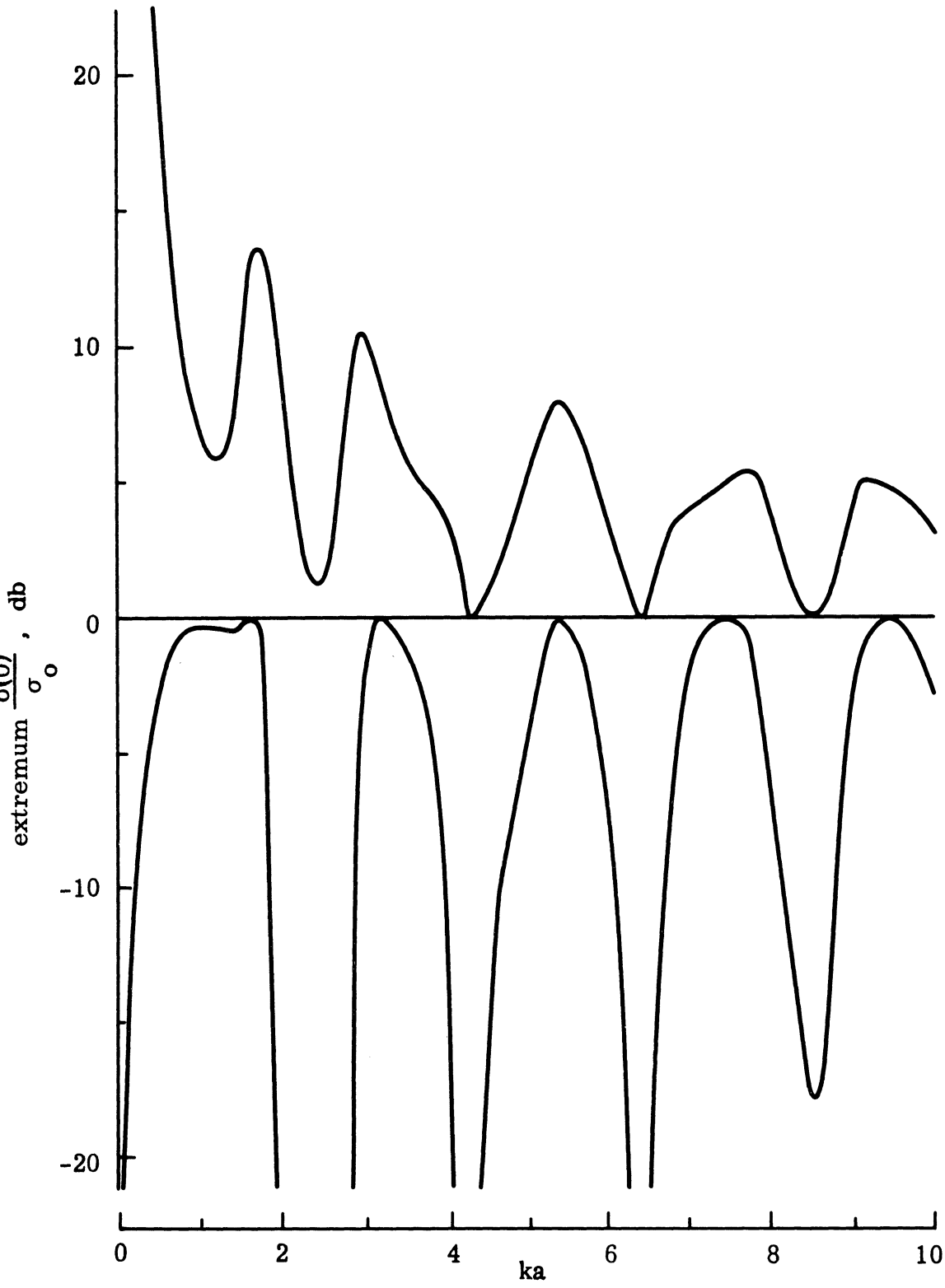

FIG. 3-19: MAXIMUM AND MINIMUM RELATIVE BACK SCATTERING CROSS SECTION FOR PASSIVE LOADING AT $\theta_o = 120^o$

θ_o somewhere in the neighborhood of 60^o. As θ_o is changed to 30^o, this value decreases to 15 db and, for $\theta_o = 120^o$, it is a mere 12.8 db. The maximum average enhancement for the range $1 \leqslant ka \leqslant 10$ also appears to take a similar pattern. With $\theta_o = 60^o$ it is 11.2 db, but with $\theta_o = 30^o$ and 120^o it decreases to 7.8 and 4.7 db respectively.

Figures 3-13, 3-14 and 3-16, 3-17 show the passive loading admittance required to attain the given extremum scattering with $\theta_o = 45^o$ and 60^o respectively. In the case of a minimum return, the optimum passive loading $\left[Y_\ell/Y\right]_{min}$ is given by $\left[Y_\ell/Y\right]_0$ when Re $\left[Y_\ell/Y\right]_0 \gtrsim 0$, but when the Re $\left[Y_\ell/Y\right]_0 \lesssim 0$, the optimum real part is set zero and the corresponding imaginary part rapidly approaches a large value (Figs. 3-13 and 3-16). For a maximum return the real part of the optimum loading $\left[Y_\ell/Y\right]_{max}$ is zero and the imaginary part is a slowly varying function with a negative slope behavior (Figs. 3-14 and 3-17).

3.4 Surface Fields for a Loaded Sphere

The expressions for the surface fields on a loaded sphere are given by equations (2.36), and from these the numerical results were computed for ka = 1.03 and ka = 4.28 with $\theta_o = 30^o$ and 90^o, respectively, when the sphere was loaded for zero back scattering. The amplitudes are presented in Figs. 3-20 through 3-23, along with those for the unloaded body.

The behavior of the surface fields on a loaded sphere is somewhat surprising. In the light of the results by Chen and Liepa (1964a) on the loading of thin cylinders, it was expected that for a sphere loaded for zero back scattering the amplitude of the surface fields would also decrease when ka is unity or less, but as the computed values indicate, this is not true. In fact, the fields are actually enhanced. An examination of the equations for the total scattered fields for the cylinder and the sphere show that they can be treated as a sum of the fields scattered by an unloaded body and the radiated fields whose strength and phase are determined by the loading parameters. In the case of a cylinder with central loading and of length $\lambda/2$

or less, the two fields are similar. When the loading is (say) chosen for zero back scattering at broadside, an overall reduction of the far fields as well as the surface fields results. For a sphere* loaded with a slot in a plane perpendicular to the direction of incidence, the unloaded scattered field and the radiated field are siddimilar, and when such a body is loaded for zero back scattering the total surface field is modified, but not necessarily reduced. This is demonstrated by the numerical computations presented here. For ka = 1.03 the loading at $\theta_o = 30^o$ increases the fields at the front of the sphere by a factor of two, and even more in the region of a load. Over the remaining surface (say, $\theta > 60^o$) the fields are slightly reduced. In the other case, ka = 4.28 with $\theta_o = 90^o$, the loading does not appreciably change the surface field amplitude, but induces in it periodically varying oscillations.

3.5 Bistatic Scattering by a Loaded Sphere

The general expressions for the scattering by a loaded sphere were derived in terms of the far field scattering amplitudes $S_1(\theta)$ and $S_2(\theta)$ in section 2.4. We normalize the bistatic cross section by the back scattering cross section of an unloaded sphere for suitability in computation, and for ease of presentation, restrict our attention to the E-plane ($\phi = 0$) and the H-plane ($\phi = \pi/2$). Thus, from (2.29) and (2.30), in the E-plane

$$\frac{\sigma(\theta, 0)}{\sigma_o} = |S_1(\theta)|^2 \tag{3.3a}$$

and in the H-plane

$$\frac{\sigma(\theta, \pi/2)}{\sigma_o} = |S_2(\theta)|^2 . \tag{3.3b}$$

To study the bistatic behavior, the two equations were programmed and computed at $\theta = 0(5)180^o$ for ka = 4.28 and for those values of ka at which the

*as well as for a cylinder with central loading of length λ or longer.

oscillations in the back scattering cross section for an unloaded sphere (see Fig. 3-1) have the extremum values. These correspond to ka = 1.03, 2.33, 3.55, etc. for the maxima and ka = 1.75, 2.96, 4.16, etc. for the minima. Two slot positions $\theta_o = 30^o$ and $\theta_o = 90^o$ were considered and the loading for zero scattering in the back direction ($\theta = 0$) was chosen. With $\theta_o = 30^o$ the loading is always passive, but with $\theta_o = 90^o$ there are values of ka where active loading is required and such, for example, is needed at ka = 2.33.

Sample calculations for ka = 1.03 with $\theta_o = 30^o$ and 90^o are shown in Figs. 3-24 through 3-27 and for ka = 4.28 with $\theta_o = 90^o$ in Figs. 3-28 and 3-29. Included, for comparison purposes, are the scattering patterns for the corresponding unloaded cases.

From these patterns, and the others that were computed, we can now estimate the beamwidths for the minima in the back scattering direction. For example, for ka = 1.03 and with $\theta_o = 30^o$ we find from Figs. 3-24 and 3-25 (dashed curves) that the total beamwidths for 20 db reduction are about 55^o and 56^o in the E-plane and H-plane respectively. Similarly, the values were estimated from the other patterns and are presented for $0 < ka < 10$ with $\theta_o = 30^o$ and $\theta_o = 90^o$ in Figs. 3-30 through 3-33. The limiting value as $ka \to 0$ is obtained from the asymptotic analysis in Section 2.5. The beamwidths are always maximum at ka = 0 and then decrease in an oscillatory manner with an increasing ka. The maximum and minimum of these oscillations occur at the same values of ka as those in the back scattering cross section for an unloaded sphere (Fig. 3-1). In general, the beamwidths are wider in the H-plane than the E-plane and overall there is about a 50 percent improvement with the slot at 30^o as compared to that at $\theta_o = 90^o$.

In the above discussion, there has been no reason to restrict the loading to zero back scattering. For instance, if we choose a loading for zero scattering in the direction $\theta = 30^o$ (in the E-plane) rather than $\theta = 0^o$, a wider beamwidth in the back scattering direction can be obtained. As shown in Fig. 3-24 (long dashes) there is almost a 30 percent improvement in the beamwidth in the E-plane, but the

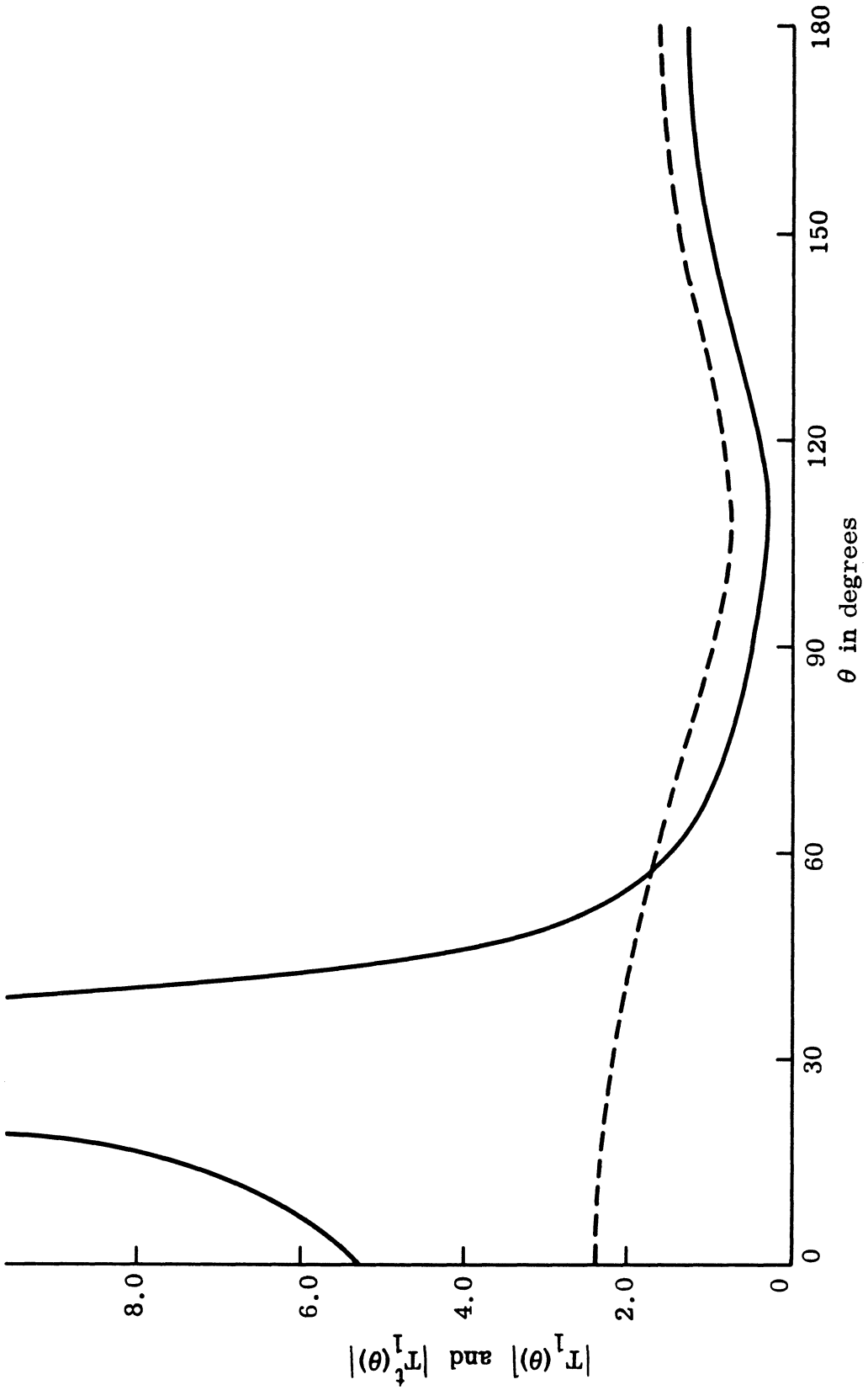

FIG. 3-20: AMPLITUDES OF SURFACE FIELD COMPONENTS FOR SPHERE LOADED FOR ZERO BACK SCATTERING (——) AND UNLOADED (– – –) SPHERE: ka = 1.03, $[Y_\ell/Y]_0 = 0.845 + i11.952$, $\theta_o = 30.$

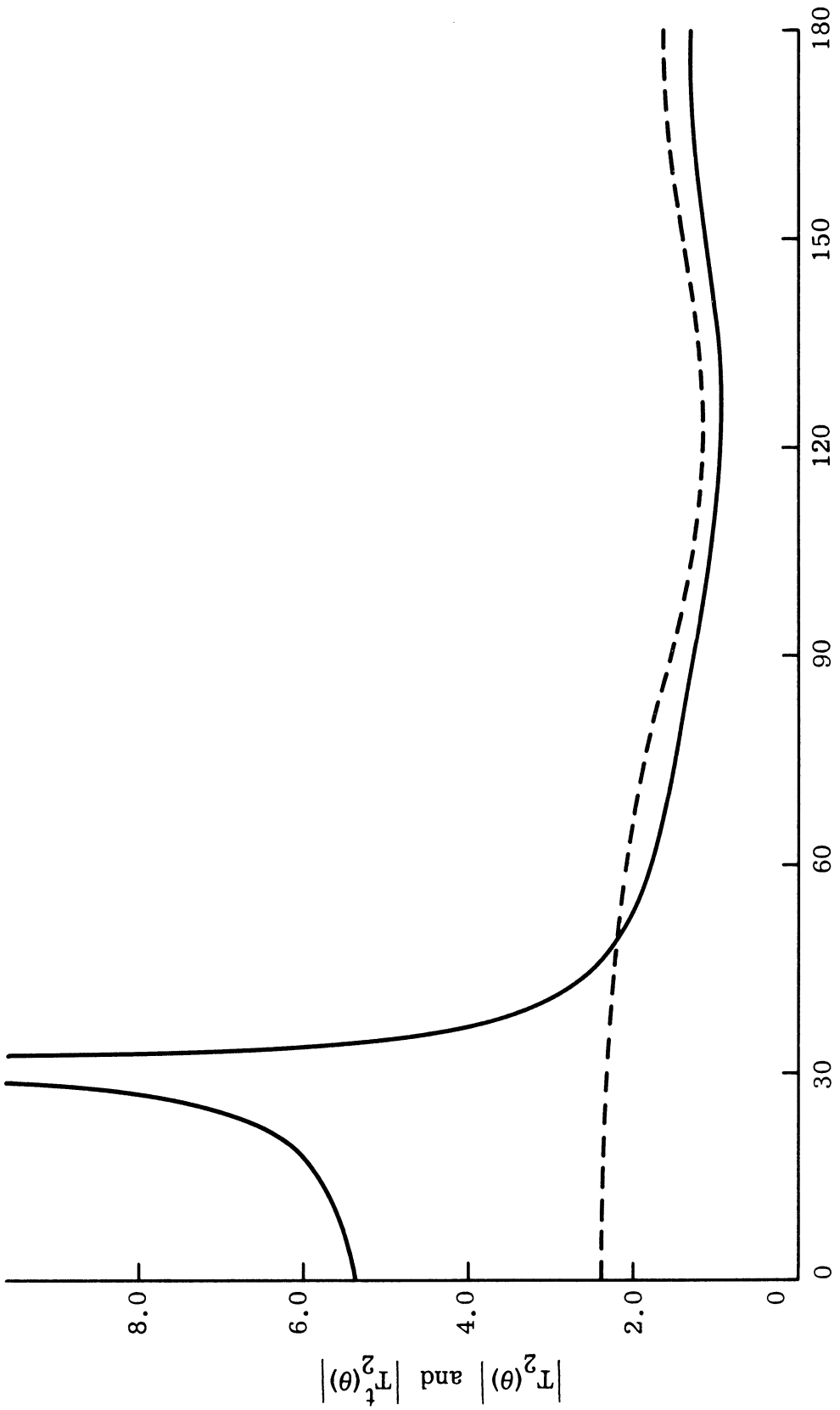

FIG. 3-21: AMPLITUDES OF SURFACE FIELD COMPONENT FOR SPHERE LOADED FOR ZERO BACK SCATTERING (——) AND UNLOADED (- - -) SPHERE: ka = 1.03, $\left[Y_\ell/Y\right]_0 = 0.847 + i11.952$, $\theta_o = 30^o$.

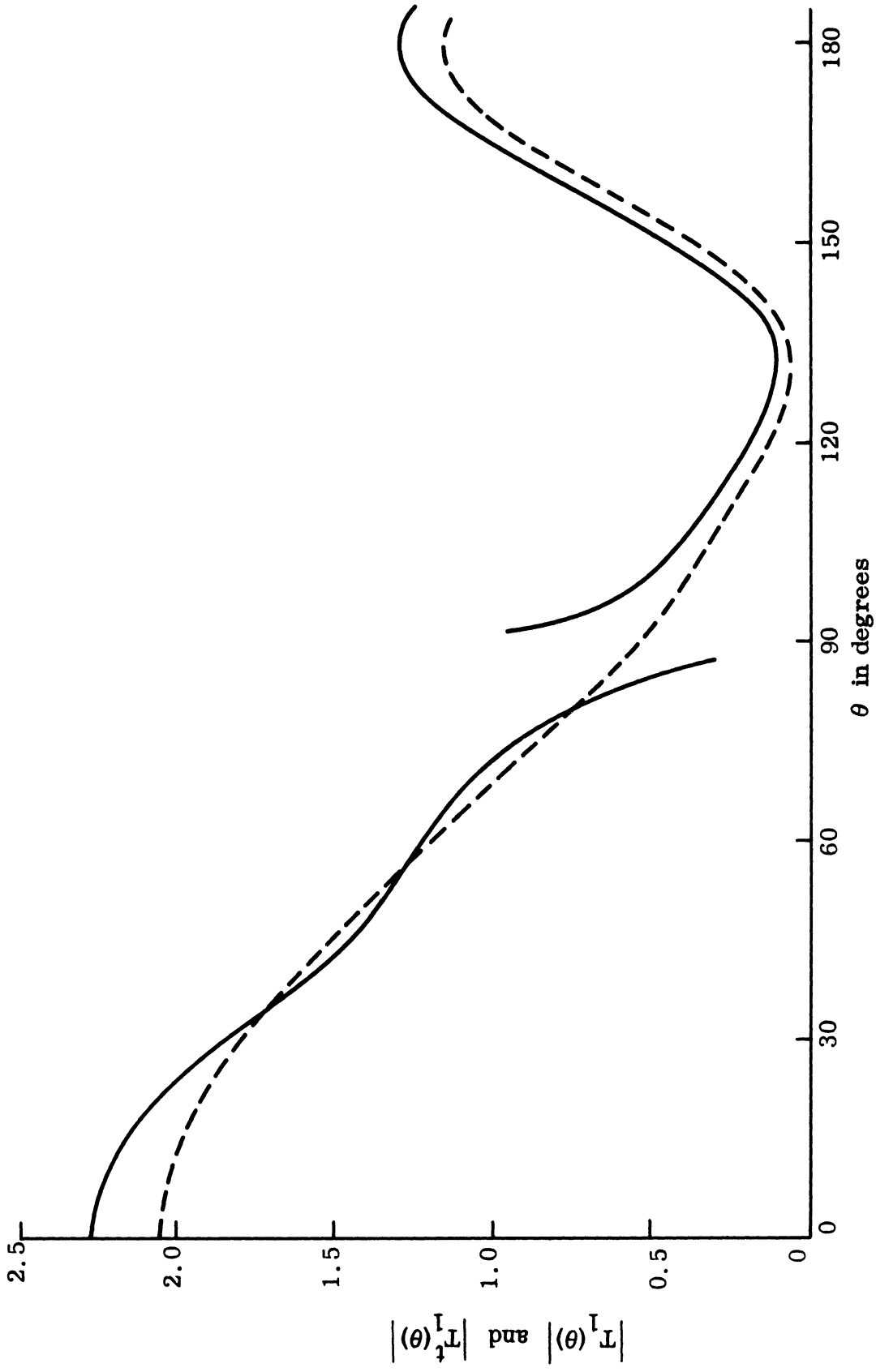

FIG. 3-22: AMPLITUDES OF SURFACE FIELD COMPONENT FOR SPHERE LOADED FOR ZERO BACK SCATTERING (——) AND UNLOADED (– – –) SPHERE: ka = 4.28, $\left[Y_\ell/Y\right]_0 = -163.742$, $\theta_o = 90^o$.

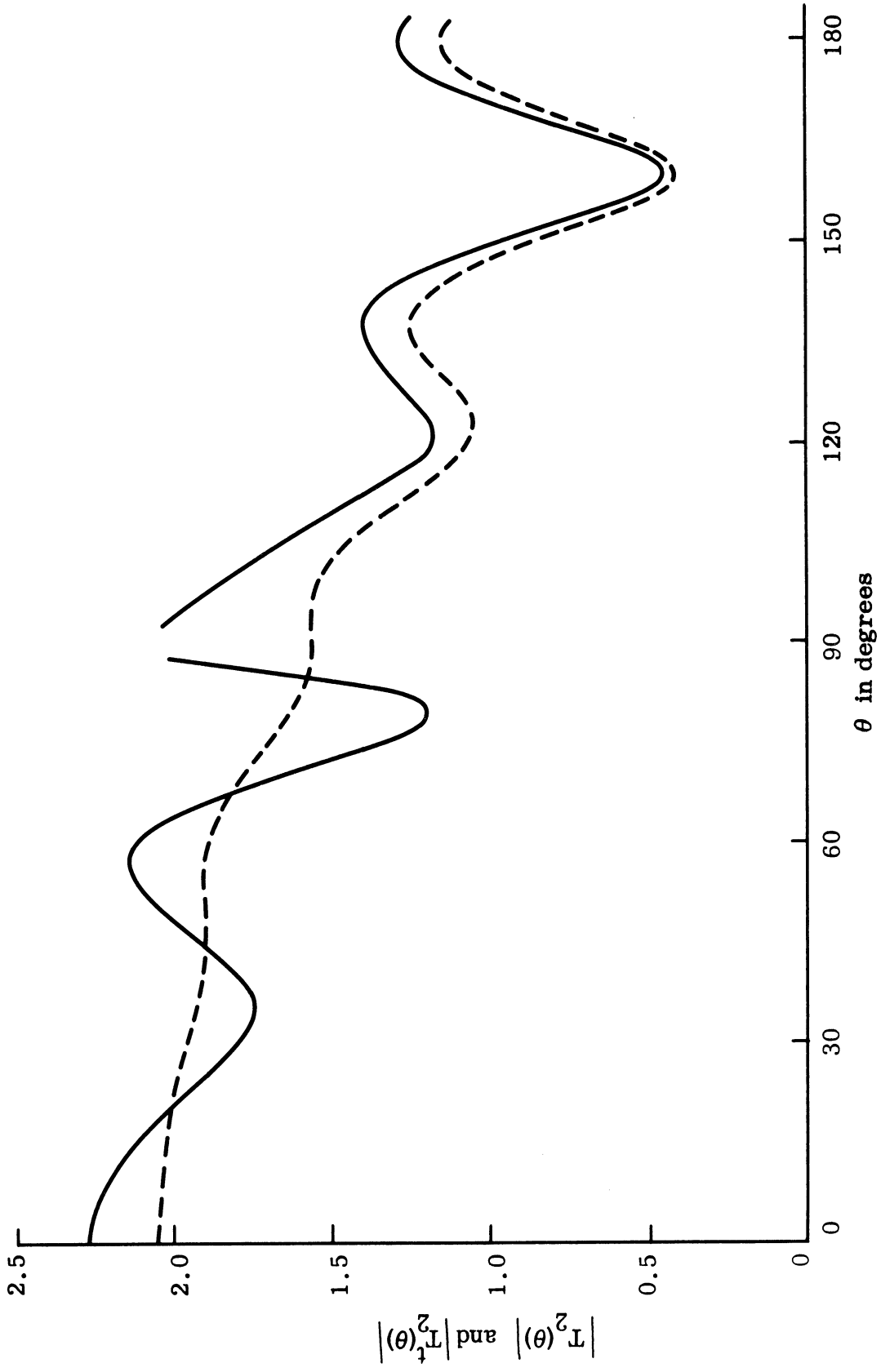

FIG. 3-23: AMPLITUDES OF SURFACE FIELD COMPONENT FOR SPHERE LOADED FOR ZERO BACK SCATTERING (——) AND UNLOADED (- - -) SPHERE: ka = 4.28, $\left[Y_\ell/Y\right]_0$ = -i63.742, $\theta_o = 90^o$.

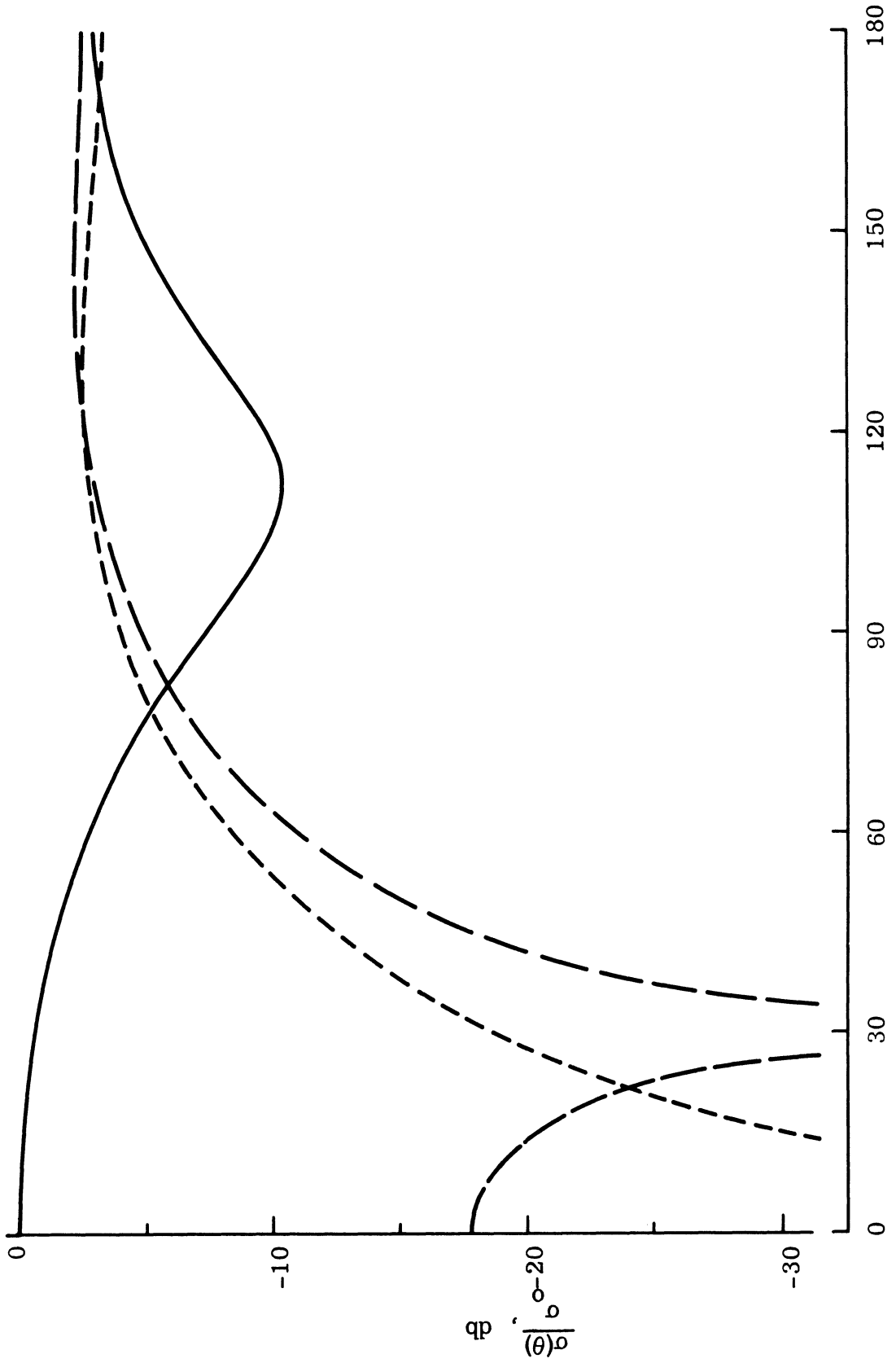

FIG. 3-24: RELATIVE BISTATIC SCATTERING CROSS SECTION IN E-PLANE ($\phi = 0$) FOR LOADED (- -, — —) AND UNLOADED (——) SPHERE: ka = 1.03 AND $\theta_o = 30^o$.

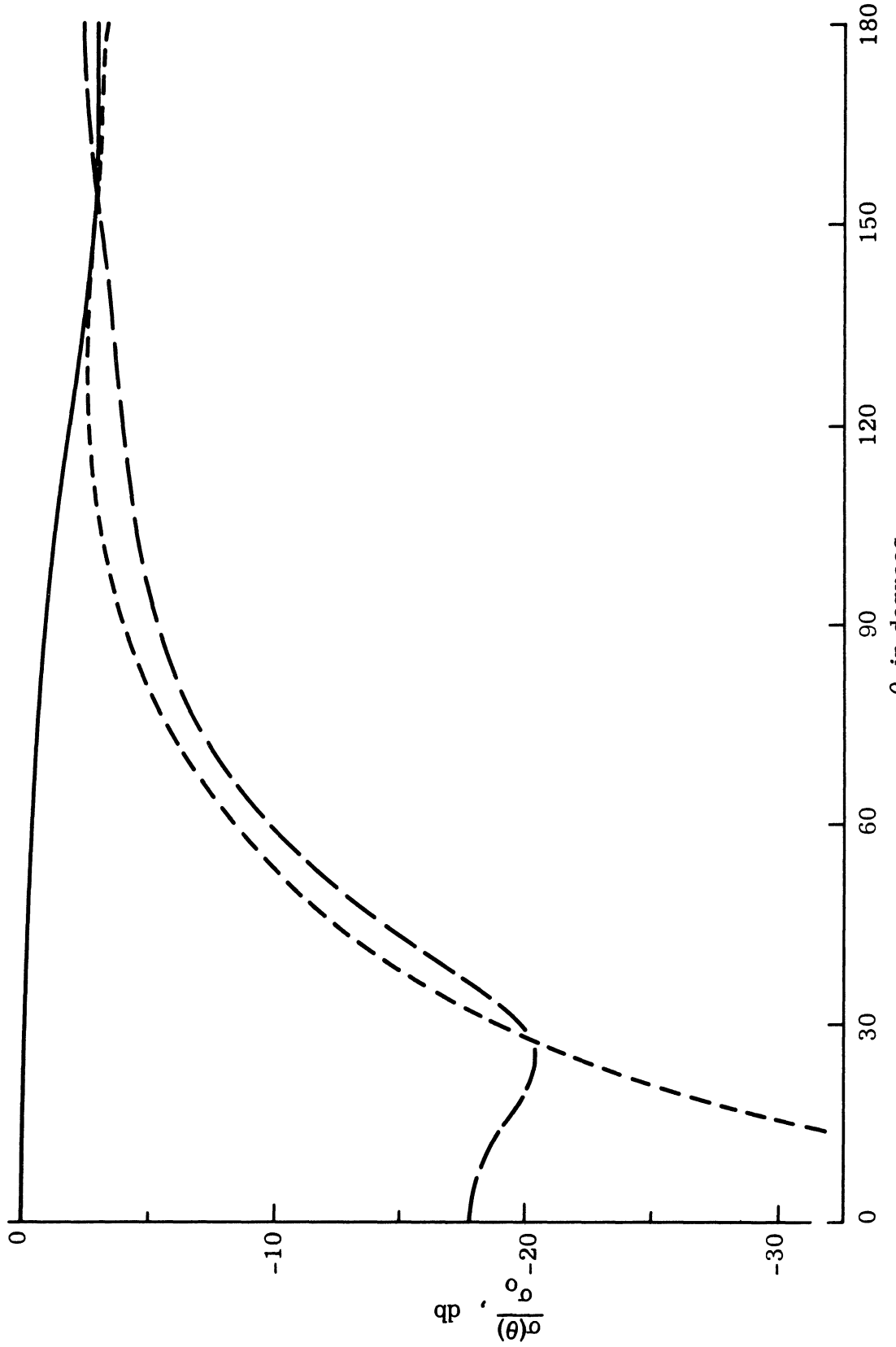

FIG. 3-25: RELATIVE BISTATIC SCATTERING CROSS SECTION IN H-PLANE ($\phi = \pi/2$) FOR LOADED (- - -, — — —) AND UNLOADED (——) SPHERE: ka = 1.03 AND $\theta_o = 30^o$.

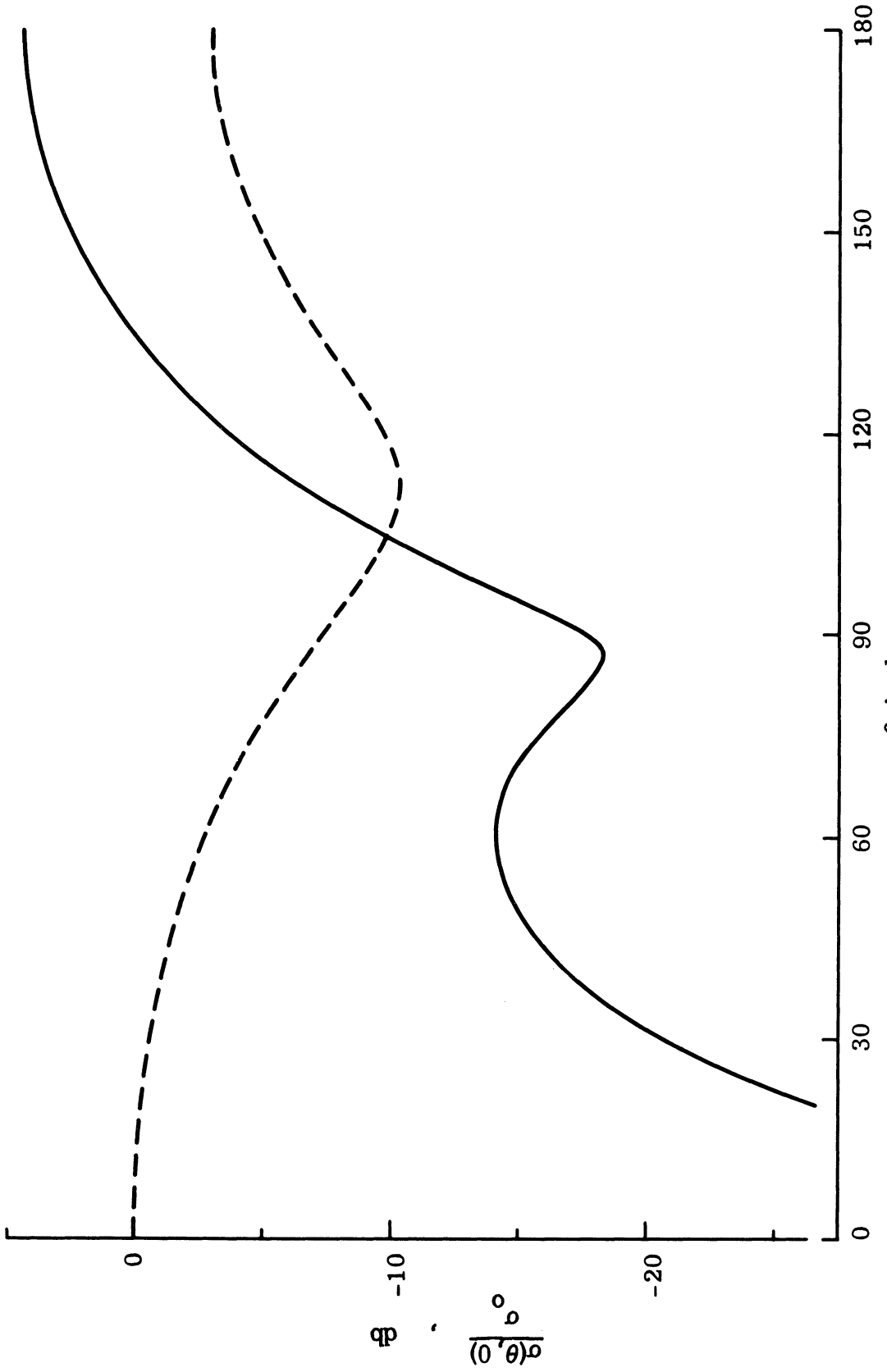

FIG. 3-26: RELATIVE BISTATIC SCATTERING CROSS SECTION IN E-PLANE ($\phi = 0$) FOR LOADED (——) AND UNLOADED (- - -) SPHERE: ka = 1.03 AND $\theta_o = 90^o$.

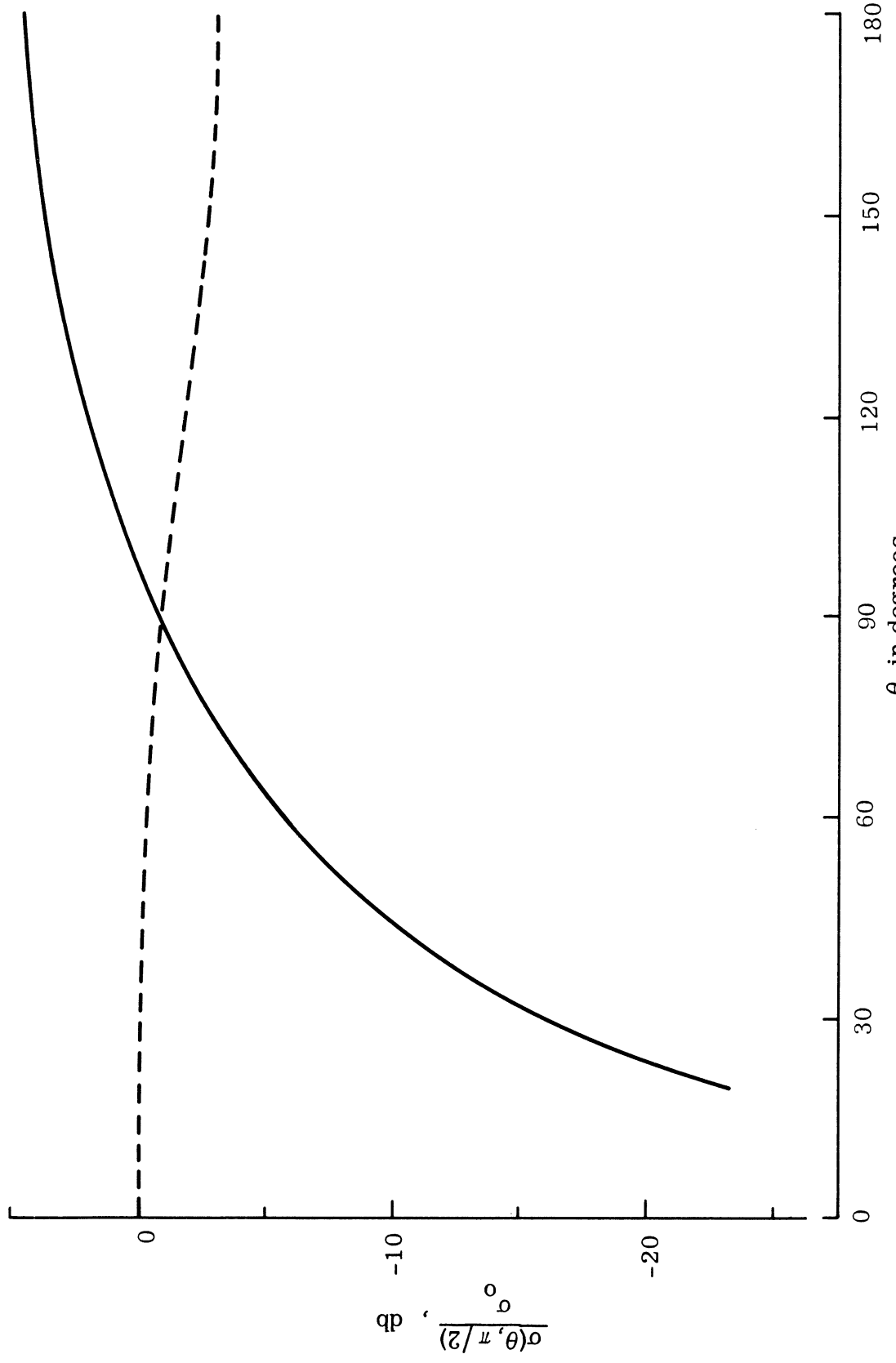

FIG. 3-27: RELATIVE BISTATIC SCATTERING CROSS SECTION IN H-PLANE ($\phi = \pi/2$) FOR LOADED (——) AND UNLOADED (– – –) SPHERE: ka = 1.03 AND $\theta_o = 90^o$.

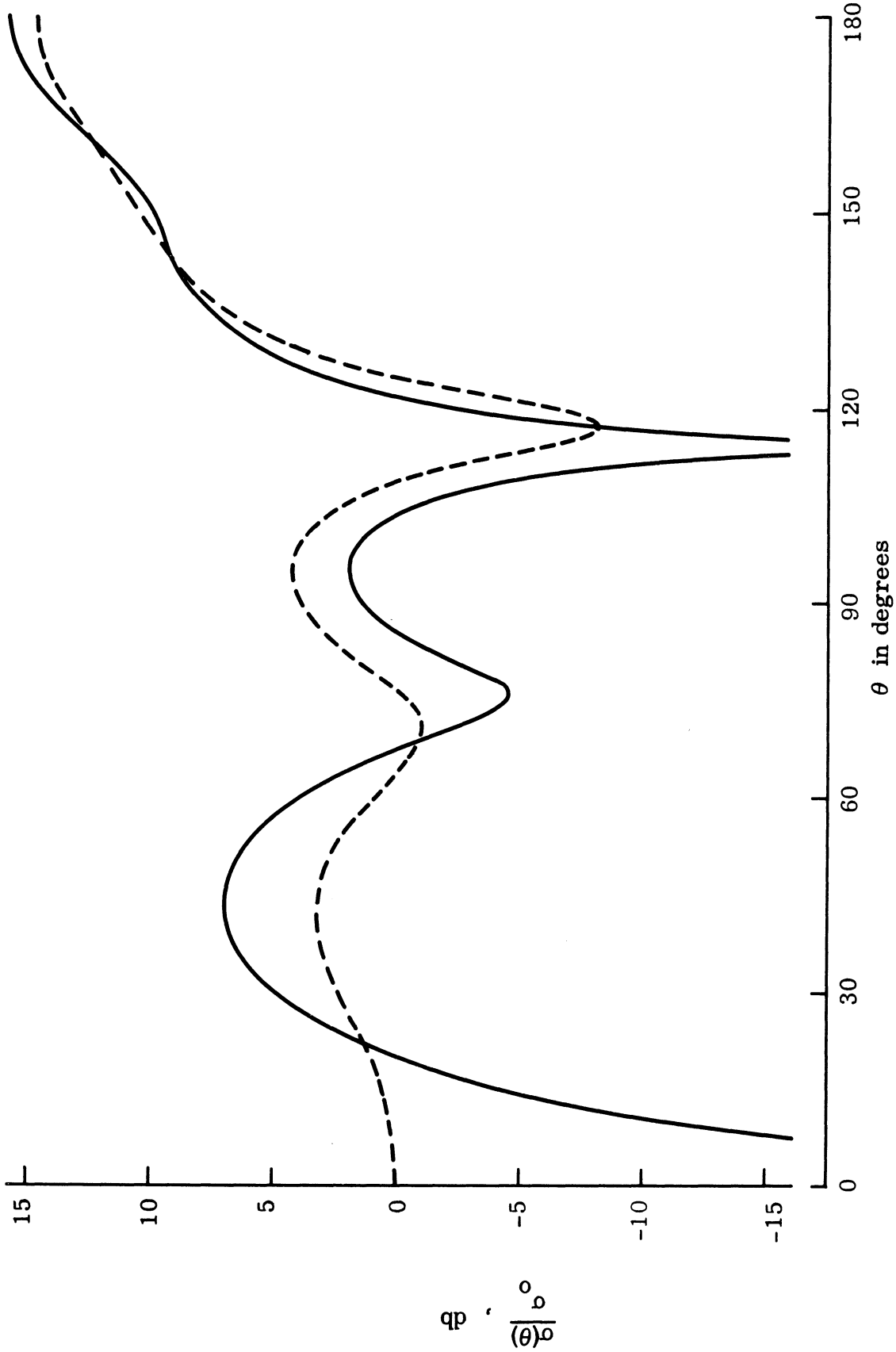

FIG. 3-28: RELATIVE BISTATIC SCATTERING CROSS SECTION IN E-PLANE ($\phi = 0$) FOR LOADED (——) AND UNLOADED (– – –) SPHERE: ka = 4.28 AND $\theta_o = 90^o$.

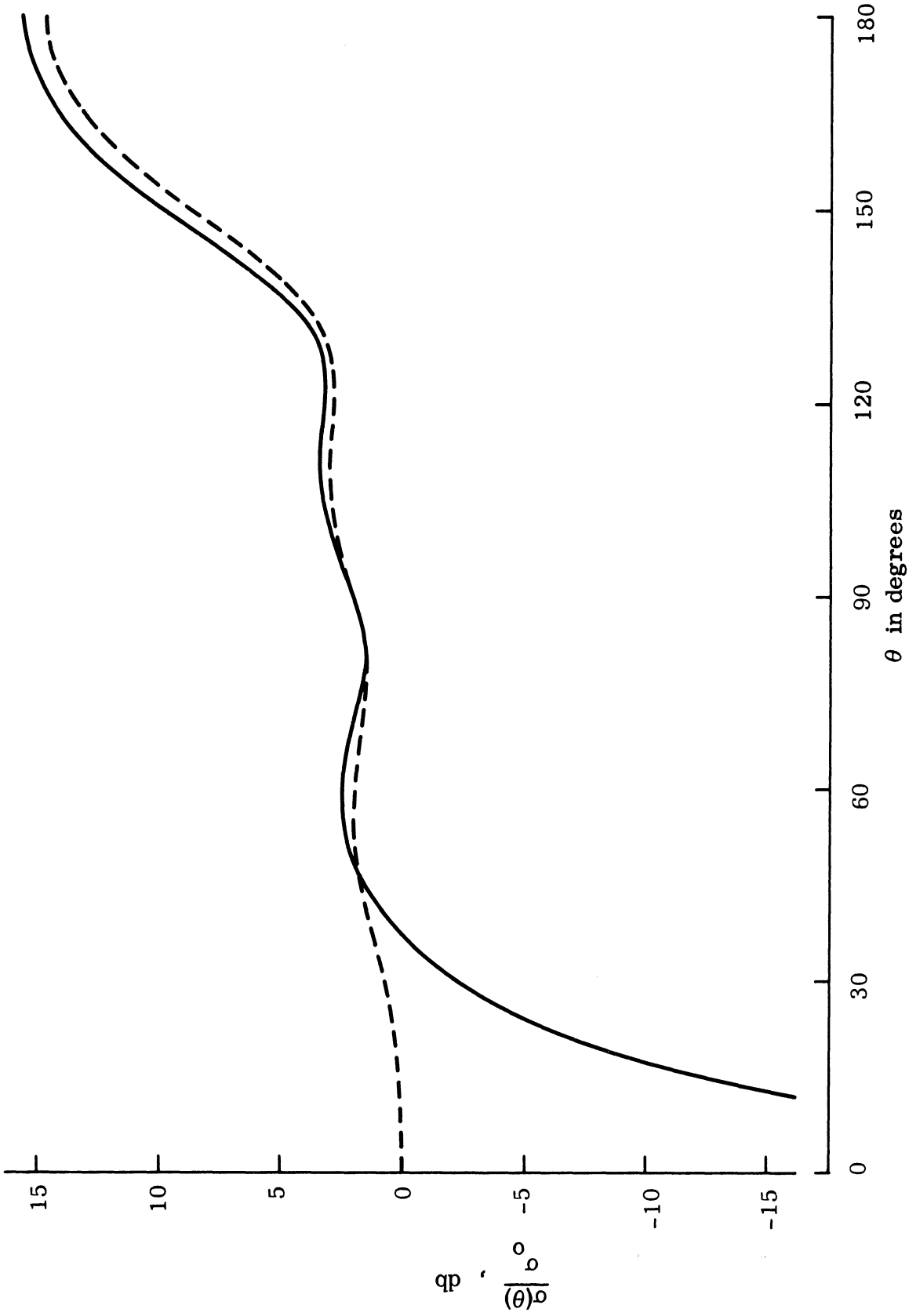

FIG. 3-29: RELATIVE BISTATIC SCATTERING CROSS SECTION IN H-PLANE ($\phi = \pi/2$) FOR LOADED (——) AND UNLOADED (– – –) SPHERE: ka = 4.28 AND $\theta_o = 90^o$.

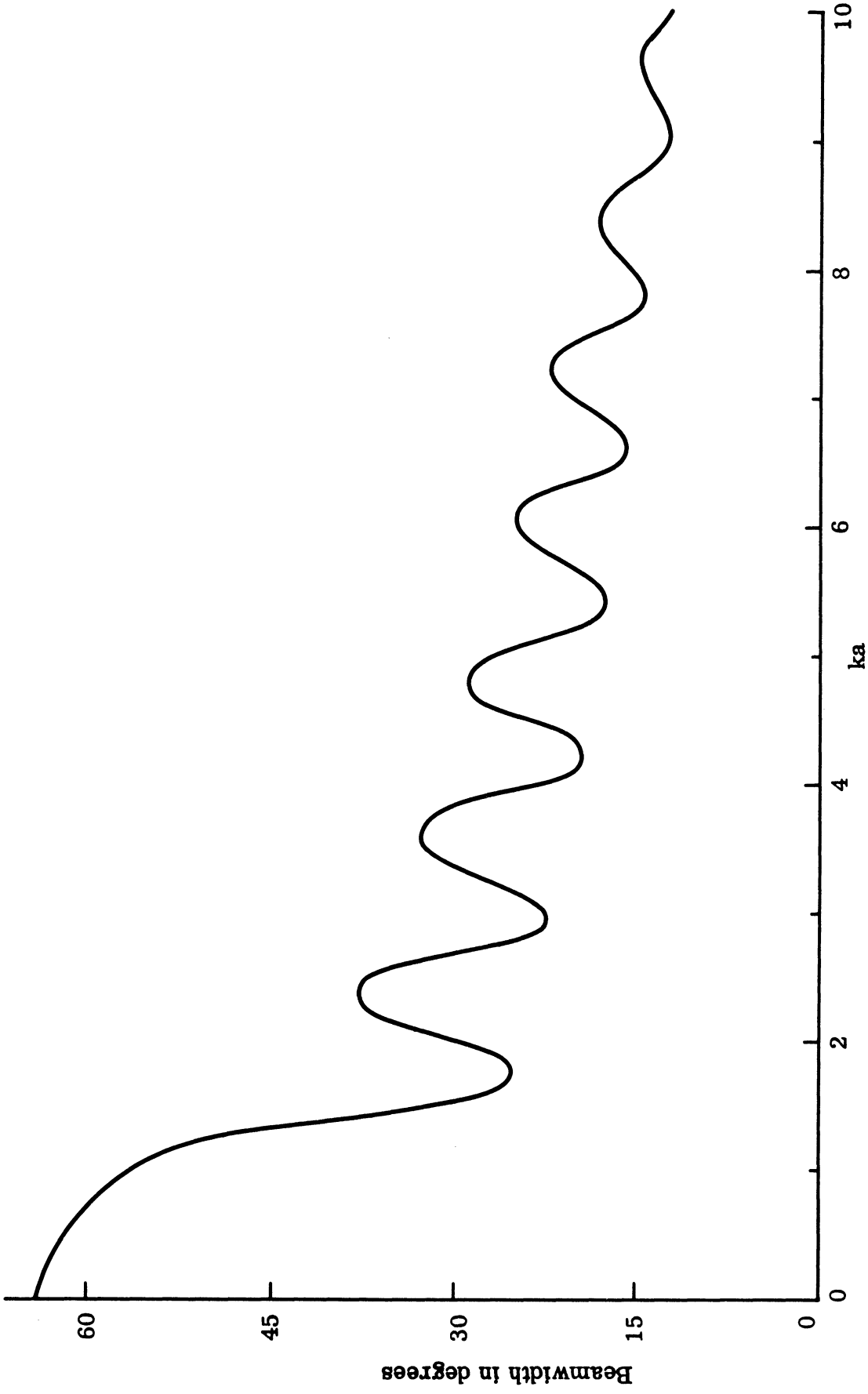

FIG. 3-30: EXPECTED BEAMWIDTH FOR 20 db REDUCTION IN E-PLANE ($\phi = 0$) WITH LOADING FOR ZERO BACK SCATTERING AT $\theta_o = 30^o$.

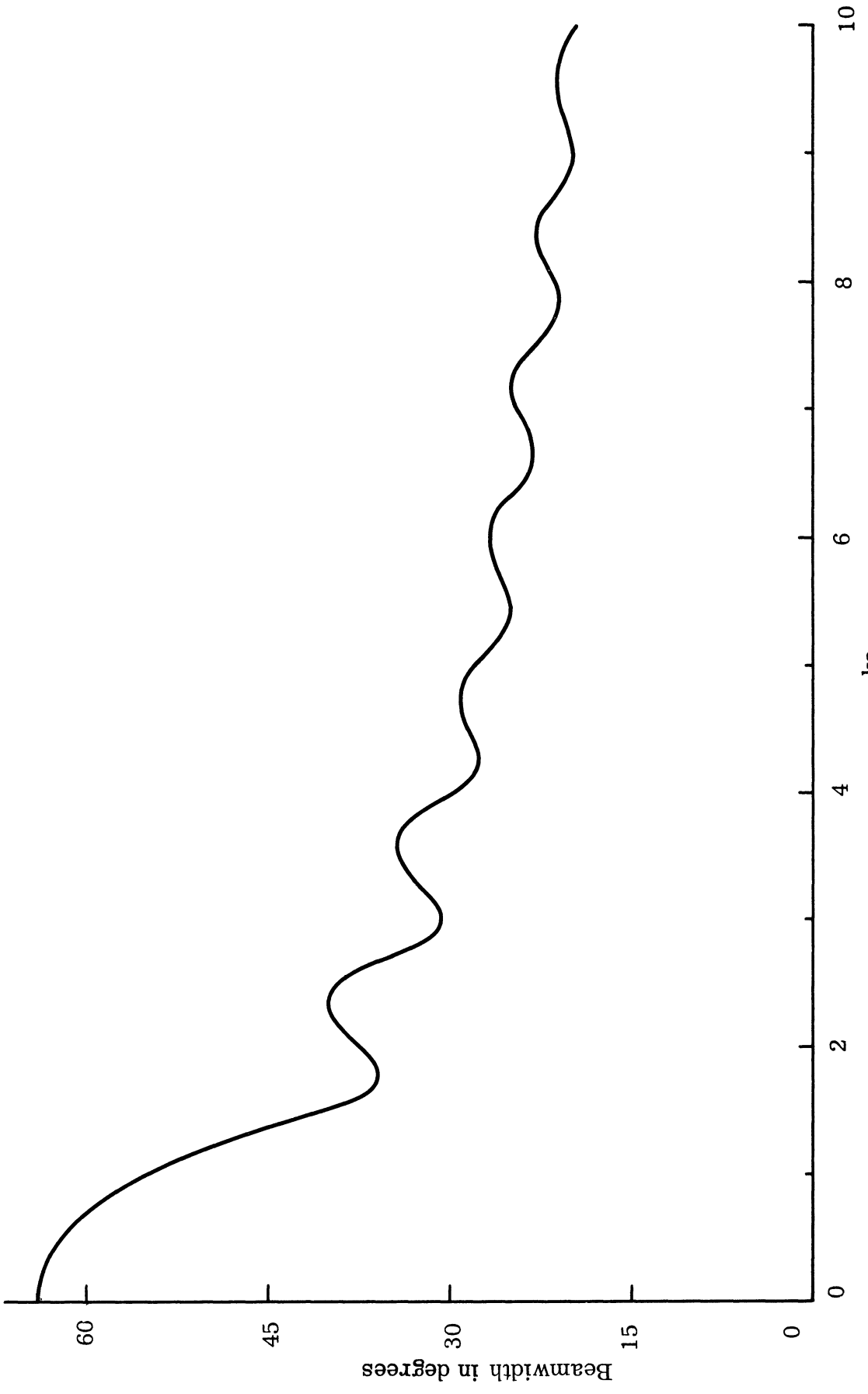

FIG. 3-31: EXPECTED BEAMWIDTH FOR 20 db REDUCTION IN H-PLANE ($\phi = \pi/2$) WITH LOADING FOR ZERO BACK SCATTERING AT $\theta_o = 30^o$.

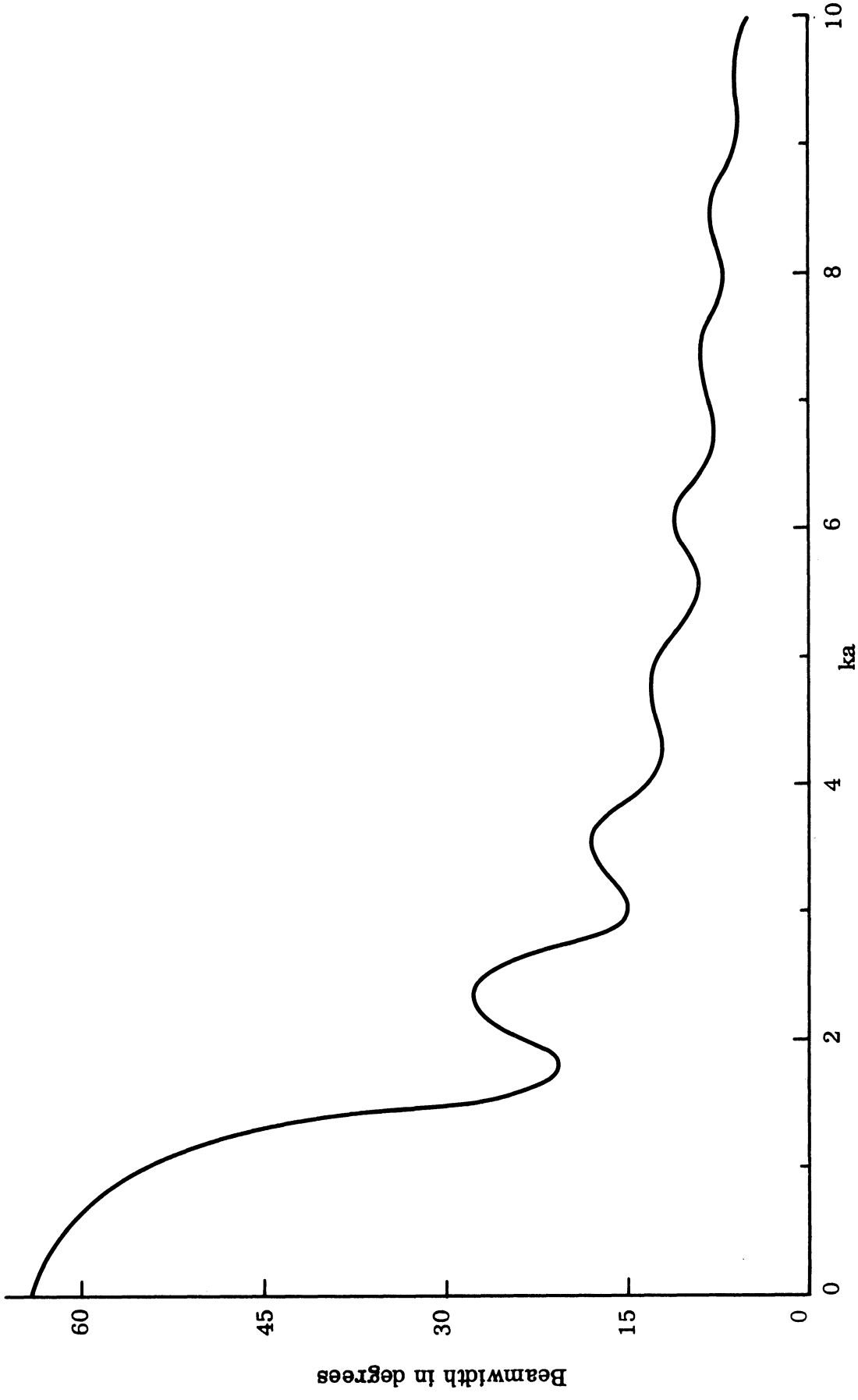

FIG. 3-32: EXPECTED BEAMWIDTH FOR 20 db REDUCTION IN E-PLANE ($\phi = 0$) WITH LOADING FOR ZERO BACK SCATTERING AT $\theta_o = 90^o$.

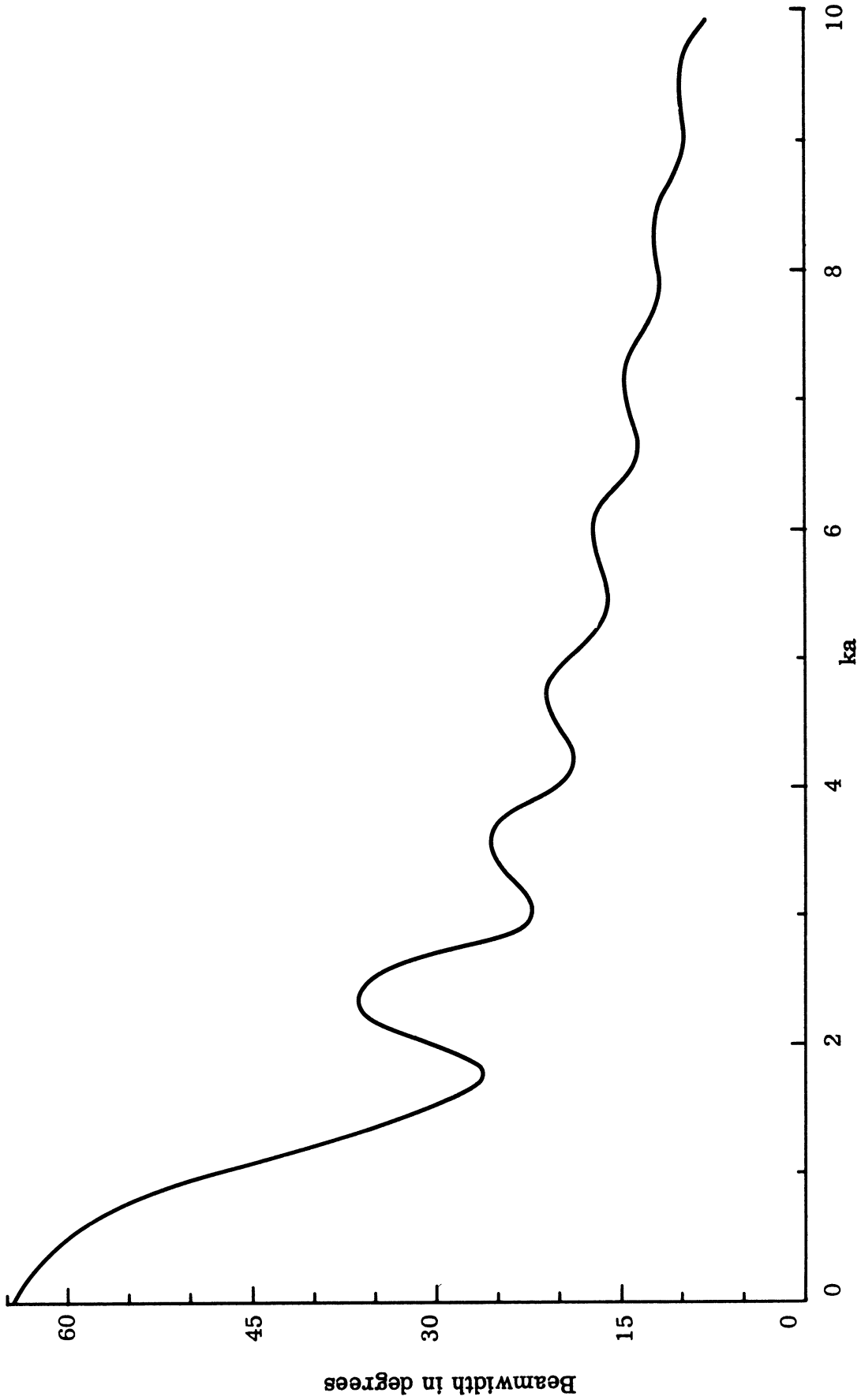

FIG. 3-33: EXPECTED BEAMWIDTH FOR 20 db REDUCTION IN H-PLANE ($\phi = \pi/2$) WITH LOADING FOR ZERO BACK SCATTERING AT $\theta_o = 90^o$.

reduction at $\theta = 0^{o}$ is 18 db as compared with the previous value of $-\infty$ db. In the H-plane there is no change in the beamwidth. If there is a need to increase the beamwidth in the H-plane, rather than the E-plane, one simply must choose the loading accordingly.

CHAPTER IV

EXPERIMENTAL STUDIES

4.1 Experimental Model

To confirm the theoretical predictions, a series of measurements were carried out on a sphere with a circumferential cavity backed slot. The model consisted of two identical solid aluminum caps joined together by means of a partially threaded shaft at the center (Figs. 4-1 and 4-2) but spaced 1/16 inch apart to form a radial cavity of the same width. The cavity was shorted at the center and the diameter of this short was determined by the size of the disc used. In all, there were 21 such discs available, and with these the inner diameter could be varied from 0.3125 inches (diameter of the shaft) to 3.133 inches (diameter of the sphere). The discs were cut from 1/16 inch aluminum sheet and except for the outer edge, had a slight undercut in thickness for positive metallic contact. At the surface of the sphere, the slot subtended an angle of approximately 2.25^{o} or 0.0392 radians.

4.2 Back Scattering vs. Loading

The back scattering measurements were made with the above model at several S- and C-band frequencies corresponding to values of ka = 2.340, 3.004, 3.090, 3.198 and 4.280. Conventional cw equipment in an anechoic room was used, except that the azimuth-amplitude recorder was replaced by a HP 415B meter for greater accuracy in reading. At each frequency, the back scattering was determined for a number of shorting discs of different diameters and the values were calibrated with respect to the back scattering from the unloaded sphere. The results are summarized in Table 4-1. The resulting normalized cross sections were then related to the cavity loading by converting the disc diameters for a given frequency to equivalent loading admittances using the formula derived in Appendix B. The results were then compared with the theoretical values computed from equation (2.28) with $\theta_o = 90^{o}$ and $\theta = 0^{o}$. The agreement was extremely gratifying.

Two sets of results are plotted in Figs. 4-3 and 4-4 for ka = 2.34 and ka = 4.28 respectively. The choice of ka is such as to present a reasonable description of the susceptive loading. When ka = 2.34, zero back scattering requires

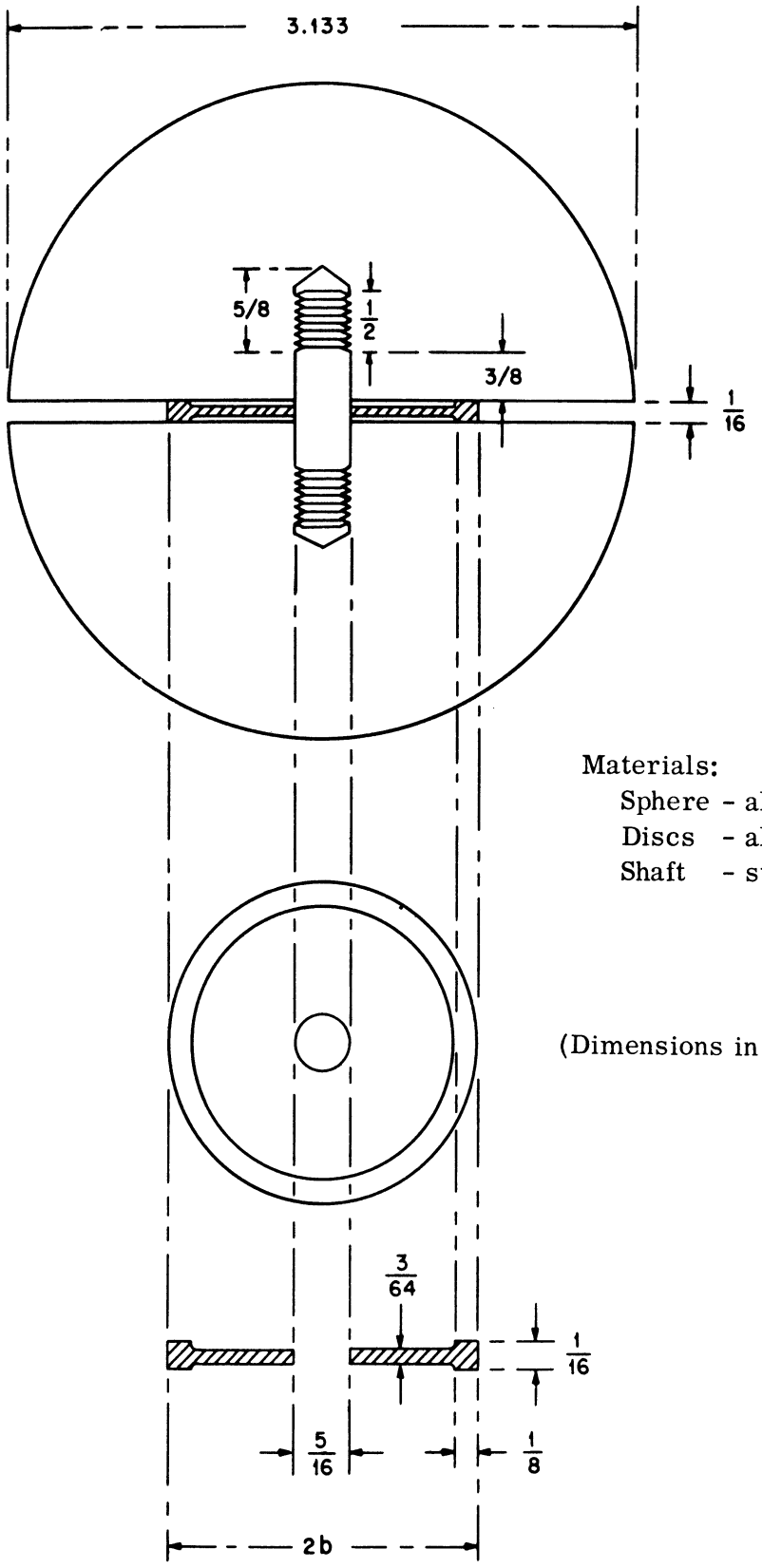

2b
0.500
0.625
0.750
0.875
1.000
1.125
1.250
1.375
1.500
1.625
1.750
1.875
2.000
2.125
2.250
2.375
2.500
2.625
2.750
2.875
3.133

Materials:
Sphere - aluminum
Discs - aluminum
Shaft - steel

(Dimensions in inches)

FIG. 4-1: SECTORIAL VIEW OF MODEL

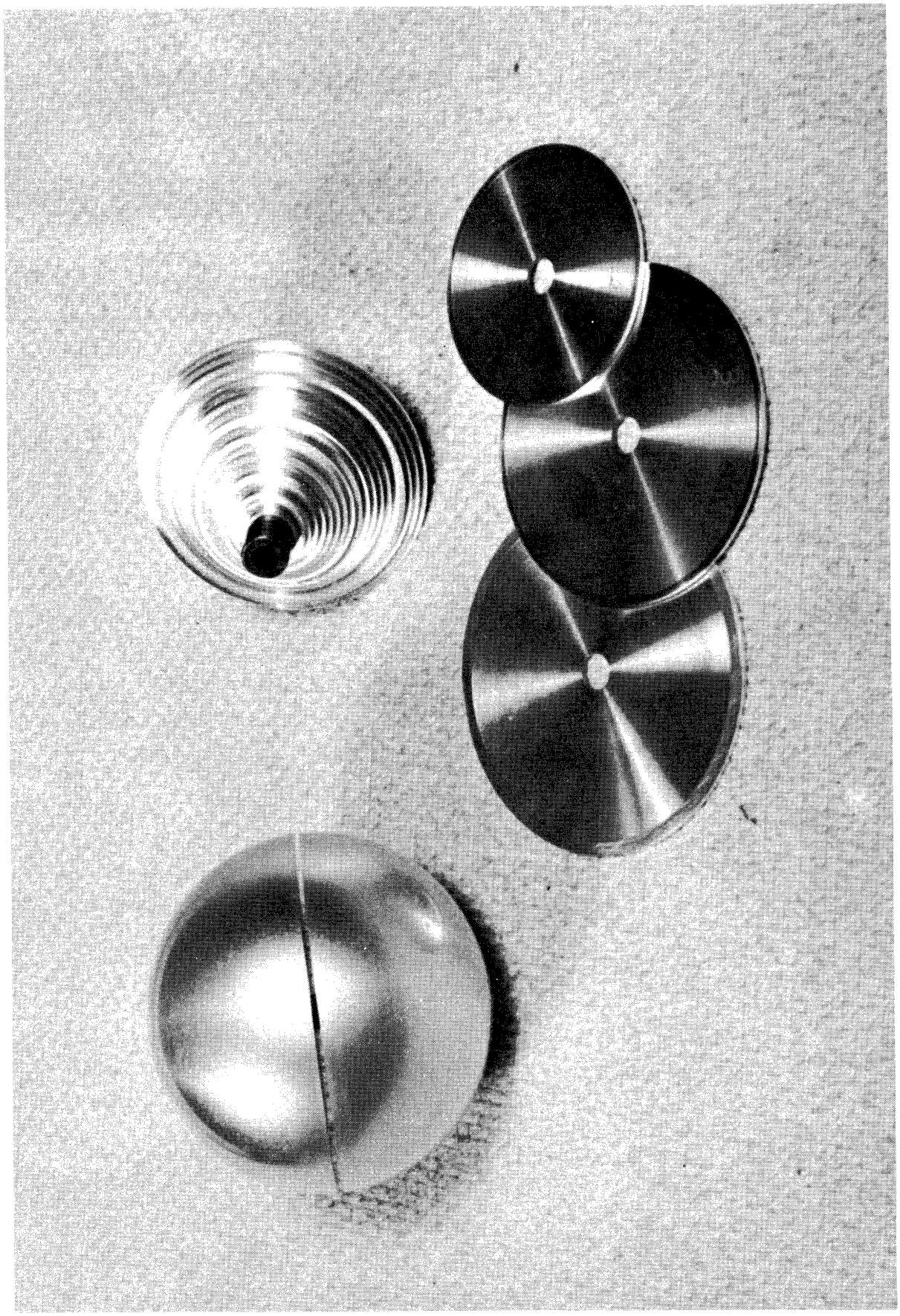

FIG. 4-2: EXPERIMENTAL MODEL

TABLE 4-1: EXPERIMENTAL DATA

Shorting disc diameter 2b, inches	Relative Return,* db				
	2.808 Gc	3.605 Gc	3.709 Gc	3.838 Gc	5.136 Gc
.3125	-0.7	-1.5	-0.7	-0.8	
.500	-0.8	-1.7	-1.7	-1.1	
.625	-0.7	-1.9	-1.8		
.750	-0.7	-2.3		-1.3	
.875	-0.6	-2.5	-2.5	-1.6	
1.000	0.0	-3.3	-2.5		
1.125	2.3	-3.8	-3.0	-2.0	
1.250	7.5	-5.6	-3.5	-2.4	1.3
1.375	6.1	-8.0	-5.6	-3.4	
1.500	3.2	-13.4	-9.4	-4.6	1.9
1.625	2.2	-0.8	-14.7	-9.6	2.3
1.750	1.6	10.4	6.4	-5.4	2.8
1.875	1.3	7.0	7.0	7.0	3.7
2.000	1.0	4.5	4.4	4.3	5.3
2.125					8.2
2.250					-2.5
2.375					-11.7
2.500	0.5	1.4	1.0	1.1	-4.8
2.625					-2.8
2.750					-1.8
2.875					-1.0
3.133	0.0	0.0	0.0	0.0	0.0

*relative to the unslotted sphere

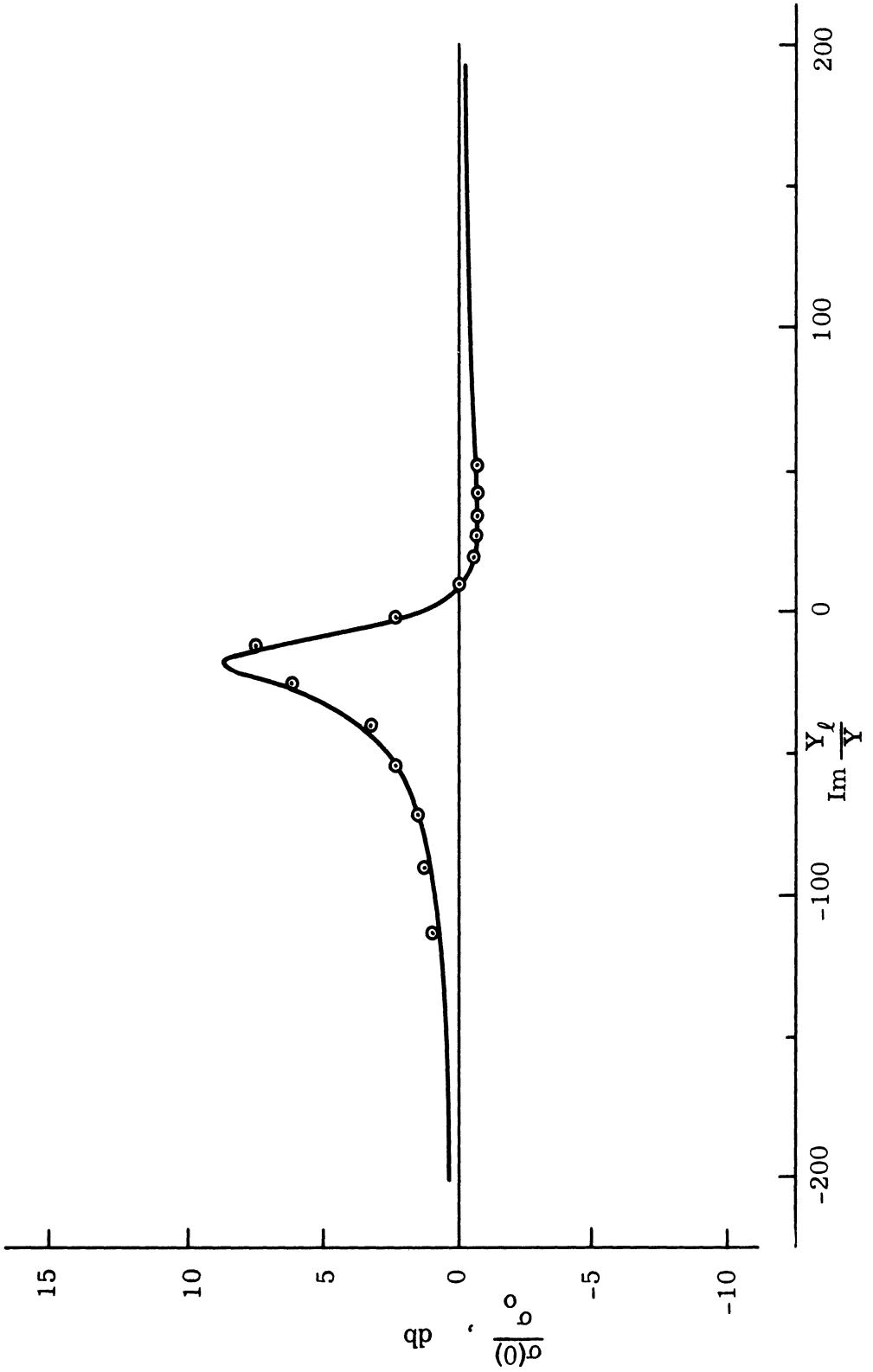

FIG. 4-3: THEORETICAL (——) AND EXPERIMENTAL (∘ ∘ ∘) RELATIVE BACK SCATTERING CROSS SECTIONS WITH SUSCEPTIVE LOADING: ka = 2.34 AND $\theta_o = 90^o$.

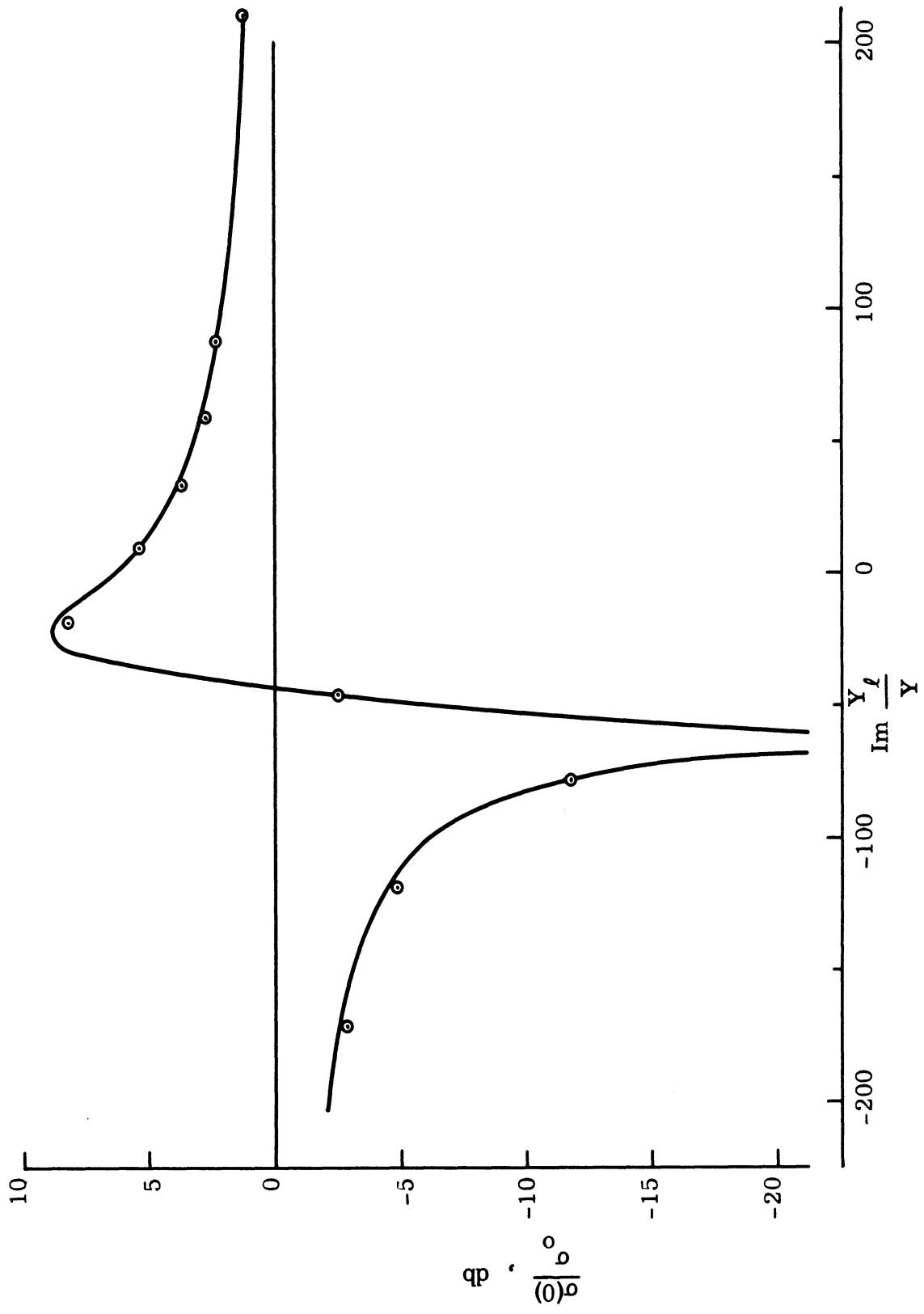

FIG. 4-4: THEORETICAL (——) AND EXPERIMENTAL (⊙⊙⊙) RELATIVE BACK SCATTERING CROSS SECTIONS WITH SUSCEPTIVE LOADING: ka = 4.28 AND $\theta_o = 90^o$.

a loading with a large negative real part (Fig. 3-9) but this, of course, is unattainable with this or any other passive cavity or network. As Fig. 4-3 indicates, there is no substantial cross section reduction (0.6 db at most), but an increase of 8.7 db is achievable for a particular value of $\text{Im}\,\frac{Y_\ell}{Y}$. Since, according to the results of Section 3.3, maximum enhancement always demands a susceptive load and maximum reduction requires a susceptive load whenever $\text{Re}\,\frac{Y_\ell}{Y}(0) < 0$, the peak and the minimum measured here are the extreme values attainable with a passive load. They agree with those predicted in Fig. 3-18. When ka = 4.28, the required loading for zero back scattering is susceptive (Fig. 3-9), and this is attainable from the cavity. The theoretical results in Fig. 4-4 show a complete cross section reduction, but since a disc for this particular susceptance was not available, the one nearest to it gave 11.7 db reduction in cross section. (For the experiment described in the next section, a shorting disc was especially made to supply a susceptance for zero back scattering, and with this over 20 db reduction in cross section resulted.) For maximum return, an enhancement of 8.8 db was expected for a particular value of susceptance and with a disc nearest to it, 8.0 db was attained.

Another value of ka for which a complete reduction in back scattering cross section can be attained with a susceptive load is ka = 3.090. The results are similar to those for ka = 4.280 (Table 4-1) except for the reversal of the peak and a null about $Y_\ell = 0$. This reversal is attributed to the sign change of $S_1^s(0)$ in equation (2.28) as ka changes from 3.090 to 4.280 while the values for $T_2(\pi/2)$ and $a\,S_1^r(0, \pi/2)$ remain essentially unchanged.

4.3 Back Scattering vs. Rotation

Although the analysis in Chapters II and III was limited to the case of a field incident in a direction perpendicular to the plane of the slot, no such constraint existed in the experimental study. Therefore it seems a worthwhile effort to carry out a sample measurement of a back scattering cross section as a function of rotation of a slotted sphere. For this a frequency corresponding to ka = 4.28 (5.136 Gc) was chosen. To obtain the loading required for the null in Fig. 4-4, a new shorting

disc of the requisite diameter was cut. The sphere was mounted on a pedestal with the slot in the vertical plane, and back scattering measurements were made for both horizontal and vertical polarizations. The results, along with the measured values for the unloaded sphere are presented in Figs. 4-5 and 4-6. The large cross section reductions are clearly evident. For both polarizations, the reduction is on the order of 22 db and although theoretically it should be infinite, the minor peaking at the center of the minimum could be caused by a small deviation in the optimum dimension of the shorting disc. However, in view of the slightly different magnitudes of cross sections for zero rotation, a more likely source of the residual contribution could be sphere-pedestal interaction, room effect, or both.

Within, say, 30^{o} of zero rotation there are obvious similarities between the back scattering patterns measured here and the bistatic patterns computed in Section 3.4. The horizontal polarization pattern (Fig. 4-3) is similar to the bistatic E-plane plot (Fig. 3-24) and the vertical polarization pattern (Fig. 4-4), to the bistatic H-plane plot (Fig. 3-25). The measured null widths are in good agreement with the corresponding bistatic values and the 5 db enhancement that was measured for the horizontal polarization is also evident in the E-plane bistatic plot.

4.4 Surface Field Measurements

To supplement the back scattering data, the surface fields were measured on a loaded, as well as an unloaded, sphere. The facility and equipment required to perform such measurements are not as common as those generally encountered in routine back scattering work and therefore a short discussion of the current measurement facility is in order.

4.4.1 Development of the Surface Field Measurement Facility

About three years ago, a limited program to study the feasibility of measuring surface fields on three dimensional objects was initiated at the Radiation Laboratory. The primary purpose of this project was to establish the basic requirements for designing a surface field measurement facility and to gain experience in the measurement techniques involved. Up to that time, there was little

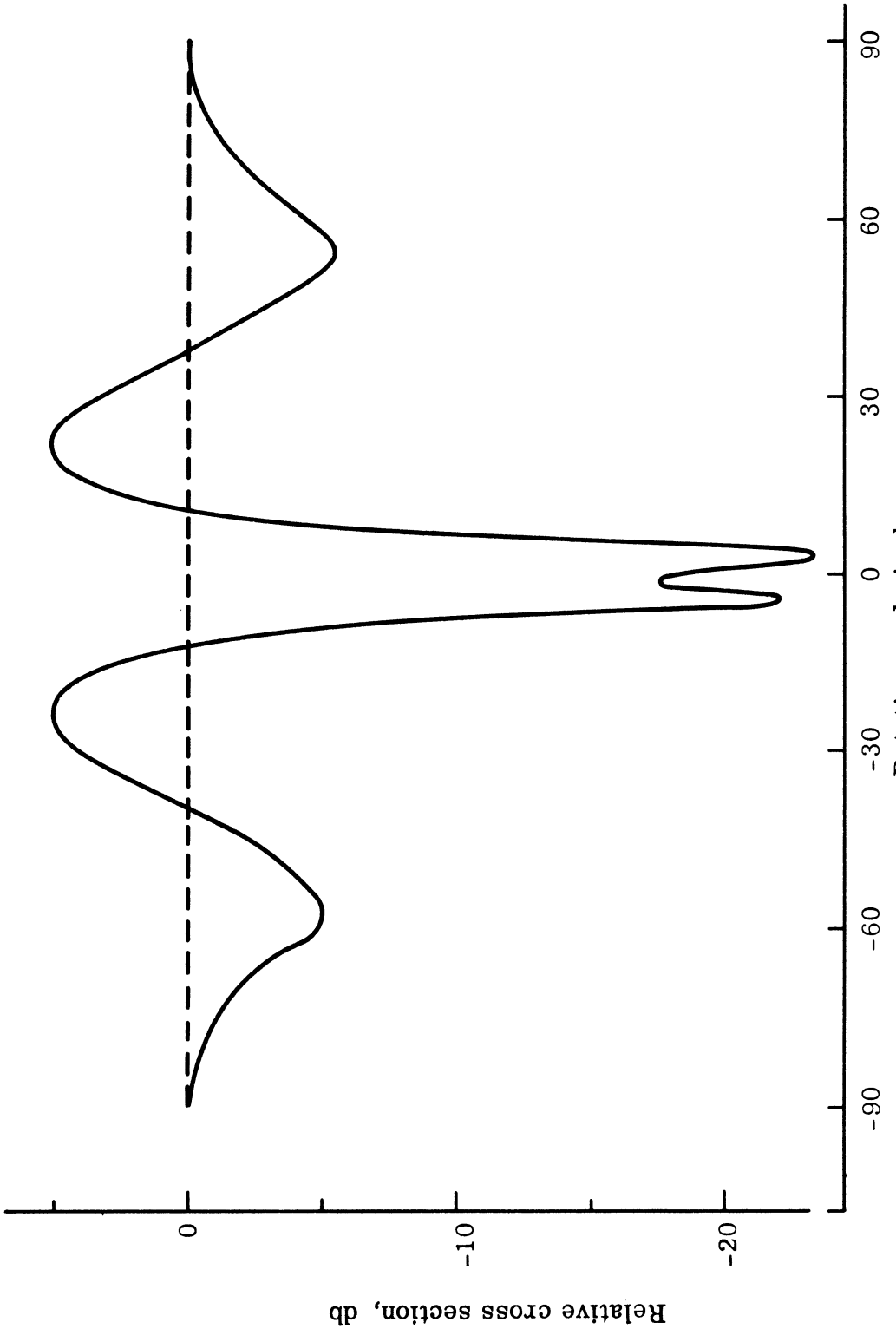

FIG. 4-5: EXPERIMENTAL BACK SCATTERING CROSS SECTIONS OF LOADED (——) AND UNLOADED (– – –) SPHERE: ka = 4.28, HORIZONTAL POLARIZATION.

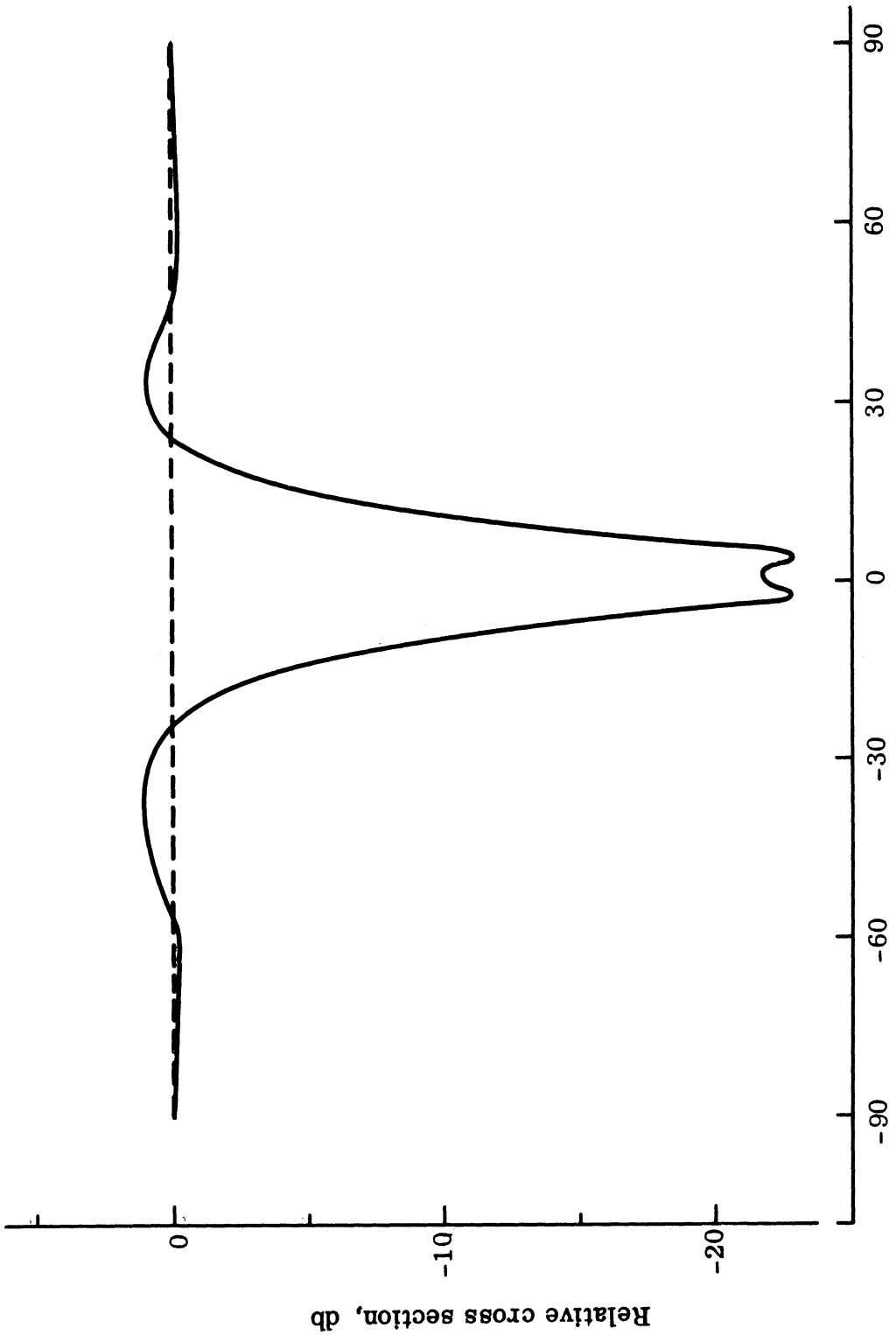

FIG. 4-6: EXPERIMENTAL BACK SCATTERING CROSS SECTIONS OF LOADED (——) AND UNLOADED (- - -) SPHERE: ka = 4.28, VERTICAL POLARIZATION.

information on surface field measurements available in the literature and any research that had been reported dealt, for the most part, with current measurements on radiating elements rather than bodies illuminated by plane electromagnetic waves. (See, for example, Reynolds, 1948; Wetzel and Brick, 1955; or Row, 1953.)

For our study, a rather crude setup, shown in Fig. 4-7, was constructed. The facility was housed in a large room, but the entire operation was confined to a region 25 by 14 feet. The experimental apparatus consisted of a signal source, an absorbing screen, and a probe with its traversing mechanism. Their arrangement is shown in Fig. 4-7.

To make measurements, the model was placed on a styrofoam pedestal located directly in front of the absorbing screen, which served to shield the traversing mechanism for the probe. The model was illuminated by a signal from the horn antenna located some 10 feet from it. The choice of frequencies was influenced by two main factors: the desire to measure models whose dimensions are comparable to or longer than a wavelength, and the necessity of having probes very small in comparison with wavelength if they are not to disturb the field unduly. The first of these forces one to higher frequencies if the models are to be of reasonable dimensions, but this in turn requires the use of extremely small probes and more accurate positioning equipment if the measurement accuracy is to be retained. Ultimately, the limit is determined by the difficulties in construction and handling of probes only a few millimeters in dimension, as well as accurate positioning of them along the required path along the surface of the body. For this reason, all the measurements were carried out in the 1 to 4 Gc frequency range.

The type of probe used depends in part on the field component to be measured. A number of different types was investigated, including a self-rectifying dipole, a two-diode balanced loop, and a simple shielded loop. The last proved most convenient for our measurements, and several versions of it, differing only in size, were constructed from miniature 50 ohm rigid coaxial line. The top

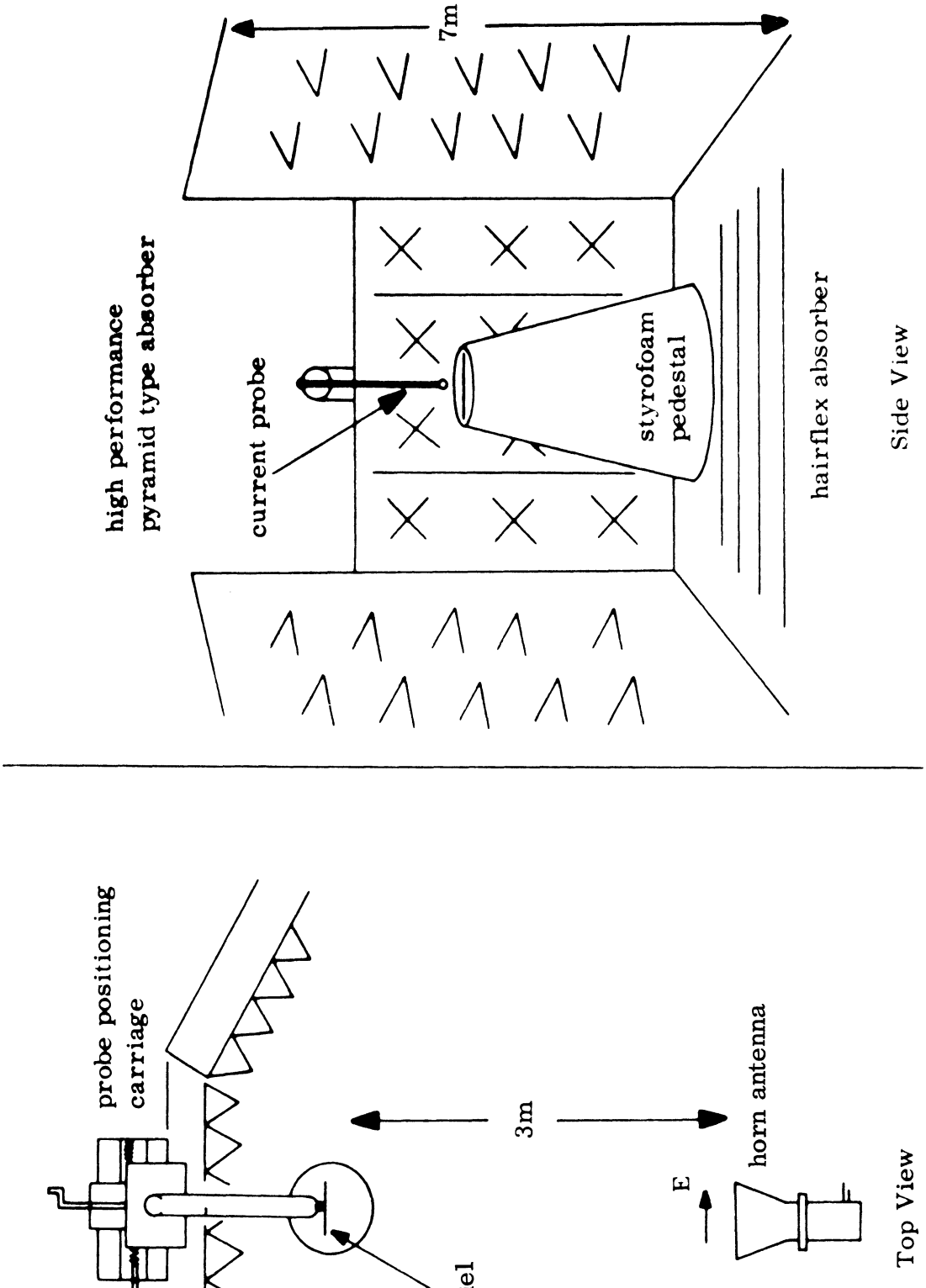

FIG. 4-7: ROOM LAYOUT.

photograph in Fig. 4-8 shows some loop probes at different stages of construction. The first representation shows a rigid coaxial line bent in a coil of several turns to ensure a circular bend. In the second and third, the excess turns have been cut off and the end, including the center conductor, soldered to form a closed, symmetric loop. The last is a completed loop in which a gap in the outer conductor has been cut and a bead of dielectric (epoxy) applied at the outer edge of this gap. This serves to keep the gap width constant and prevents the loop from "shorting" when placed against a metallic or conducting surface. Unfortunately, the reproduction is too small to show the gap or the dielectric bead. A detailed drawing of a typical loop is given in the center and in the bottom illustration are shown two different loop probes with slip-on miniature connectors. The upper probe has been bent about 5 mm from the end so that the plane of the loop is perpendicular to the lead.

Because of the relatively high loss and the flexibility in a line of such small dimensions, only about a 6-inch length of miniature coax is used. This is then connected to a larger diameter cable which together with a styrofoam beam constitutes the support for the probe. The mechanism for positioning the probe consists of two cross-coupled, horizontal motion lead-screw carriages and an associated elevating device. The coverage in the horizontal plane is about 15 by 36 cm, and the probe can be located within 0.2 mm of its intended horizontal position. The vertical adjustment or motion, however, is not as accurate due to the oscillations of the beam, and it is therefore usual to place the probe in physical contact with the model.

For detection of the signal, either a heterodyne receiver or a tuned crystal detector together with a VSWR meter was available. The receiver, naturally, gave a better sensitivity, but because of its varying gain and frequency drift, the conventional crystal detector was generally used.

While this setup was in operation, the current distribution on a number of different models was investigated. These models included thin cylinders, long wires measured for near end-on incidence, spheres, cone-spheres, and cylinders with impedance loading at the center for cross section reduction. For these

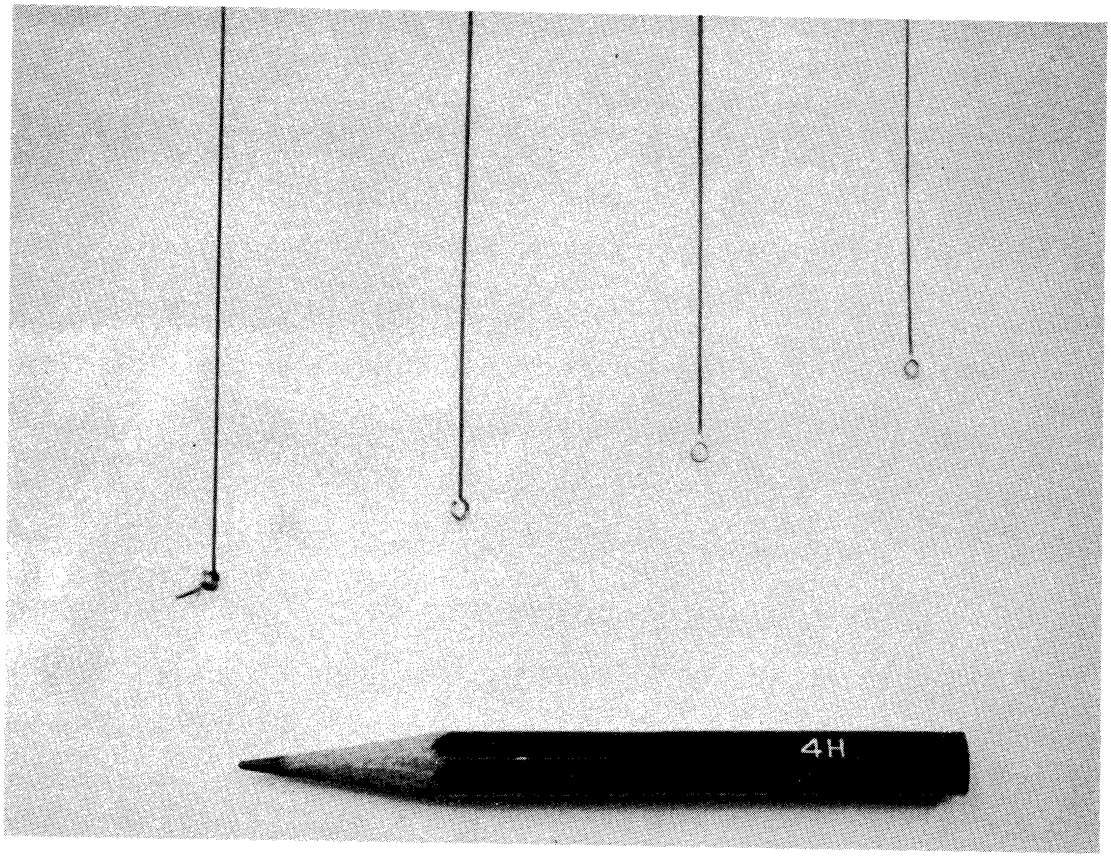

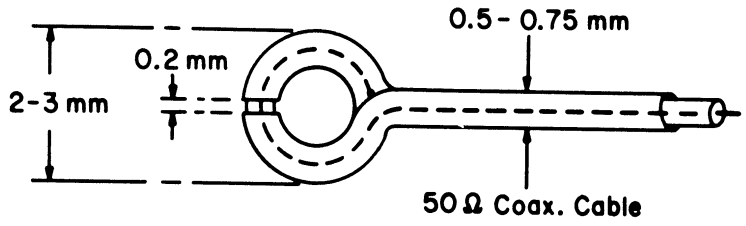

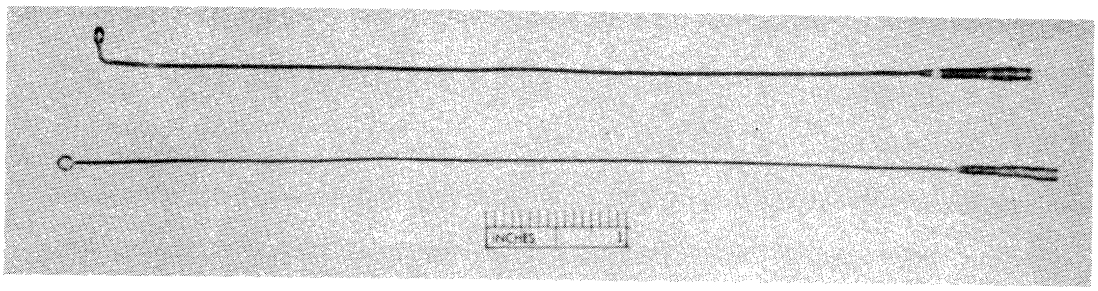

FIG. 4-8: CONSTRUCTION OF CURRENT PROBES.

loaded cylinders especially, the current measurements were extremely helpful. In a theoretical study, Chen and Liepa (1964a, b) used approximate techniques as is done for all cylinders of finite length, and therefore it was essential to verify experimentally the accuracy of these results as well as to predict the frequency range over which the solutions are valid. The current measurements did exactly that. In addition, they were helpful in determining the equivalent shunt capacitance of the gap which was to be added in parallel with the input impedance of the cavity.

4.4.2 The New Facility

As mentioned earlier, the main purpose of the above study was to gather information for the construction of a permanent, large scale surface field measurement facility. Such has now been constructed and is being used for measuring the amplitude and phase (when required) on bodies of various shapes. The anechoic chamber is 45 feet in length and 10 feet in height. It is of a tapered design with the illuminating antenna placed at the small aperture and the model near the other end of the chamber. A remotely controllable mechanism for positioning the probe is mounted above the chamber and the probe, with its coaxial lead and wooden support tower, extends vertically through the ceiling. The motion of the probe is controlled from the console by the range operator; the probe can be moved in a direction specified by either rectangular or cylindrical coordinates. A detailed description of this surface field measurement facility has been given by Knott et al (1965).

The surface field measurements for the loaded and unloaded spheres were performed in the new chamber. The model was the same as that used for back scattering measurements, and the frequency was 5.136 Gc, corresponding to $ka = 4.28$. For the unloaded case, the model was merely loaded with a disc of the same diameter as the sphere, while for the loaded case, the disc which gave over 20 db reduction in cross section was used.

The photographs in Fig. 4-9 show the model in position for measurements. In (a) is shown the overall view from the incident signal direction, and in (b) a close-up, detailed view of the loading slot and the probe. The loop of the probe is

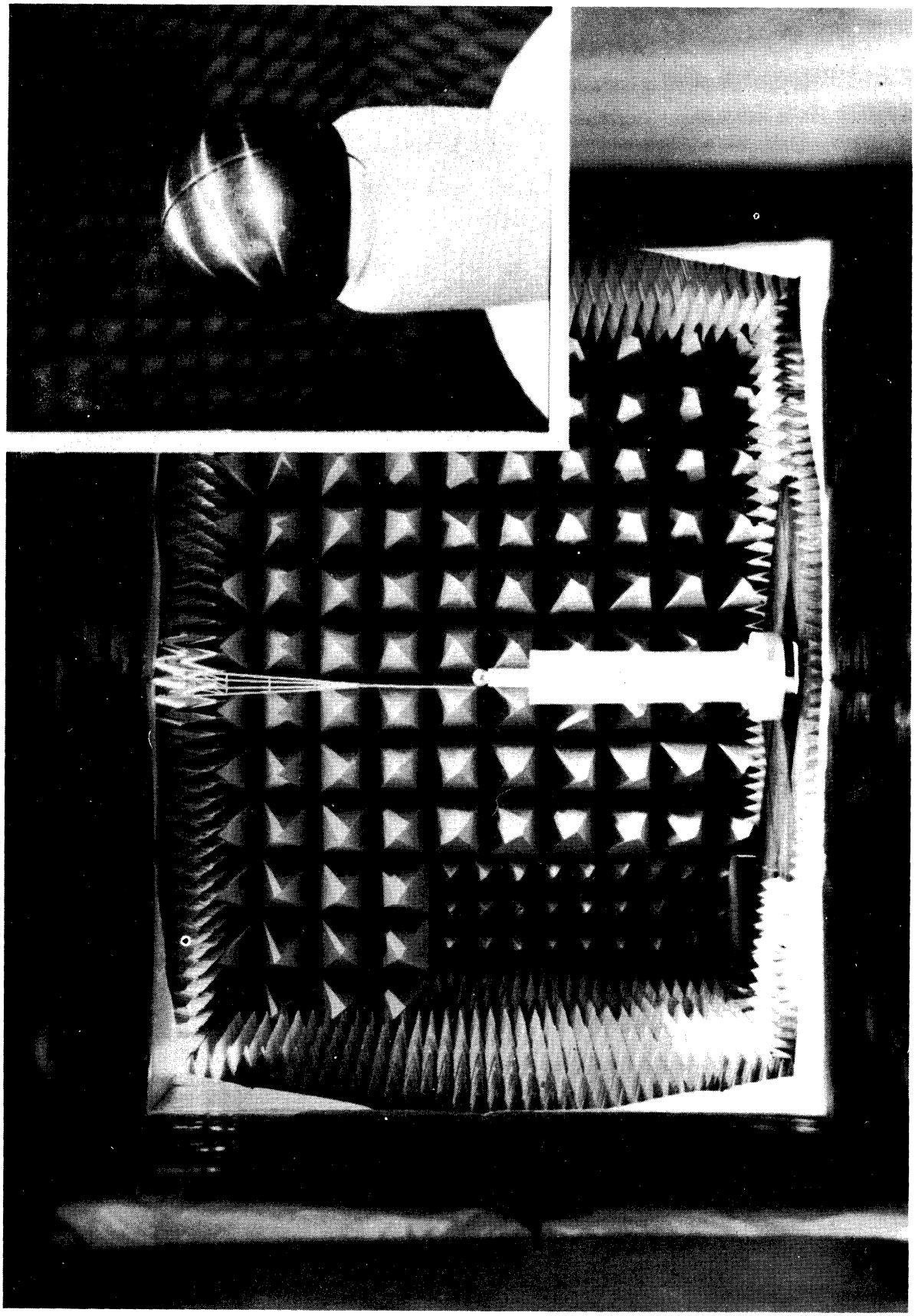

FIG. 4-9: MEASURING OF SURFACE FIELD ON A LOADED SPHERE

in the horizontal plane and is in physical contact with the surface, spaced only by a small epoxy bead to prevent any conduction current flow. The incident wave is horizontally polarized and the loaded model is oriented with the slot normal to the direction of incidence.

The data was taken at 10-degree intervals as the probe was traversed along the horizontal great circle. The measurements, normalized to coincide with the theoretical value at $\theta = 0^{o}$ for an unloaded sphere, are presented in Figs. 4-10 and 4-11 for the unloaded and loaded case respectively. The theoretical values from Chapter III are presented here for comparison.

There were two reasons for measuring the fields on the solid sphere. One was to obtain the reference level for the recorded relative data and the other to determine the performance of the chamber and associated equipment. A sphere rather than some other three dimensional body was chosen because, at present, it is the only body for which the fields are known exactly and numerical data have been extensively tabulated. When the experimental results from a sphere are in good agreement with the theoretical values, it is a not a guarantee, but rather a good indication of the accuracy of measurements for other shapes. For example, if we compare the two sets of data presented here, we see that the errors or discrepancies in one are of the same order as in the other, and in both cases the measured values are slightly lower in the shadow region. This difference, which is about 0.5 db, can be attributed to the interaction of the model with the styrofoam support pedestal.

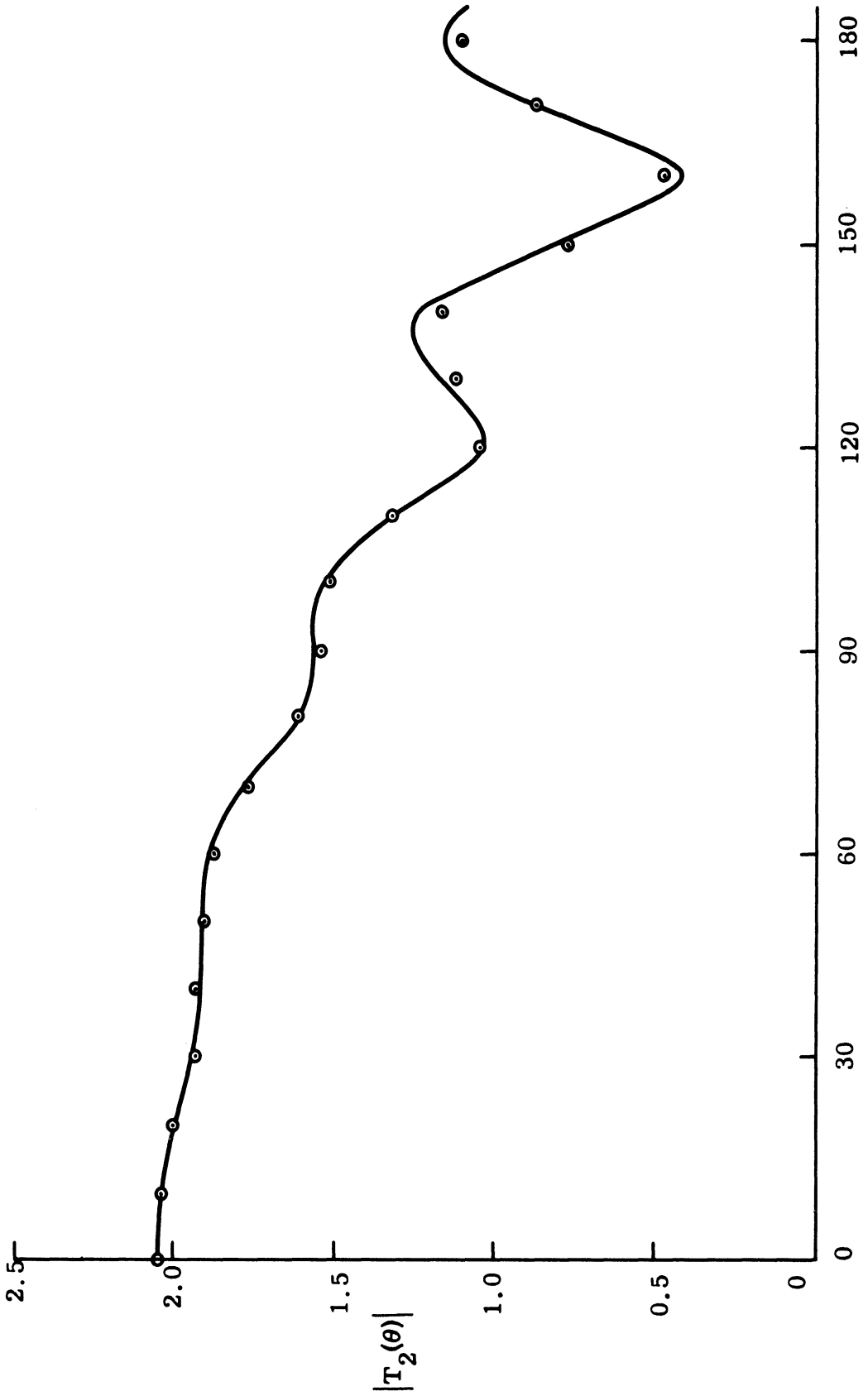

FIG. 4-10: THEORETICAL (——) AND EXPERIMENTAL (o o o) AMPLITUDES OF SURFACE FIELD COMPONENT ON AN UNLOADED SPHERE FOR ka = 4.28.

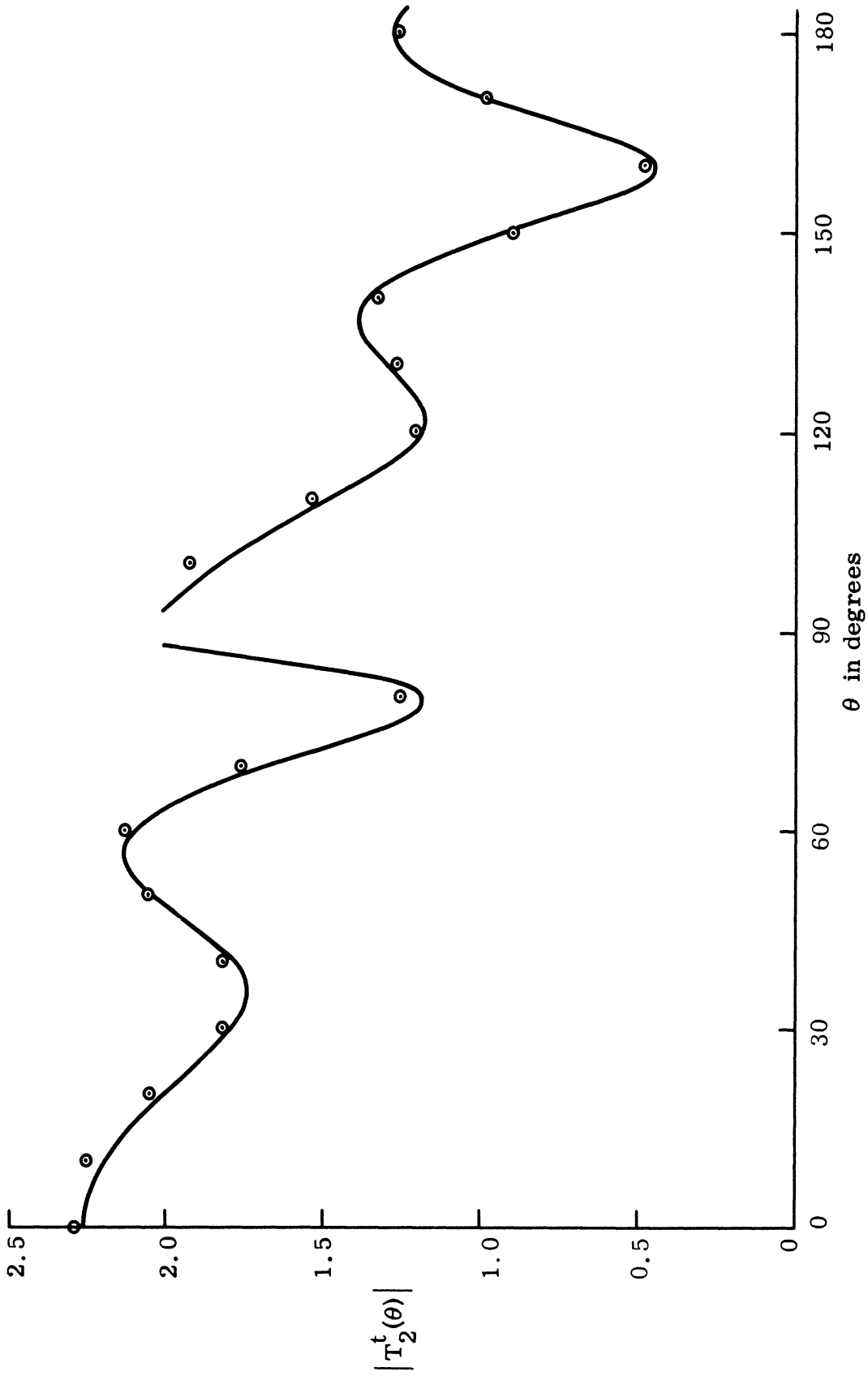

FIG. 4-11: THEORETICAL (——) AND EXPERIMENTAL (o o o) AMPLITUDES OF SURFACE FIELD COMPONENT ON A LOADED SPHERE FOR ka = 4.28 AND LOADED FOR ZERO BACK SCATTERING AT $\theta_o = 90^o$.

CHAPTER V

STUDY OF TOTAL SCATTERING

5.1 Exact Theory

The total scattering cross section is a measure of the total energy scattered by a target and is usually defined as (Jackson, 1962)

$$\sigma_s = \frac{1}{4\pi} \int_S \sigma(\theta, \phi) d\Omega \quad , \tag{5.1}$$

where S is a surface enclosing the object, $d\Omega$ an element of solid angle, and $\sigma(\theta, \phi)$ the bistatic radar cross section for the object. An equivalent expression is the ratio of the total power scattered by an object to the incident power density (King and Wu, 1959), viz.,

$$\sigma_s = P_s/P_i \ . \tag{5.2a}$$

Similarly, the total absorption cross section is defined as

$$\sigma_a = P_a/P_i \ , \tag{5.2b}$$

where P_a is the power absorbed by the object, and the sum $\sigma_s + \sigma_a$ is known as extinction cross section (van de Hulst, 1957).

A useful relation between the extinction cross section and the scattering amplitudes in the forward direction ($\theta = \pi$) is given by the forward scattering theorem. This was first discovered in quantum mechanics and since then its equivalent in electromagnetic theory has received a number of different proofs, as, for example, Schiff (1954) and Bolljahn and Lucke (1956). In the latter reference the theorem has been derived for the case of a plane wave incidence and in terms of our notation it may be written as

$$\sigma_s = \frac{4\pi}{k^2} \operatorname{Re} S_1^s(\pi)$$

for an unloaded body and

$$\sigma_a + \sigma_s = \frac{4\pi}{k^2} \operatorname{Re} S_1(\pi)$$

for a loaded body. $S_1^s(\pi)$ and $S_1(\pi)$ are the scattering amplitudes defined by equations (2.6a) and (2.24a) for the unloaded and loaded spheres respectively.

There are two methods of evaluating the total scattering cross section. One involves integration of the differential cross section $\sigma(\theta, \phi)$, and the other, computation of the forward scattering amplitude and calculation of the power absorbed by the object. For a loaded sphere, this is then the power absorbed by the load. Due to the complexity of $\sigma(\theta, \phi)$ for a loaded sphere, we proceed to evaluate the total cross section by the second method, which is relatively straightforward.

For forward scattering ($\theta = \pi$), just as for back scattering, there is no cross-polarized component and the field can be represented by a single scattering amplitude

$$S_1(\pi) = S_1^s(\pi) + \frac{Y}{Y_\ell + Y_r} 2\pi \sin\theta_o T_2(\theta_o) a S_1^r(\pi, \theta_o) .$$

To find σ_a, or the power absorbed by the object, we employ the definition of input admittance introduced in Section 2.4. It is assumed that the surface of the sphere is lossless and that the power is absorbed only by the cavity-backed slot. For an asymmetrically excited slot, the average complex power input per unit length of the slot is

$$w = \frac{Y_\ell}{4\pi a \sin\theta_o} v \cos\phi \widetilde{v \cos\phi} , \qquad (5.3)$$

where Y_ℓ is the input admittance of the slot and the tilde denotes the complex conjugate. The peak voltage that is excited across the slot is, from equation (2.27),

$$v = \frac{Y}{Y_\ell + Y_r} 2\pi a \sin\theta_o T_2(\theta_o)$$

and when it is substituted in (5.3), the total absorbed power becomes

$$P_a = \mathrm{Re} \int_0^{2\pi} w a \sin\theta_o \, d\phi$$

$$= (\pi a \sin^2\theta)^2 \left| \frac{Y}{Y_\ell + Y_r} T_2(\theta_o) \right|^2 \mathrm{Re}\, Y_\ell$$

and the absorption cross section

$$\sigma_a = 2(\pi a \sin\theta_o)^2 \left| \frac{Y}{Y_\ell + Y_r} T_2(\theta_o) \right|^2 \mathrm{Re} \frac{Y_\ell}{Y} .$$

The total scattering cross section, normalized to its physical optics value πa^2, is then

$$\frac{\sigma_s}{\pi a^2} = \frac{4}{(ka)^2} \mathrm{Re}\, S_1(\pi) - 2\pi \sin^2\theta_o \left| \frac{Y}{Y_\ell + Y_r} T_2(\theta_o) \right|^2 \mathrm{Re} \frac{Y_\ell}{Y} . \quad (5.4)$$

We now want to find the extremum value of (5.4) subject to passive loading, i.e. $\mathrm{Re} \frac{Y_\ell}{Y} \geqslant 0$. $\mathrm{Im} \frac{Y_\ell}{Y}$, on the other hand, has no restriction and may take any value. For simplicity, we now introduce the following definitions:

$$T_2(\theta_o) = t_1 + it_2$$

$$\frac{Y_\ell + Y_r}{Y} = x + iy$$

$$Y_r/Y = g_1 + ig_2$$

$$Y_\ell/Y = \ell_1 + i\ell_2$$

$$S_1^s(\pi) = s_1 + is_2$$

$$aS_1^r(\pi, \theta_o) = r_1 + ir_2 . \quad (5.5)$$

When these are substituted in equation (5.4) we find

$$\frac{\sigma_s}{\pi a^2} = B_1 + \frac{B_2}{x^2+y^2} + \frac{B_3 x}{x^2+y^2} + \frac{B_4 y}{x^2+y^2} \quad , \tag{5.6a}$$

where

$$B_1 = \frac{4}{(ka)^2} s_1$$

$$B_2 = 2\pi \sin^2\theta_o (t_1^2 + t_2^2) g_1$$

$$B_3 = 2\pi \sin\theta_o \left\{ \frac{4}{(ka)^2} (t_1 r_1 - t_2 r_2) - \sin\theta_o (t_1^2 + t_2^2) \right\}$$

$$B_4 = \frac{8\pi}{(ka)^2} \sin\theta_o (t_1 r_2 + t_2 r_1) \; . \tag{5.6b}$$

The extremum values of (5.6), for $g_1 \geqslant 0$, are given in Appendix A. The maximum value is

$$\max. \frac{\sigma_s}{\pi a^2} = B_1 + \frac{B_4^2}{2} \frac{1}{-(B_2 + B_3 g_1) + \sqrt{(B_2 + B_3 g_1)^2 + B_4^2 g_1^2}} \tag{5.7a}$$

and the minimum value,

$$\min. \frac{\sigma_s}{\pi a^2} = B_1 + \frac{B_4^2}{2} \frac{1}{-(B_2 + B_3 g_1) - \sqrt{(B_2 + B_3 g_1)^2 + B_4^2 g_1^2}} \; , \tag{5.7b}$$

$$\text{for } g_1 \geqslant x_{min.}$$

$$= B_1 - \frac{B_3^2 + B_4^2}{4B_2} \quad , \qquad \text{for } g_1 \leqslant x_{min.} \tag{5.7c}$$

where

$$x_{min.} = - \frac{2B_2 B_3}{B_3^2 + B_4^2} \; .$$

The results simplify considerably when $\theta_o = 90^o$. From equation (2.35a)

$$a S_1^r(\pi, \pi/2) = \frac{(ka)^2}{4} T_2(\pi/2)$$

or

$$r_1 + ir_2 = \frac{(ka)^2}{4}(t_1 + it_2)$$

and with this condition we have

$$B_1 = \frac{4}{(ka)^2} S_1$$

$$B_2 = 2\pi(t_1^2 + t_2^2)g_1$$

$$B_3 = -4\pi t_2^2$$

$$B_4 = 4\pi t_1 t_2 \quad . \tag{5.8}$$

The numerical calculations of (5.7) with $\theta_o = 90^o$ and the constants defined by (5.8) are presented in Fig. 5-1. To emphasize the enhancement or reduction, the values are normalized relative to the total cross section of an unloaded sphere, namely

$$\frac{\sigma_{so}}{\pi a^2} = \frac{4}{(ka)^2} s_1$$

$$= B_1 \quad .$$

Let us consider first the maximum total scattering. If we allow an active slot, it is obvious that there is no limit to the maximum scattering attainable. Of more practical interest is the maximum scattering attainable with passive loading. As shown in Fig. 5-1, a large enhancement occurs for small values of ka, but decreases rapidly as ka is increased. Whereas at ka = 0.5 the enhancement is 20 db, at ka = 1.0 it is 8 db and at ka = 5.0 it is already less than 1 db.

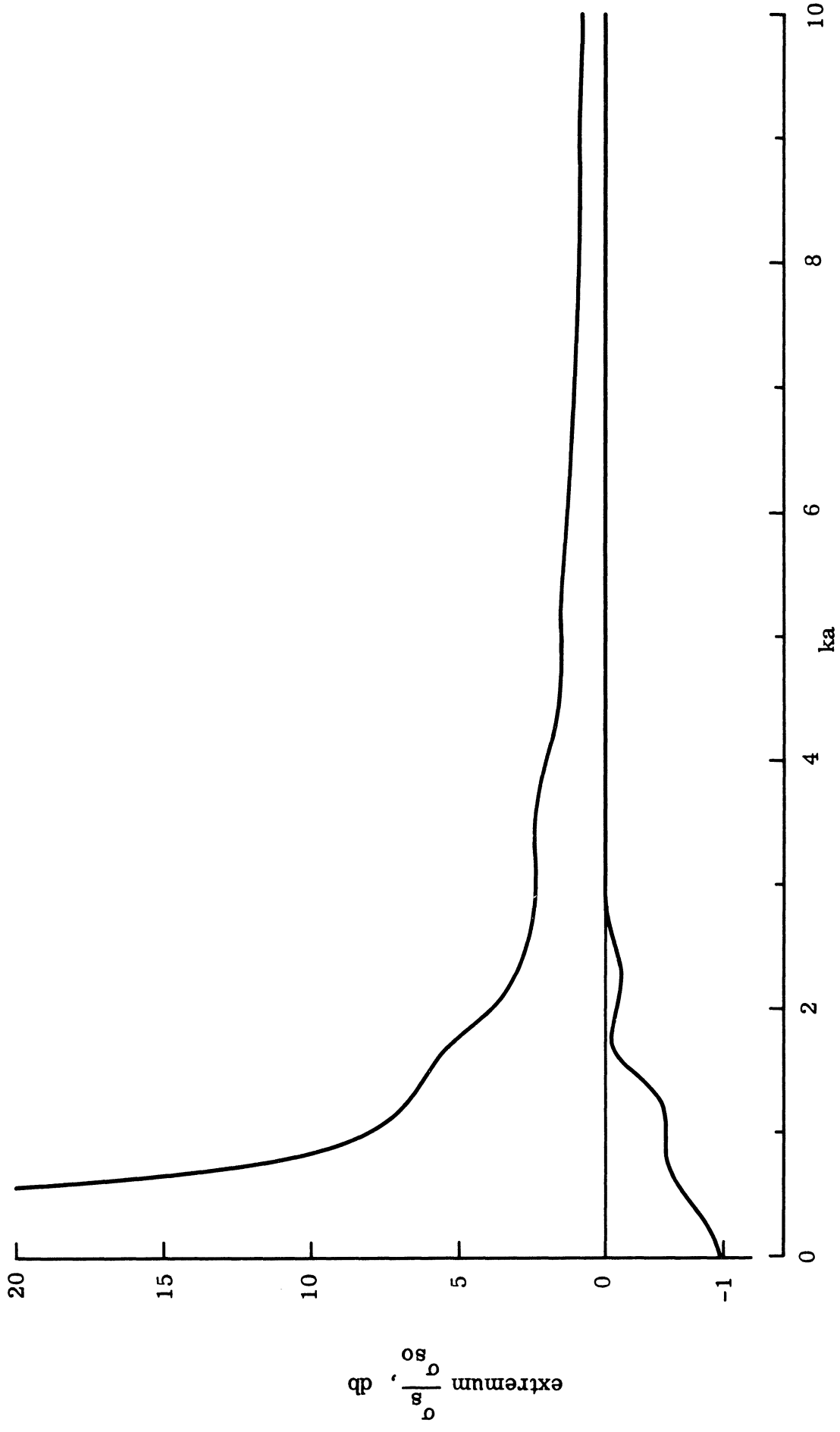

FIG. 5-1: NORMALIZED MAXIMUM AND MINIMUM TOTAL SCATTERING CROSS SECTIONS FOR PASSIVE LOADING AT $\theta_o = 90^o$.

The lower curve in Fig. 5-1 gives the minimum total scattering for a passive load. As we see, there is practically no reduction for large values of ka, and even when ka is around unity, the maximum reduction is a mere 0.5 db. From this we deduce that the loading of the sphere does not reduce its scattering, but rather redirects it from one direction to another. And this, of course, is evident in the bistatic scattering patterns in Figs. 3-24 through 3-29. The question now arises as to whether an improvement can be achieved if active loading is allowed. In such a case there would be no restriction on ℓ_1, the condition

$$g_1 + \ell_1 = x_{min.}$$

would always be satisfied, and the total cross section would then be given by equation (5.7c). However, when the results for Fig. 5-1 were calculated, the condition $g_1 \leqslant x_{min.}$ was met for all values of ka, implying that the same minimum total cross section is achieved with active or passive loading.

5.2 Low Frequency Approximation

In Section 2.5 the expressions for the low frequency scattering behavior of a loaded sphere were obtained. They are rather simple, and we can easily find the total cross section by direct integration of the differential cross sections. Substitution of equation (2.29) into (5.1) leads to a normalized total scattering cross section

$$\frac{\sigma_s}{\pi a^2} \sim \frac{1}{\pi (ka)^2} \int_0^{\pi} \int_0^{2\pi} \left(|S_1(\theta)|^2 \cos^2\phi + |S_2(\theta)|^2 \sin^2\phi \right) \sin\theta \, d\phi \, d\theta \ ,$$

where, for low frequencies, the scattering amplitudes are given by equations (2.41). Upon integration, we get

$$\frac{\sigma_s}{\pi a^2} \sim \frac{10}{3} (ka)^4 + \frac{27}{8} \pi^2 (ka)^2 \frac{1}{x^2 + y^2} + 3\pi (ka)^3 \frac{y}{x^2 + y^2} \ , \qquad (5.9)$$

where x and y are the loading parameters defined in equation (5.5). The first

term on the right hand side represents the scattering by an unloaded sphere, and the other two are direct consequences of the loading and disappear when the cavity is shorted ($y \to -\infty$).

It is of interest to compare this result with the formula previously obtained from the forward scattering theorem. For small values of ka, and using the expressions derived in Section 2.5, the constants for $\theta_o = \pi/2$ in equation (5.8) reduce to

$$B_1' = \frac{10}{3}(ka)^4$$

$$B_2' = \frac{27}{8}\pi^2(ka)^2$$

$$B_3' = -\pi(ka)^6$$

$$B_4' = 3\pi(ka)^3$$

and the total scattering, from (5.6a), becomes

$$\frac{\sigma_s}{\pi a^2} \sim \frac{10}{3}(ka)^4 + \frac{27}{8}\pi^2(ka)^2 \frac{1}{x^2+y^2} - \pi(ka)^6 \frac{x}{x^2+y^2} + 3\pi(ka)^3 \frac{y}{x^2+y^2} .$$

Except for the third term on the right hand side, this expression is identical to equation (5.9). The absence of this term in (5.9) is due to the assumption (in Section 2.5) that $x \ll 1$ and therefore its presence or absence, for all practical purposes, has not effect on numerical results.

The extremum values for (5.9) are given again in Appendix A, and upon substitution of the corresponding values we find

$$\text{max.} \quad \frac{\sigma_s}{\pi a^2} \sim \frac{10}{3}(ka)^4 + \frac{6}{(ka)^2}$$

$$\text{min.} \quad \frac{\sigma_s}{\pi a^2} \sim \frac{10}{3}(ka)^4 - \frac{6(ka)^4}{9+(ka)^6} ,$$

or, when normalized to the total scattering cross section of an unloaded sphere,

$$\max. \frac{\sigma_s}{\sigma_{so}} \sim 1 + \frac{9}{5} \frac{1}{(ka)^6} \tag{5.10a}$$

$$\min. \frac{\sigma_s}{\sigma_{so}} \sim 1 - \frac{9}{5} \frac{1}{9+(ka)^6} \quad . \tag{5.10b}$$

Numerical comparison of this result with the exact computed values in Fig. 5-1 indicates that the above equations are accurate within 10 percent up to $ka = 1.0$.

CHAPTER VI
DISCUSSION

6.1 Some Practical Considerations for Obtaining the Desired Loading

We have seen in the chapter on experimental studies that when the optimum loading is purely susceptive, it can be supplied by a simple radial cavity of variable depth. For zero back scattering there are only a few values of ka where the optimum loading is susceptive, and these depend on the slot position θ_o. For instance, with the slot at $\theta_o = 45^o$, there is only one value of ka (in the range $0 < ka \leqslant 10$ considered) where the real part of the optimum loading for zero back scattering crosses the zero value, but with $\theta_o = 90^o$ there are six such frequencies. For maximum return, however, the optimum loading is susceptive for all ka (cf. Figs. 3-14 and 3-17) and the loading requirement can be met with a lossless radial cavity at any value of ka.

Unfortunately the variation of susceptance with frequency for the radial cavity (or any other lossless network) is the direct opposite of that required to reduce or enhance the back scattering cross section. As a result, the loading can be satisfied only where the two loading curves intersect, and narrow bandwidths are therefore to be expected. To determine the actual bandwidths encountered with susceptive loading, we examine the case when the sphere is loaded for zero back scattering with ka = 4.28 and $\theta_o = 90^o$. The required optimum loading and that supplied by the radial cavity, such as used in the experimental model, are shown in Fig. 6-1. The depth for the cavity was chosen so as to satisfy the optimum loading at ka = 4.28. It is evident that the corresponding curves, especially for the real part, have completely different behaviors and, as a result, a minute deviation in frequency from the critical value results in a large difference between the desired and the supplied loading. The cross section corresponding to the cavity loading is shown in Fig. 6-2. As expected, a complete reduction is achieved at ka = 4.28 and this reduction is highly frequency sensitive. For example, for a 10 db reduction in the cross section the bandwidth is 6.5 percent and decreases to only 2 percent when a 20 db reduction in the cross section is desired.

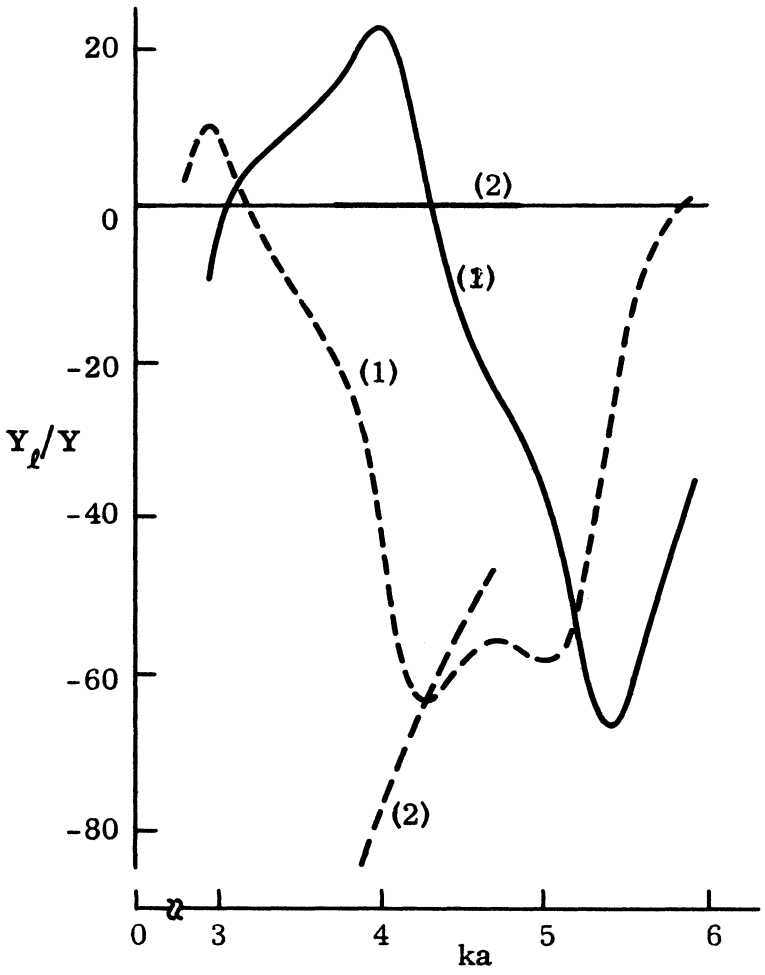

FIG. 6-1: REAL (——) AND IMAGINARY (– – –) PARTS OF (1) NORMALIZED LOADING ADMITTANCE FOR ZERO BACK SCATTERING WITH $\theta_o = 90^o$ AND (2) LOADING SUPPLIED WITH LOSSLESS RADIAL CAVITY.

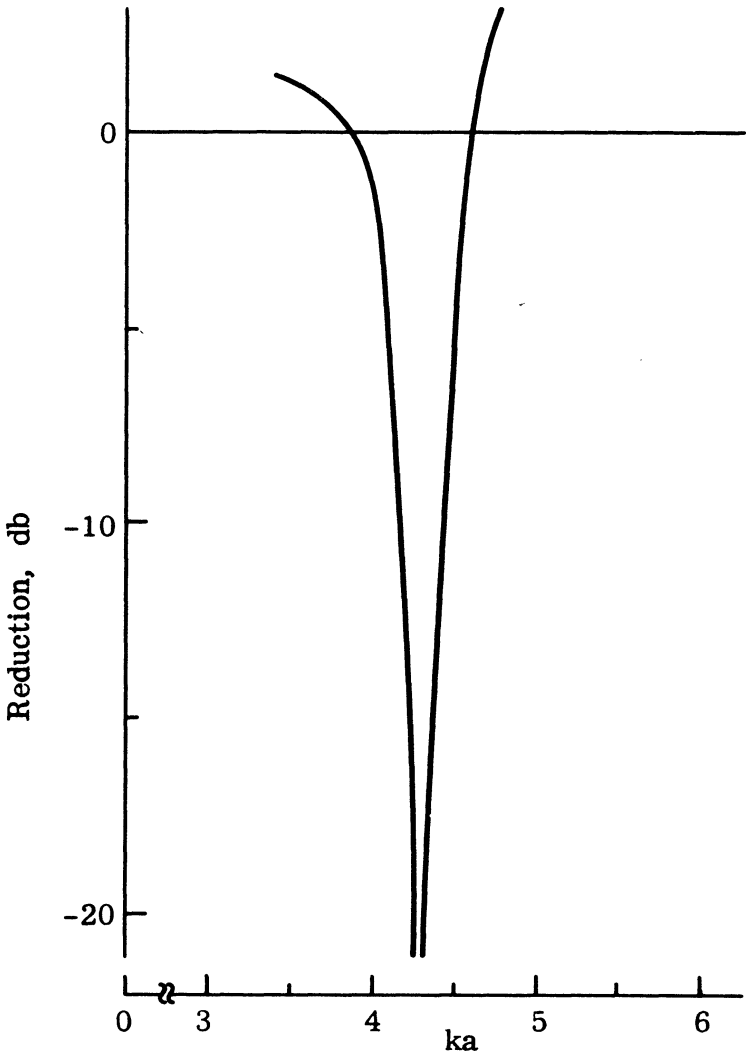

FIG. 6-2: REDUCTION IN BACK SCATTERING WITH SUSCEPTIVE LOADING AT $\theta_o = 90^o$.

For wider bandwidths and increased scattering control, it is clear that such simple susceptive loading alone will not suffice and that more sophisticated loading techniques must be developed. From a practical viewpoint there appear to be two different methods of approach. One method would be to use a number of lumped two-port networks, whose frequency response is determined by the optimum loading, and distribute these around a sphere to simulate a distributed loading. The resultant admittance Y_ℓ in such a case would be

$$Y_\ell = nY_L + Y'_\ell$$

where n is the number of loading points or elements used, Y_L the admittance of each element, and Y'_ℓ the inherent admittance of the slot and the back-up cavity. This cavity could be similar to the one used in the experimental model. The number of loading points will depend on the accuracy to which the optimum loading must be attained. A rough estimate is that this number may be as high as 10 ka, where ka is the maximum value in the frequency range considered. Once n and Y'_ℓ are known, Y_L can be found from the above equation and from then on the problem is strictly one of network synthesis. It would involve the study of the realizability conditions and synthesis procedures for functions such as Y_L when both the real and imaginary parts are specified over a finite frequency range. In addition, a network to generate this function would need to be determined.

The other method would be to consider the cavity as a distributed network or a non-uniform transmission line loaded in a prescribed manner to achieve the requisite loading. For small bandwidths, of order 5 to 10 percent for 20 db reduction, a cavity such as used in the experimental model could be filled with a lossy dielectric, or even ferrite materials, to supply the required complex loading for certain frequencies. The formula for the input admittance derived in Appendix B still applies, but it must be modified slightly to accept the complex values of k and Y. For wider bandwidths, however, the loading of the cavity must be considered as a synthesis problem. The work by Sharpe (1962) and Youla (1964) on the analysis and synthesis of non-uniform transmission lines could probably be extended and applied to the synthesis of radial transmission lines and cavities.

Perhaps a loading that is easier to realize physically may result from either of two related problems that should be considered in a future study. One problem would be to examine the effect of coplanar multiple slot loading with the slots perpendicular to the direction of incidence, and the other would be to solve the boundary value problem for a single slot loading, but with the slot located arbitrarily with respect to the direction of incidence.

In the case of multiple slot loading the analysis would be an extension of the results for a single slot presented here. A cursory study has shown that double loading does have certain advantages. For example, by using two slots we could make either $S_1(\theta)$ or $S_2(\theta)$ zero for two adjacent values of θ (as compared to one value for a single load), or make both $S_1(\theta)$ and $S_2(\theta)$ zero for a single value of θ. Correspondingly, it is expected that with the proper choice of the slot positions, loading admittances whose frequency characteristics are more suited for physical realizability would be obtained. Overall, it appears that with double loading, twice as much controllability is obtained as with a single load, but the use of multiple loading adds to the difficulty of adequate numerical treatment.

Encouraging as it may be, the slots would still be excited by an asymmetric voltage requiring a distributed (or lumped distributed) loading which is rather cumbersome to achieve. However, this is not the case in the problem of loading a sphere with a single slot arbitrarily located with respect to the direction of incidence. Whereas in the problem that we have considered only a single asymmetric mode was excited in the slot, now the slot would be, in general, excited by an infinite set of modes. In particular, when the direction of the incident wave is such that its electric vector is perpendicular to the plane of the slot, a zeroth mode would predominate and by independently controlling this mode it should be possible to control the scattering behavior of the sphere. For such a loading, the slot should be backed by a radial cavity of the type used in our experimental model, but with a lumped load at the center. Such a load would affect only the zeroth mode and would appear nonexistent to all the higher modes. It is expected that the frequency characteristics for this loading would be similar to those for a thin cylinder, and that the scattering control would be less effective than that

for an asymmetrically excited single slot loading. Nevertheless a possibility of using a single lumped load would alone justify an investigation of a single slot loading with arbitrary illumination.

6.2 Conclusions

In the preceding sections we have considered the scattering behavior of a metallic sphere loaded with a slot in a plane perpendicular to the direction of incidence. The slot was assumed to be of small but finite width with a constant electric field across it, and under this assumption, the analysis for the external fields is exact. Expressions for the scattered far field components, as well as the total surface field components, were derived and then used to investigate the modification to the scattering cross section produced by various admittances of the slot. All investigation was limited to the frequency range $0 < ka \leqslant 10$.

The loading admittance necessary for a particular modification is in general complex, with negative or positive real part, corresponding to an active or passive load respectively. The loading required to reduce the back scattering cross section to zero has been examined in some detail. For any given slot position θ_o, the ranges of ka in which the real part of the loading admittance is positive or negative alternate with one another, and the location of these active or passive bands are functions of the slot position. For example, with the slot at the shadow boundary ($\theta_o = 90^o$), there are three different active bands, but as the slot is moved toward the front, these bands appear to move towards increasing ka. With $\theta_o = 45^o$, the first band does not commence until ka = 4.25, and with $\theta_o = 30^o$, it appears somewhere beyond ka = 10.0. However, any further movement of the slot towards the front introduces a new active band at ka = 1.5 and due to this, it seems that for back scattering reduction with passive loading, the load should be somewhere between $\theta_o = 30^o$ and $\theta_o = 60^o$. The exact position of the slot will depend on the limitations imposed by the realizability and synthesis requirements of the loading.

In contrast, an increase of almost 20 db in back scattering cross section can be achieved for a particular value of ka with passive loading, and maximum

enhancement occurs when the loading slot is near 60^{o}. When a sphere is loaded for zero back scattering, the angular beamwidth for 20 db reduction in bistatic operation is maximum (64^{o}) as $ka \rightarrow 0$. It is then independent of the loading position θ_o and has the same value in either the E-plane or the H-plane. At $ka = 2.0$, the beamwidth is about 50 percent of the initial value and at $ka = 10.0$ it has decreased to only about 25 percent. Quantitatively the beamwidths are wider with $\theta_o = 30^{o}$ than $\theta_o = 90^{o}$ and also wider in the H-plane as compared to the E-plane. An improvement in the beamwidth can be obtained by selecting a loading for maximum width (with a null between 15^{o} and 30^{o}) rather than for a null at $\theta = 0^{o}$. The bistatic scattering patterns indicate, in addition to the beamwidths, that whenever the sphere is loaded for back scattering reduction there is enhancement in the forward direction. It appears that the loading, such as studied here, does not in general reduce the total cross section, but rather modifies the scattering pattern by redirecting the scattered energy from one direction to another. Studies of the total scattering behavior do indeed confirm this.

To verify some of the theoretical conclusions, a spherical model was constructed. The model had a circumferential slot at $\theta_o = 90^{o}$ backed by a radial cavity whose depth could be varied by using shorting discs of various diameters. Since the loading was purely susceptive, emphasis was placed on the frequency where complete reduction in back scattering can be obtained, namely $ka = 4.28$. The back scattering from this model was measured for different loading discs which, in turn, were related to the corresponding loading admittance by an input admittance formula for the asymmetrically excited radial cavity. Agreement between the measured and computed back scattering cross sections was excellent, and with the loading disc corresponding to the optimum loading for zero back scattering, over 20 db in cross section reduction was achieved. The theory was further verified by measuring the surface fields on the same model loaded for zero back scattering and comparing the data with the computed values. Again the agreement was excellent.

REFERENCES

Adams, E.F. and R.L. Hippisley (1947) Smithsonian Mathematical Formulae and Tables of Elliptic Functions, Smithsonian Miscellaneous Collections, 74, No. 1.

Ås, B.O. and H.J. Schmitt (1958) "Back Scattering Cross Section of Reactively Loaded Cylindrical Antennas", Harvard University Cruft Laboratory Scientific Report No. 18.

Bailin, L.L. and S. Silver (1956) "Exterior Electromagnetic Boundary Value Problems for Spheres and Cones", IRE Trans. Ant. and Prop., AP-4, pp 5-16.

Bechtel, M.E. (1962) "Scattering Coefficients for the Backscattering of Electromagnetic Waves from Perfectly Conducting Spheres", Cornell Aeronautical Laboratory Report No. AP/R18-1.

Bolljahn, J.T. and W.S. Lucke (1956) "Some Relationships between Total Scattered Power and the Scattered Field in the Shadow Zone", IRE Trans. Ant. and Prop., AP-4, pp 69-71.

Chen, K-M (1965a) "Minimization of Back Scattering of a Cylinder by Double Loading", IEEE Trans. Ant. and Prop., AP-13, pp 262-270.

Chen, K-M (1965b) "Minimization of Back Scattering of a Cylinder with a Moderate Radius by Loading Method", Michigan State University Technical Report No. 1, Contract AF 33(615)-1656.

Chen, K-M and V.V. Liepa (1964a) "The Minimization of the Back Scattering of a Cylinder by Central Loading", IEEE Trans. Ant. and Prop., AP-12, pp 576-582.

Chen, K-M and V.V. Liepa (1964b) "The Minimization of the Radar Cross Section of a Cylinder by Central Loading", The University of Michigan Radiation Laboratory Report No. 5548-1-T.

Ducmanis, J.A. and V.V. Liepa (1965) "Surface Field Components for a Perfectly Conducting Sphere", The University of Michigan Radiation Laboratory Report No. 5548-3-T.

Green, R.B. (1963) "The General Theory of Antenna Scattering", The Ohio State University Report No. 1223-17.

Harrington, R.F. (1963) "The Electromagnetic Scattering by Antennas", IEEE Trans. Ant. and Prop., AP-11, p 596.

Harrington, R.F. (1964) "Theory of Loaded Scatterers", Proc. IEE (London), 111, pp 617-623.

Hey, J.S., G.S. Stewart, J.T. Pinson, and P.E.V. Prince (1956) "The Scattering of Electromagnetic Waves by Conducting Spheres and Discs", Proc. Phys. Soc. B, 69, pp 1038-1049.

Hu, Y-Y (1958) "Backscattering Cross Section of a Center-Loaded Cylindrical Antenna", IRE Trans. Ant. and Prop., AP-6, pp 140-148.

van de Hulst, H.C. (1957) Light Scattering by Small Particles, John Wiley and Sons, Inc., New York.

Iams, H.A. (1950) "Radio Wave Conducting Device", U.S. Patent No. 2,578,367.

Jackson, J.D. (1962) Classical Electrodynamics, John Wiley and Sons, Inc., New York.

Kazarinoff, N.D. and T.B.A. Senior (1962) "A Failure of Creeping Wave Theory", IRE Trans. Ant. and Prop., AP-10, pp 634-638.

King, R.W.P. (1956) The Theory of Linear Antennas , Harvard University Press, Cambridge, Mass.

King, R.W.P. and T.T. Wu (1959) The Scattering and Diffraction of Waves, Harvard University Press, Cambridge, Mass.

Knott, E.F., V.V. Liepa and T.B.A. Senior (1965) "A Surface Field Measurement Facility", Proc. IEEE, 53, pp 1105-1107.

Meissner, A. (1929) "Transmitting Antennas for Broadcasting", Proc. IRE, 17, pp 1178-1184.

Reynolds, D.K. (1948) "Surface-Current and Charge Measurements on Flat Metal Sheets", Harvard University Cruft Laboratory Report No. TR-53.

Row, R.V. (1953) "Microwave Diffraction Measurements in a Parallel Plate Region", J. Appl. Phys., 24, pp 1448-1452.

Schiff, L.I. (1954) "On an Expression for the Total Cross Section", Prog. Theor. Phys.,11, pp 288-290.

Senior, T.B.A. and R.F. Goodrich (1964) "Scattering by a Sphere", Proc. IEE (London), 111, pp 907-916.

Sharpe, C.B. (1962) "An Alternative Derivation of Orlov's Synthesis Formula for Non-uniform Lines", Proc. IEE (London), 109, pp 226-229.

Sletten, C.J., P. Blacksmith, F.S. Holt, and B.B. Gorr (1964) "Scattering from Thick Reactively Loaded Rods", in "The Modification of Electromagnetic Scattering Cross Sections in the Resonance Region", A Symposium Record, 1, USAF Cambridge Research Laboratories Report No. AFCRL-64-727(I), pp 67-87.

Stratton, J.A. (1941) Electromagnetic Theory, McGraw-Hill Book Co., Inc., New York.

Watson, G.N. (1948) A Treatise on the Theory of Bessel Functions, The Mac-Millan Co., New York.

Weinberg, L. (1963) "New Technique for Modifying Monostatic and Multistatic Radar Cross Sections", IEEE Trans. Ant. and Prop., AP-11, pp 717-719.

Wetzel, L. and D.B. Brick (1955) "An Experimental Investigation of High Frequency Current Distributions on Conducting Cylinders", Harvard University Cruft Laboratory Report No. SR-4.

Youla, D.C. (1964) "Analysis and Synthesis of Arbitrary Terminated Lossless Nonuniform Lines", IEEE Trans. Circuit Theory, CT-11, pp 363-372.

APPENDIX A

AN EXTREMUM PROBLEM

In Chapters III and V, the following extremum problem arises: given

$$\Gamma = A+B\frac{1}{x^2+y^2}+C\frac{x}{x^2+y^2}+D\frac{y}{x^2+y^2} \tag{A.1}$$

where A, B, C and D are real constants, find the maximum and minimum values of Γ subject to the condition $x \geqslant g_1 > 0$. In addition, A and B are positive.

From equation (A.1)

$$\Gamma = \frac{Ax^2+Ay^2+B+Cx+Dy}{x^2+y^2} \tag{A.2}$$

and since there is no restriction on y, we can obtain an extremum of (A.2) by setting the derivative of Γ with respect to y equal to zero. Thus

$$\frac{Ax^2+Ay^2+B+Cx+Dy}{x^2+y^2} = \frac{2Ay+D}{2y} \tag{A.3}$$

and when substituted in (A.2), the extremum values are given by

$$\Gamma_{ext.} = A+\frac{D}{2y} \quad . \tag{A.4}$$

The variables x and y are not independent now, but are related by equation (A.3). Solving explicitly for y in (A.3)

$$y = \frac{1}{D}\left\{-(B+Cx) \pm \sqrt{(B+Cx)^2+D^2x^2}\right\}$$

and then substituting it in equation (A.4), we find

$$\Gamma_{max} = A+\frac{D^2}{2}\frac{1}{-(B+Cx)+\sqrt{(B+Cx)^2+D^2x^2}} \tag{A.5a}$$

$$\Gamma_{min} = A-\frac{D^2}{2}\frac{1}{(B+Cx)+\sqrt{(B+Cx)^2+D^2x^2}} \quad . \tag{A.5b}$$

Investigating the behavior of these two equations as functions of x, we observe that as $x \to 0$

$$\Gamma_{max} \to \infty$$

$$\Gamma_{min} \to A - \frac{D^2}{4B}$$

and as $x \to \pm\infty$

$$\Gamma_{max} \to A + \frac{C}{2x} + \frac{\sqrt{C^2+D^2}}{|x|}$$

$$\Gamma_{min} \to A + \frac{C}{2x} - \frac{\sqrt{C^2+D^2}}{|x|}$$

We can obtain the least value of Γ_{min} by setting its derivative with respect to x equal to zero. However, the same result is obtained much more easily if we minimize the denominator in equation (A.5b). Thus,

$$x_{min} = -\frac{2BC}{D^2+C^2} \tag{A.6}$$

and the corresponding minimum value is

$$\Gamma_{min} = A - \frac{C^2+D^2}{4B} \quad . \tag{A.7}$$

A sketch for the extremum values of Γ with $C < 0$ is shown in Fig. A-1. In case $C > 0$, the curves are similar, but reversed about the Γ-axis. The x_{min} then is on the negative axis, but g_1 remains on the positive side. Recalling the restriction $x \geq g_1 > 0$ placed on x, it is easily seen from the diagram that the maximum value is given by

$$\Gamma_{max} = A + \frac{D^2}{2} \frac{1}{-(B+Cg_1) + \sqrt{(B+Cg_1)^2 + D^2 g_1^2}} \tag{A.8}$$

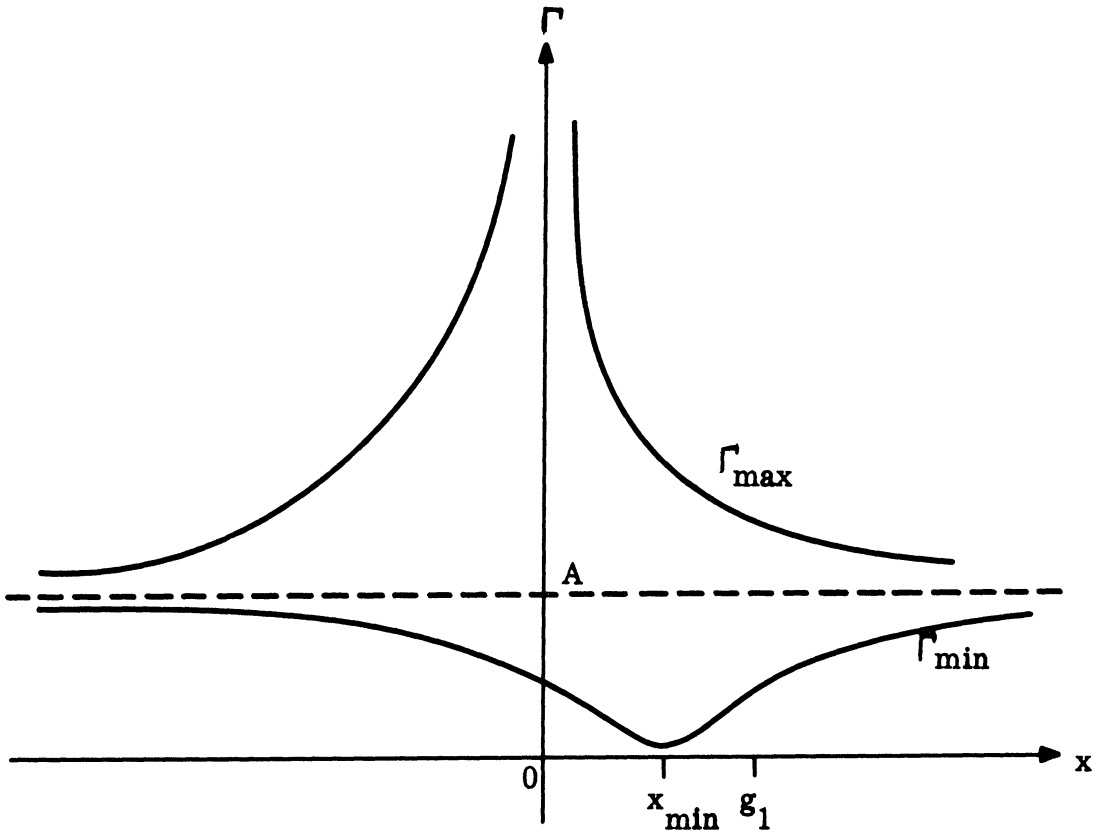

FIG. A-1: EXTREMUM VALUES OF Γ WITH C < 0.

and the minimum value by

$$\Gamma_{min} = A - \frac{D^2}{2} \frac{}{(B+Cg_1)+\sqrt{(B+Cg_1)^2+D^2g_1^2}} , \qquad \text{(A.9a)}$$

when $x_{min} < g_1$

$$= A - \frac{C^2+D^2}{4B} , \qquad \text{when } x_{min} > g_1 \qquad \text{(A.9b)}$$

where x_{min} is given by equation (A.6).

APPENDIX B

THE INPUT ADMITTANCE OF AN ASYMMETRICALLY EXCITED RADIAL CAVITY

In order to use the experimental model of Chapter IV to verify the theoretically predicted scattering behavior of the slotted sphere, it is necessary to relate the input admittance of the cavity to its dimensions, frequency, and, in particular, to the radius b of the inner conductor. Bearing in mind that the slot is of small width centered on $\theta_o = \pi/2$, it would appear sufficient to regard the cavity as a radial one, and in terms of the cylindrical polar coordinates (r, ϕ, z) where

$$x = r\cos\phi, \qquad y = r\sin\phi, \qquad z = z,$$

the situation is now as shown in Fig. B-1.

The cavity is of width $d = a\delta$ and is shorted at $r = b$. At the outer edge $r = a$ it is excited by a voltage $-v\cos\phi$ (the sign difference with respect to the voltage implied by equation (2.10a) is a consequence of the fact that $\hat{z} = -\hat{\theta}$ at $\theta = \pi/2$) and since it is assumed that $d \ll \lambda$, the components E_r and E_ϕ of the electrical field within the cavity can, for all practical purposes, be neglected. The only E component remaining is then E_z, and this must satisfy the wave equation which, in cylindrical coordinates, is

$$\frac{1}{r}\frac{\partial}{\partial r}\left(r\frac{\partial}{\partial r}E_z\right) + \left(k^2 + \frac{1}{r^2}\frac{\partial^2}{\partial\phi^2}\right)E_z = 0 .$$

The general solution for $0 < b \leqslant r \leqslant a$ is

$$E_z = \sum_{n=-\infty}^{\infty}\left\{E_n J_n(kr) + F_n N_n(kr)\right\} e^{in\phi} , \qquad (B.1)$$

where $J_n(kr)$ and $N_n(kr)$ are cylindrical Bessel functions of the first and second kinds respectively, and E_n and F_n are constants to be determined. The boundary conditions on the sides of the cavity are satisfied automatically by (B.1). At the

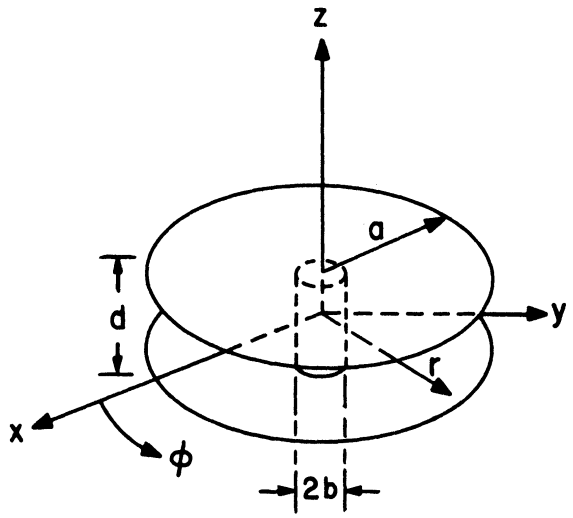

FIG. B-1: GEOMETRY OF THE RADIAL CAVITY.

inner and outer surfaces, however, the conditions are

$$E_z = 0 \qquad \text{for } r = b$$

$$= \frac{v}{d}\cos\phi \qquad \text{for } r = a \ ,$$

and on substituting in (B.1), we obtain

$$E_z = \frac{v}{d}\,\frac{J_1(kr)\,N_1(kb) - N_1(kr)\,J_1(kb)}{J_1(ka)\,N_1(kb) - N_1(ka)\,J_1(kb)}\cos\phi \ . \tag{B.2}$$

The corresponding circumferential component of the magnetic field can be found from Maxwell's equations, and is

$$H_\phi = -iY\frac{v}{d}\,\frac{J_1'(kr)\,N_1(kb) - N_1'(kr)\,J_1(kb)}{J_1(ka)\,N_1(kb) - N_1(ka)\,J_1(kb)}\cos\phi \ . \tag{B.3}$$

Since both E_z and H_ϕ are functions of ϕ, we shall again employ the concept of admittance density, as for the radiation admittance in Section 2.3. The power flow across the aperture and into the cavity is

$$w = -\int_{-d/2}^{d/2} \frac{1}{2}(\underline{E} \times \underline{\tilde{H}}) \cdot \hat{r}\, dz$$

$$= \frac{1}{2}\,\frac{v\cos\phi}{d}\int_{-d/2}^{d/2} H_\phi\, dz$$

$$= \frac{1}{2}\, v\cos\phi\, H_\phi \ ,$$

from which we have

$$y_\ell = \frac{\left[H_\phi\right]_{r=a}}{v\cos\phi} \ .$$

The total input admittance Y_L follows on integrating this around the circumference of the cavity, and hence

$$Y_\ell = -iY\,2\pi\,\frac{a}{d}\,\frac{J_1'(ka)\,N_1(kb) - N_1'(ka)\,J_1(kb)}{J_1(ka)\,N_1(kb) - N_1(ka)\,J_1(kb)} \quad . \tag{B.4}$$

As $b \to a$

$$Y_\ell \to -iY\,2\pi\,\frac{a}{d}\cdot\frac{1}{k(a-b)} \quad ,$$

and the admittance therefore approaches $-i\infty$ with decreasing cavity depth. On the other hand, as $b \to 0$ (a condition which is equivalent to an asymmetrically excited radial cavity open at the center)

$$Y_\ell \to -iY\,2\pi\,\frac{a}{d}\,\frac{J_1'(ka)}{J_1(ka)} \quad . \tag{B.5}$$

We also remark that if the cavity were filled with a medium of refractive index n, the expression for the admittance would follow immediately from equation (B.4) on replacing k by nk and Y by the intrinsic admittance of the medium. Thus for real n, numerical values can be obtained by scaling those for an air-filled cavity.

The expression for Y_ℓ has been programmed for an IBM 7090 computer to give data for any ka and a/d as a function of kb. For the sphere used in the experimental study the diameter was 3.133 inches, the gap width 0.0625 inches, and the spacing discs enabled 2b to be varied in 22 steps from a minimum of 0.3125 inches to 3.133 inches. In order to have the computed data directly applicable to the experimental model, kb was written in the form

$$kb = ka\,\frac{x}{3.133} \quad ,$$

and the data was printed out for the first 22 values of the inner diameter x (in inches) appropriate to the shorting discs. Because of the infinity when b = a, the largest x computed was 3.0. Typical values of the relative admittance Y_ℓ/Y are

shown in Fig. B-2. The value $2b = 0.3125$ inches corresponds to the diameter of the center screw in the experimental model, and $2b = 2.322$ inches is the diameter of the loading disc which supplies the optimum loading for zero back scattering at $ka = 4.28$.

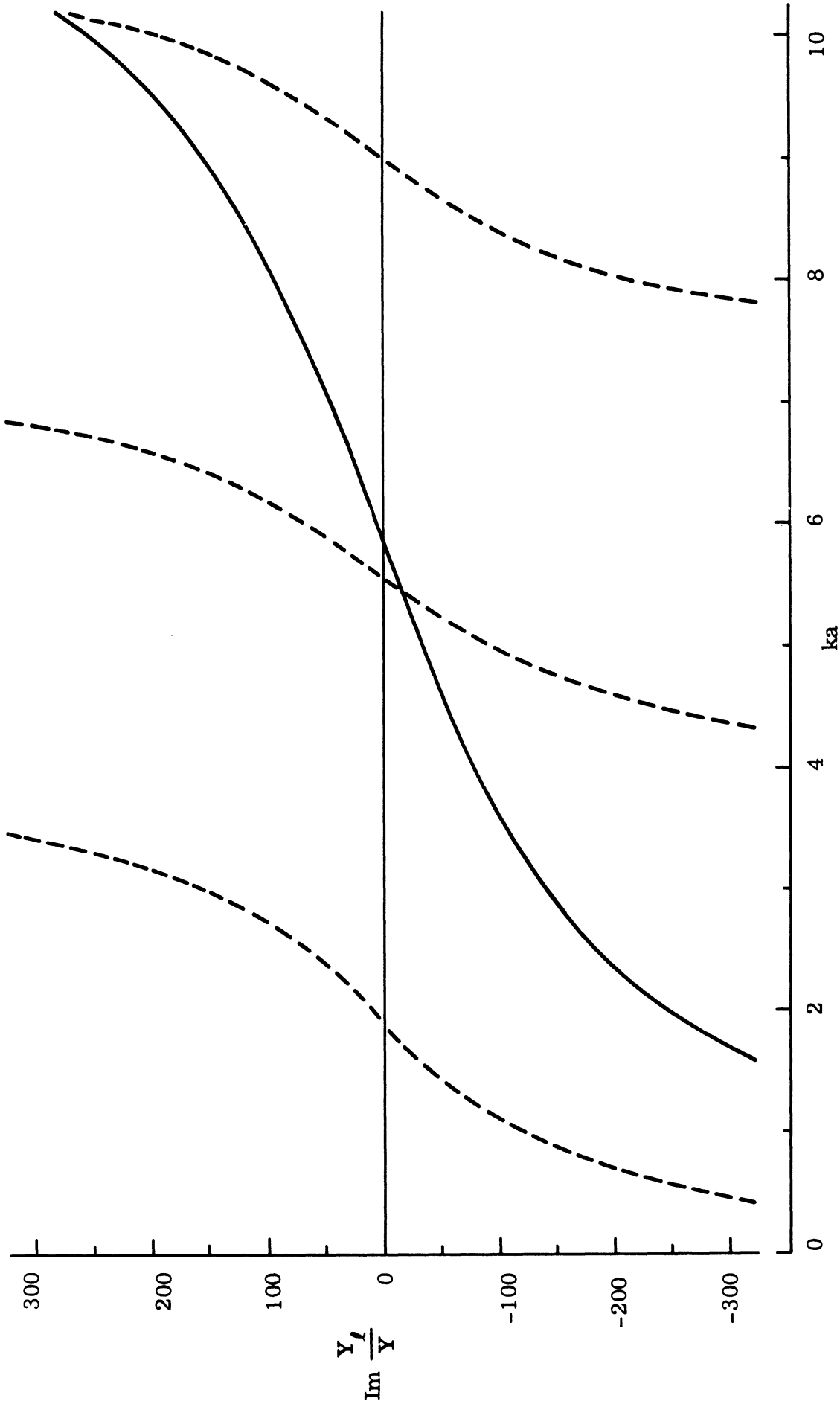

FIG. B-2: NORMALIZED LOADING ADMITTANCE OF ASYMMETRICALLY EXCITED RADIAL CAVITY FOR 2b = 0.3125 INCHES (- - -) AND 2b = 2.322 INCHES (——): 2a = 3.133 AND d = 0.064 INCHES.

Unclassified

Security Classification

DOCUMENT CONTROL DATA - R&D

(Security classification of title, body of abstract and indexing annotation must be entered when the overall report is classified)

1. ORIGINATING ACTIVITY (Corporate author)
The University of Michigan
Department of Electrical Engineering
Radiation Laboratory

2a. REPORT SECURITY CLASSIFICATION
UNCLASSIFIED

2b. GROUP

3. REPORT TITLE
Theoretical and Experimental Study of the Scattering Behavior of a Circumferentially-Loaded Sphere

4. DESCRIPTIVE NOTES (Type of report and inclusive dates)
Technical Report

5. AUTHOR(S) (Last name, first name, initial)
Liepa, Valdis V.
Senior, Thomas B.A.

6. REPORT DATE	7a. TOTAL NO. OF PAGES	7b. NO. OF REFS
February 1966	116	34

8a. CONTRACT OR GRANT NO.	9a. ORIGINATOR'S REPORT NUMBER(S)
AF 19(628)-2374	5548-5-T
b. PROJECT NO. 5635	
c. Task 563502	9b. OTHER REPORT NO(S) (Any other numbers that may be assigned this report)
d.	

10. AVAILABILITY/LIMITATION NOTICES
U.S. Government agencies may obtain copies of the report directly through DDC.

Other qualified users shall request through CFSTI

11. SUPPLEMENTARY NOTES	12. SPONSORING MILITARY ACTIVITY
	Air Force Cambridge Research Laboratories L.G. Hanscom Field Bedford, Massachusetts

13. ABSTRACT

The electromagnetic scattering behavior of a metallic sphere loaded with a circumferential slot in a plane perpendicular to the direction of incidence is investigated. The slot is assumed of small but finite width with a constant electric field across it, and under this assumption, the analysis of external fields is exact. The scattered field is obtained by superposition of the field diffracted by an unloaded sphere and that radiated from the excited slot, with the radiation strength and phase determined by the loading parameters. Thus the scattering behavior is determined by the loading admittance and the position of the slot.

The numerical study is restricted to the frequency range corresponding to $0<ka\leqslant 10.0$, and the results presented are primarily for passive loading. The maximum and minimum back scattering cross sections and the loading needed to attain these are presented for different loading positions. The bistatic scattering patterns are computed for a sphere loaded for zero back scattering and from these the back scattering null widths are obtained. The extreme total scattering cross sections are evaluated using the forward scattering theorem and, for small values of ka, the result is compared with that obtained by direct integration of the differential cross sections.

Experimental data, obtained using a metallic sphere with an equatorial slot backed by a radial cavity of adjustable depth, is presented for the surface field and back scattering measurements. The results are compared with the computed data.

DD FORM 1 JAN 64 1473

Unclassified

Security Classification

14. KEY WORDS	LINK A		LINK B		LINK C	
	ROLE	WT	ROLE	WT	ROLE	WT
Metallic sphere Scattering and Diffraction Cross section control Impedance loading						

INSTRUCTIONS

1. ORIGINATING ACTIVITY: Enter the name and address of the contractor, subcontractor, grantee, Department of Defense activity or other organization *(corporate author)* issuing the report.

2*a*. REPORT SECURITY CLASSIFICATION: Enter the overall security classification of the report. Indicate whether "Restricted Data" is included. Marking is to be in accordance with appropriate security regulations.

2*b*. GROUP: Automatic downgrading is specified in DoD Directive 5200.10 and Armed Forces Industrial Manual. Enter the group number. Also, when applicable, show that optional markings have been used for Group 3 and Group 4 as authorized.

3. REPORT TITLE: Enter the complete report title in all capital letters. Titles in all cases should be unclassified. If a meaningful title cannot be selected without classification, show title classification in all capitals in parenthesis immediately following the title.

4. DESCRIPTIVE NOTES: If appropriate, enter the type of report, e.g., interim, progress, summary, annual, or final. Give the inclusive dates when a specific reporting period is covered.

5. AUTHOR(S): Enter the name(s) of author(s) as shown on or in the report. Enter last name, first name, middle initial. If military, show rank and branch of service. The name of the principal author is an absolute minimum requirement.

6. REPORT DATE: Enter the date of the report as day, month, year; or month, year. If more than one date appears on the report, use date of publication.

7*a*. TOTAL NUMBER OF PAGES: The total page count should follow normal pagination procedures, i.e., enter the number of pages containing information.

7*b*. NUMBER OF REFERENCES: Enter the total number of references cited in the report.

8*a*. CONTRACT OR GRANT NUMBER: If appropriate, enter the applicable number of the contract or grant under which the report was written.

8*b*, 8*c*, & 8*d*. PROJECT NUMBER: Enter the appropriate military department identification, such as project number, subproject number, system numbers, task number, etc.

9*a*. ORIGINATOR'S REPORT NUMBER(S): Enter the official report number by which the document will be identified and controlled by the originating activity. This number must be unique to this report.

9*b*. OTHER REPORT NUMBER(S): If the report has been assigned any other report numbers *(either by the originator or by the sponsor)*, also enter this number(s).

10. AVAILABILITY/LIMITATION NOTICES: Enter any limitations on further dissemination of the report, other than those imposed by security classification, using standard statements such as:

(1) "Qualified requesters may obtain copies of this report from DDC."

(2) "Foreign announcement and dissemination of this report by DDC is not authorized."

(3) "U. S. Government agencies may obtain copies of this report directly from DDC. Other qualified DDC users shall request through

_____."

(4) "U. S. military agencies may obtain copies of this report directly from DDC. Other qualified users shall request through

_____."

(5) "All distribution of this report is controlled. Qualified DDC users shall request through

_____."

If the report has been furnished to the Office of Technical Services, Department of Commerce, for sale to the public, indicate this fact and enter the price, if known.

11. SUPPLEMENTARY NOTES: Use for additional explanatory notes.

12. SPONSORING MILITARY ACTIVITY: Enter the name of the departmental project office or laboratory sponsoring *(paying for)* the research and development. Include address.

13. ABSTRACT: Enter an abstract giving a brief and factual summary of the document indicative of the report, even though it may also appear elsewhere in the body of the technical report. If additional space is required, a continuation sheet shall be attached.

It is highly desirable that the abstract of classified reports be unclassified. Each paragraph of the abstract shall end with an indication of the military security classification of the information in the paragraph, represented as *(TS)*, *(S)*, *(C)*, or *(U)*.

There is no limitation on the length of the abstract. However, the suggested length is from 150 to 225 words.

14. KEY WORDS: Key words are technically meaningful terms or short phrases that characterize a report and may be used as index entries for cataloging the report. Key words must be selected so that no security classification is required. Identifiers, such as equipment model designation, trade name, military project code name, geographic location, may be used as key words but will be followed by an indication of technical context. The assignment of links, rules, and weights is optional.